DETERMINATION OF THE PARTICLE INTERACTIONS – RHEOLOGY – SURFACE ROUGHNESS RELATIONSHIP FOR DENTAL CERAMICS

A Thesis Submitted to
the Graduate School of Engineering and Sciences of
İzmir Institute of Technology
in Partial Fulfillment of the Requirement for the Degree of

MASTER OF SCIENCE

in Chemistry

by
Mürşide KES

July 2007
İZMİR

We approve the thesis of **Mürşide KES**

Date of Signature

..... **20 July 2007**
Assoc. Prof. Dr. Hürriyet POLAT
Supervisor
Department of Chemistry
Izmir Institute of Technology

..... **20 July 2007**
Prof. Dr. Orhan ÖZTÜRK
Department of Physics
Izmir Institute of Technology

..... **20 July 2007**
Assoc. Prof. Dr. Gökhan AKSOY
School of Dentistry
Ege University

..... **20 July 2007**
Prof. Dr. Levent ARTOK
Head of Department
Izmir Institute of Technology

.....
Prof. Dr. M. Barış ÖZERDEM
Head of The Graduate School

ACKNOWLEDGMENTS

I would like to express my grateful thanks to my thesis supervisor, Assoc. Prof. Hürriyet POLAT for her guidance, understanding, motivations and endless support during this study and preparation of this thesis. I also would like to thank to Assoc. Prof. Gökhan AKSOY at Ege University for his valuable comments on dental ceramics and Prof. Dr. Mehmet POLAT and Prof. Dr. Orhan ÖZTÜRK for their valuable criticisms.

I am also thankful to IZTECH (2006 IYTE 14) for financial support for this study and Assoc. Prof. Cihangir DURAN at Gebze Institute of Technology for his kind help in Zeta Potential and Particle Size measurements and Dt. Niler Özdemir for her help in preparation of dental ceramics and IYTE Center of Material Research members for their assistance in SEM, EDS, XRD and AFM measurements.

I am also grateful to Serkan KELEŞOĞLU for his help and motivation during the study.

Finally, I would like to thank to my family for their support, continued patience, encouragement and help throughout my studies.

ABSTRACT

DETERMINATION OF THE PARTICLE INTERACTIONS – RHEOLOGY – SURFACE ROUGHNESS RELATIONSHIP FOR DENTAL CERAMICS

In this study, relationship between particle interactions, rheology and surface roughness for dental ceramics was determined. For this purpose IPS Empress 2 veneer powder was chosen and characterized with XRD, SEM, EDS, Zeta Potential and Particle Size measurements.

Particle interactions have been interpreted in the light of DLVO Theory for distilled water and electrolyte solutions at different concentrations (0.1, 0.25, 0.5, 0.75, 1 M NaCl and $CaCl_2$). The results indicated that interactions between particles change with electrolyte concentration and valency. Electrical Double Layer Thickness (Debye Length) compresses and Energy Barrier height decreases as electrolyte concentration and valency increase mean that there is agglomeration between particles.

In order to understand the rheological properties of the system shear rate versus shear stress and shear rate versus viscosity graphs were interpreted for the same environmental conditions, distilled water and electrolyte solutions at different concentrations. It was obtained that at low electrolyte conditions particles formed agglomerates, however at high electrolyte conditions the system reached equilibrium where particles formed gel structures due to their non-Newtonian behaviour.

The results obtained from rheological measurements were compared with the results obtained from AFM, profilometer and SEM measurements for the surfaces prepared with IPS Empress 2 veneer powder and it was concluded that in the presence of electrolytes (Na^+ and Ca^{2+}) surface roughness increased at low concentrations due to agglomeration of particles whereas surface roughness decreased at high concentrations most probably due to gelation in the system. Moreover, this situation was supported with contact angle measurements where contact angle mean values are high and ditributions are wide at low electrolyte concentrations while contact angle mean values are small and distributions are narrow at high concentrations

ÖZET

DENTAL SERAMİKLERİN TANELER ARASI İLİŞKİLER – REOLOJİ – YÜZEY PÜRÜZLÜLÜĞÜ İLİŞKİSİNİN BELİRLENMESİ

Bu çalışmada dental seramiklerin taneler arası ilişkiler – reoloji - yüzey pürüzlülüğü ilişkisi incelenmiştir.

Taneler arası ilişkiler saf su ve değişik konsantrasyonlardaki (0.1, 0.25, 0.5, 0.75, 1M NaCl ve $CaCl_2$) elektrolit çözeltileri için DLVO Teorisi kullanılarak belirlenmiştir. Elde edilen veriler taneler arası ilişkilerin elektrolit konsantrasyonu ve değerliği ile değiştiğini göstermiştir. Elektrolit konsantrasyonu ve değerliği arttıkça Elektriksel Çift Tabaka (Debye Uzunluğu) bastırılmakta ve Enerji Bariyer Yüksekliği düşmektedir bu da taneler arasında aglomerasyon olduğunu göstermektedir.

Saf su ve değişik konsantrasyonlardaki elektrolit çözeltilerindeki seramik toz reoloji grafikleri çizilerek sistemin reolojik özellikleri anlaşılmaya çalışılmıştır. Düşük elektrolit konsantrasyonlarında tanelerin aglomere olduğu gözlenirken belli bir konsantrasyondan sonra dengeye ulaştığı ve jelleşmenin olduğu gözlenmiştir.

Reoloji ölçümlerinden elde edilen sonuçlar ile seramik yüzeylerin AFM, profilometre ve SEM ölçümleri sonucunda elde edilen sonuçlar karşılaştırılmış ve elektrolit ortamında yüzey pürüzlülüğünün düşük konsantrasyonlarda tanelerin aglomere olmasından dolayı arttığı ancak yüksek konsantrasyonlarda sistemdeki jelleşmeden dolayı yüzey pürüzlülüğünün azaldığı belirlenmiştir. Ayrıca bu durum kontak açısı ölçümleriyle de desteklenmiştir. Düşük elektrolit konsantrasyonlarında ortalama kontak açısı değerleri yüksek ve dağılımı geniş iken yüksek elektrolit konsantrasyonlarında ortalama kontak açısı değerleri düşük ve dağılımı dar olarak gözlemlenmiştir.

TABLE OF CONTENTS

LIST OF FIGURES

LIST OF TABLES

CHAPTER 1

INTRODUCTION

1.1. Statement of the Problem

Biomaterials are used to repair or replace diseased, damaged or aged body parts. Synthetic polymers, metals, ceramics, inorganics and natural macromolecules (biopolymers) may be used as biomaterials. These materials must not produce toxic substances and must be compatible with body tissues (Callister 2001). Ceramics, glasses and glass-ceramics are suitable for repair and replacement of hard tissues whereas polymeric materials are used for cardiovascular system applications. Once these materials are implanted they will come in contact with cells, proteins, tissues, organs and organ systems in human body. The form of the material, how it interfaces with the tissue, and its time of use will determine the required material properties. Therefore there are several types of biomaterials depending on application type as listed in Table 1.1.

Table 1.1. Materials for use in the body
(Source: Park and Bronzino 2003, Park and Lakes 1992)

Materials	Examples
Polymers (nylon, silicone rubber, polyester, polytetrafluoroehtylene, etc.)	Sutures, blood vessels, hip socket, ear, nose, other soft tissues
Metals (Ti and its alloys, Co-Cr alloys, stainless steels, Au, Ag, Pt, etc.)	Joint replacements, bone plates and screws, dental root implants, pacer and suture wires
Ceramics (aluminum oxide, calcium phosphates including hydroxyapatite, carbon)	Dental; femoral head of hip replacement, Coating of dental and orthopedic implants
Composites (carbon-carbon, wire or fiber reinforced bone cement)	Joint implants, heart valves

Ceramics are defined as the art and science of making and using solid articles that have as their essential component inorganic nonmetallic materials. (Kingery et al. 1976). Ceramics are generally hard. Other characteristics of ceramic materials are their high melting temperatures and low conductivity of electricity and heat. (Park and Bronzino 2003)

In recent years, it has been realized that ceramics and their composites can also be used to augment or replace various parts of the body, particularly bone. Thus, the ceramics used for the latter purposes are classified as bioceramics. Their relative inertness to the body fluids, high compressive strength, and aesthetically pleasant apperance led to the use of ceramics in dentistry. (Park and Bronzino 2003)

The types of ceramic materials used in biomedical applications may be divided into three classes according to their reactivity with the environment:

i) biodegradable or resorbable ceramics: calcium phosphates and calcium aluminates

ii) relatively bioinert (nonabsorbable) ceramics: alumina, zirconia, silicone nitrides, carbons

iii) bioactive or surface reactive (semi-inert) ceramics: glass ceramics, dense hydroxyapatites.

(Hench 1991, Hench 1993, Hench 1980, Hentrich et al. 1971, Graves et al. 1972, Park and Lakes 1992, Bhat 2002).

1.2. Literature Survey

Ceramics have been traditionally preferred as a dental restorative material because of their esthetic quality and excellent biocompatibility. Their ability to yield relatively smooth surfaces, which minimizes plaque deposition and tissue inflammation, is another important reason for their preference in dental applications. Therefore, the degree of surface roughness of dental ceramics and its effect on biocompatibility has been widely studied (Kuwata 1980, Quirynen et al. 1990, Quirynen and Bollen 1995, Fuzzi et al. 1996, Bollen et al. 2000, Yin et al. 2003, Fleming et al. 2004, Fleming et al. 2005, Ahmad et al. 2005, Curtis et al. 2005). Surface roughness also determines the degree of abrasion caused by one tooth on another. Since ceramics are usually harder materials than natural tooth, if they are not treated to smoothness, their abrasive effects

will create series of problems in the oral environment (Kawai and Urano 2001) In the cooling stage of the fired ceramic, some micro cracks develop on the ceramics surface, increasing the surface roughness and decreasing the strength of material due to stresses accumulating within the crack sites. These factors reduce the performance of the ceramic restorative materials in oral environment (Piddock et al. 1991, Anusavice and Hojjatie 1991, Anusavice et al. 1992, Oh et al. 2002). However, in the literature there is no study about the rheology of dental ceramics and effect of rheology and the particle interactions on the surface roughness.

1.3. Scope of the Study

The purpose of this study was to investigate the effect of interparticle relations by taking rheological characteristics of the dental ceramics into account on the final surface roughness.

For this purpose, to understand the rheological properties of the system, shear stress versus shear rate graphs of dental ceramics were drawn. These studies were repeated for different environmental conditions such as distilled water and electrolyte solutions at different concentrations, then the relations between these conditions and their rheological properties were determined. In addition, rheological results were interpreated by considering the particle relations which has been calculated by DLVO theory. To use DLVO theory, zeta potential and particle sizes were measured.

The relation between particle interactions – rheological properties and the surface roughness was determined by AFM, SEM and profilometer that provide surface roughness degrees and contact angle study to indicate the wettability and roughness of the surfaces.

CHAPTER 2

PROPERTIES OF DENTAL CERAMICS, RHEOLOGY AND INTERPARTICLE RELATIONS

2.1. Dental Ceramics

Dental ceramics are generally used to restore damaged, diseased, or fractured teeth because of their excellent aesthetics, wear resistance, chemical inertness, low thermal conductivity, and low thermal diffusivity. In addition, they match the characteristics of tooth structure fairly well (Anusavice 1992).

The ceramic material known as porcelain holds a special place in dentistry, because it is still considered to produce aesthetically the most pleasing result. Its colour, translucency and vitality cannot as yet be matched by any material except other ceramics. As people retain their teeth for much longer than in the past, the need for aesthetically acceptable restorations is continuing to increase (Van Noort 2002). Because ceramic materials are the materials of choice for esthetic, biocompatible, and long-term functional indirect restorations (ADA Council of Scientific Affairs).

2.1.1. Composition of Dental Ceramics

The earliest dental porcelains were mixtures of kaolin ($Al_2O.2SiO_2.2H_2O$), feldspar ($K_2O.Al_2O_3.6SiO_2$) and quartz (SiO_2), and were quite different from earthenware, stoneware and domestic porcelain, as indicated in the Figure 2.1 and Table 2.1.

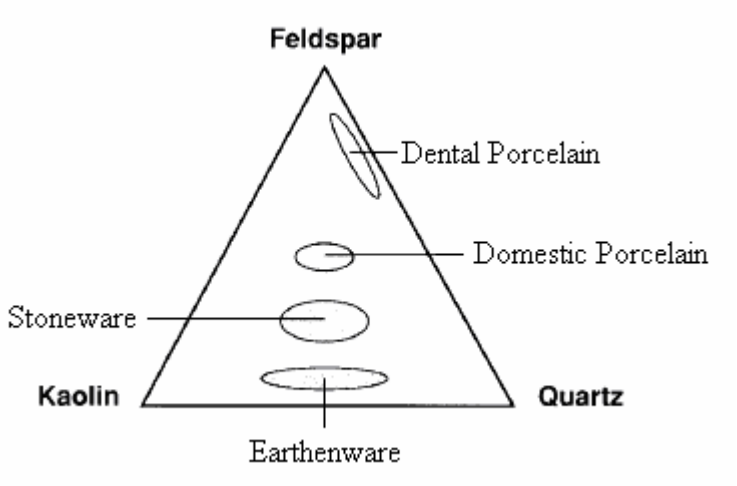

Figure 2.1. Relative composition of ceramic products
(Source: Van Noort 2002)

Table 2.1. Composition of household and dental porcelains
(Source: Van Noort 2002)

Porcelain	**% Kaolin**	**% Quartz**	**% Feldspar**
Household	50	20 – 25	25 – 30
Dental	0	25	65

Kaolin is a hydrated aluminum silicate ($Al_2O.2SiO_2.2H_2O$) and acts as a binder, increasing the ability to mould the unfired porcelain. It is opaque, however, when present, even in very small quantities, it meant that the earliest dental porcelains lacked adequate translucency. Thus, for dental porcelains the kaolin was omitted and could therefore be considered to be a feldspathic glass with crystalline inclusions of silica.

The feldspars are mixtures of potassium aluminosilicate ($K_2O.Al_2O_3.6SiO_2$) and sodium aluminosilicate, also known as albite ($Na_2O.Al_2O_3.6SiO_2$). Feldspars are naturally occuring substances, so the ratio between the potash (K_2O) and the soda (Na_2O) will vary somewhat. This affects the properties of the feldspar, in that the soda tends to lower the fusion temperature and the potash increases the viscosity of the molten glass.

The composition of the many ceramic materials used in dentistry is a complex of variable components that modify strength and aesthetic properties. (Crispin 1994). A number of oxides present in dental porcelain powders in order to obtain the natural look of teeth.

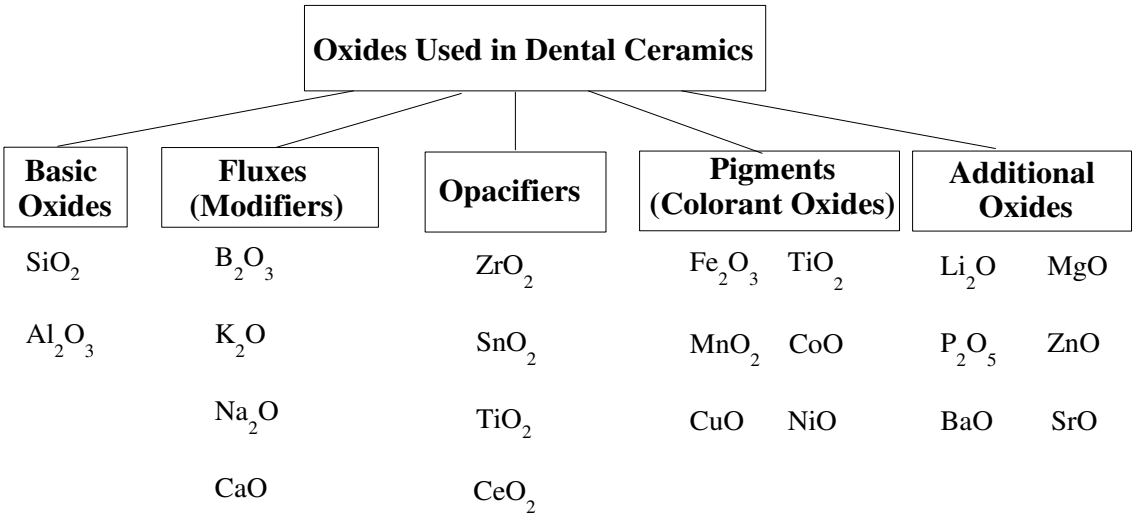

Figure 2.2. Typical Oxides Used in Dental Ceramics

2.1.1. 1. Basic Oxides

Silica and alumina are the basic oxides used in dental porcelains.

2.1.1.1.1. Silica (Silicon Dioxide, SiO_2)

It is the principle glass forming oxide. The quartz remains unchanged during the firing process and acts as a strengthening agent. It is present as a fine crystalline dispersion throughout the glassy phase that is produced by the melting of the feldspar. The feldspar fuses when it melts, forming a glassy matrix (Van Noort 2002). It comprises more than 60% of most dental ceramics (WEB_1 2006).

Decreasing SiO_2 increases the melt fluidity while increasing raises the melting temperature, acid resistance, lowers expansion, increases hardness and gloss and devitrification. It is normal to use as much as possible in any glaze to keep expansion low, to prevent crazing, and enhance body/glaze fired strength. However, in certain boracic and feldspathic compositions it can increase crazing so that other low expansion oxides may be needed to reduce glaze expansion (WEB_1 2006).

2.1.1.1.2. Alumina (Aluminum Oxide, Al_2O_3)

Dental porcelains require a high resistance to slump or pyroplastic flow and it is therefore necessary to produce samples with a high viscosity as well as low firing temperatures. Alumina is the hardest and probably the strongest oxide known. It provides hard, impermeable ceramic of very high strength and chemical resistance (McLean 1979) and combines well with silica to give body and stability (McMillan 1979).

Alumina controls the flow of the glaze melt, preventing it from running off the ware. It is thus called an intermediate oxide because it helps build strong chemical links between fluxes and silica. Alumina is second in importance to silica and combines with silica and basic fluxing oxides to prevent crystallization and give body and chemical stability to a glaze.

It is the prime source of durability in glazes. It increases melting temperature, improves tensile strength, lowers expansion, and adds hardness and resistance to chemical attack. If a glaze contains too much alumina, then it may not melt enough but will likely be more hard and durable if firing temperature is increased. If a glaze has inadequate alumina, then it is likely that it will lack hardness and strength at any temperature.

Increasing Al_2O_3 stiffens the melt and gives it stability over a wider range of temperatures. The addition of alumina prevents devitrification (crystallization) of glazes during cooling because the stiffer melt resists free movement of molecules to form crystalline stuctures.

Since alumina stiffens the glaze melt, it will prevent the growth of crystals during cooling because it is more difficult for the specific oxides needed to form the crystal, to travel to the site of formation. Thus most highly crystalline glazes have very little alumina.

The ratio of silica to alumina is mainly responsible for the degree of matteness in glazes. Low silica high alumina glazes produce matte effects. A ratio of 5:1 is matte, 10:1 is glossy. In the absence of boron, ratios of less than 5:1 are generally quite matte, ratios of greater than 8:1 are usually glossy in the absence of high titania (TiO_2), zinc, magnesia (MgO), or calcia (CaO) (WEB_1 2006).

2.1.1.2. Fluxes (Modifiers)

Currently dental ceramics are essentially feldspathic glasses with oxides added (B_2O_3, K_2O, Na_2O_3, and CaO) to lower the firing (sintering) temperature and increase thermal expansion, which is needed for bonding (Crispin 1994 and McLean 1979).

2.1.1.2.1. Boric Oxide (B_2O_3)

Boric oxide is a powerful flux included in glass formulations to lower the softening temperature of the glass (Combe 1986 and McLean 1979). Its low expansion makes it valuable in preventing crazing. In low temperature glazes, it both substitutes for fluxes of high-expansion, and for silica which cannot be present in large amounts. Its reactivity helps to form good clay-glaze interfacial zones that inhibit crazing. The action of B_2O_3 depends upon the ratio of bases to silica existing before the addition. If the ratio is greater than 1:2, the glaze will tend toward opalescence and crazing; if less toward clear and transparent. Increasing silica at the expense of boric oxide to make glaze harder, more durable, and brilliant (WEB_1 2006).

2.1.1.2.2. PotassiumOxide (K_2O)

K_2O is considered together with sodium, since the two almost always occur together and have very similar properties. K_2O generally promotes higher melt viscosity than Na_2O. It is a heavy oxide and in general hosts the brightest colors of all fluxes. It is usually preferred even to soda (Na_2O) for a more brilliant glossy glaze and longer firing range. Relatively high expansion tends to contribute to crazing in higher amounts. During the firing of porcelain there is always the danger of excessive pyroplastic flow, which may result in rounding of the edges and loss of tooth form. It is important that the correct amount of potash is present to prevent this (WEB_1 2006).

2.1.1.2.3. Sodium Oxide (Soda, Na_2O)

Sodium oxide is a good example of a modifying oxide which is a slightly more powerful flux than potassium. The introduction of soda into the glass results in changes

of the properties including reduction of viscosity of the glass and increase in the thermal expansion coefficient therefore it should be used in moderate amounts in glazes lacking silica and alumina promote crazing. Also it decreases tensile strength and elasticity compared to other common bases. High soda glazes can often be soluble and easily scratched. Soda works well with boric oxide and also lithia and potassium in low temperature glazes (McMillan 1979, WEB_1 2006).

2.1.1.2.4. Calcium Oxide (Calcia, CaO)

Calcium oxide is an extremely stable compound and the principle flux in medium and high temperature glazes. Calcia usually hardens a glaze and makes it more scratch and acid resistant. Its expansion is intermediate. Hardness, stability, and expansion properties of silicates of soda and potash are almost always improved with the addition of CaO.

High CaO glazes tend to devitrify (crystallize). This occurs either because of the high melt fluidity imparted by CaO at higher temperatures or because of the readiness with which CaO forms crystals.

CaO can mottle glaze surfaces at high temperatures if significant amounts are present. High molar amounts of calcia combined with adequate silica and preferably lower alumina will form a calcium silicate crystal matte (WEB_1 2006).

2.1.1.3. Opacifiers

The addition of concentrated colour frits to dental porcelain is insufficient to produce a life-like tooth effect since the translucency of the porcelain is too high. In particular the dentine colours require greater opacity if they are to stimulate natural dentine overlaid by enamel. An opacifying agent generally consists of metal oxide ground to a very fine particle size (<5 μm) to prevent a speckled appearance in the porcelain. Common oxides used are Zirconium oxide, Tin oxide, Titanium oxide, and Cerium oxide (McLean 1979).

2.1.1.3.1. Zirconium Dioxide (ZrO_2)

Zirconium oxide is the most popular and effective opacifyig agent. It gives a harsher glassy white and is an extremely refractory material. In amounts below 5%, where it does not yet opacify, zircon can be added to transparent glazes to produce a harder surface.

2.1.1.3.2. Tin Oxide (SnO_2)

It is a very white powder of low density and quite refractory. Tin is about twice as more effective in producing opacity than zircon. Tin oxide has been used primarily as an opacifier in amounts of 5-15% in all types of glazes. The amount required varies according to the composition and temperature. The mechanism of the opacity depends on the white tin particles being in suspension in the molten glass. At higher temperatures, these particles will start to dissolve and opacity will begin to be compromised.

Larger amounts of tin in lower temperature glazes have a refractory effect, stiffening the melt and increasing the incidence of pinholing and crawling like zirconium oxide. Tin is an effective opacifier to transform transparent glazes to white (WEB_1 2006).

2.1.1.3.3. Titanium Oxide (Titania, TiO_2)

Titania is a complex material because it opacifies, variegates, and crystallizes glazes. It also modifies existing colors from metals like Cr, Mn, Fe, Co, Ni, Cu. It discolors if any iron oxide is present. Titania can act as a modifier and within a narrow range it will combine with fluxes to make a glass. It can also act in a flux-like way in very high silica melts.

In amounts below 1% titania can dissolve completely in a glaze melt. In slightly greater amounts it can give a bluish-white flush to transparent glazes depending on their amount of alumina. Above 2% it begins to significantly alter the glaze surface and light reflectance properties through the creation of minute crystals. This crystal mechanism gives soft colors and pleasant opacity, and breaks up and mottles the surface. In the 2-

6% range, it increasingly variegates the glaze surface. Large amounts (10-15%) will tend to produce an opaque and matte surface if the glaze is not overfired. They will also subdue color and can add sparkle to the surface. Small amounts (i.e. 0.1%) can be used to intensify and stabilize colors. It can alter and intensify existing color and opacity in a glaze (WEB_1 2006).

2.1.1.3.4. Cerium Oxide (CeO)

It is used as a replacement for tin opacifier in porcelain enamel. In combination with titanium, cerium produces a yellow glass. It is restricted to low temperatures.

2.1.1.3.5. Other Opacifiers

These include calcium phosphate when problems with off-coloring to greys and antimony to give yellow color.

2.1.1.4. Pigments

The greatest colour problem encountered in dental porcelain is the slightly greenish hue. In order to dampen down this effect and to produce life-like dentine and enamel colours the basic dental porcelain frit must be coloured with high temperature resistant pigments. Different pigments are used in the ceramic to impart colour (McLean 1979, Crispin 1994).

2.1.1.4.1. Iron Oxide (Ferric Oxide, Fe_2O_3)

Iron compounds are the most common coloring agent in ceramics. Fe_2O_3 generally behaves as a refractory antiflux material in a glaze melt, combining with alkalis. Oxidation iron-red glazes, for example, can have very low alumina contents yet do not run off ware because the iron acts like alumina to stabilize and stiffen the melt. However these glazes likely will have somewhat reduced durability.

Fe_2O_3 is very affected by a reducing atmosphere where it can act as a flux in both bodies and glazes at high temperatures. Higher amounts of iron exhibit dramatically increased fluidity.

Fe_2O_3 is the most natural state of iron oxide where it is combined with the maximum amount of oxygen. In oxidation firing it remains in this form to typically produce amber to yellow up to 4% in glazes (especially with lead and calcia), tans around 6% and browns in greater amounts. In the 20% range, matteness is typical. In oxidation iron glazes calcia likes to form yellow crystalline compounds with the Fe_2O_3 producing a lime matte. Without the calcia, glossy brown glazes are formed.

2.1.1.4.2. Manganese Dioxide (MnO_2)

Manganese is a colorant using in bodies and glazes, producing blacks, browns, and purples. Smaller amounts are easily dissolved in most glaze melts, however, around the 5% threshold, the manganese will precipitate and crystallize. In large amounts (i.e. 20%), metallic surfaces are likely. Below 1080^{o}C, it can give coffee color browns when used with tin.

2.1.1.4.3. Cobalt Oxide (CoO)

Cobalt is a powerful and often less than 1% will give strong color and stable colorant used in glass, glaze, enamel. CoO is the stable form that combines with the glass melt to produce color. Because cobalt is quite soluble in glaze melts, it has little or no opacifying effect. It is very color dependable under both oxidizing and reducing furnace conditions, fast and slow firing.

Cobalt is used in combination with manganese and selenium to mask excess yellow coloration. This effect works best when silica is not too high and there is adequate alumina.

2.1.1.4.4. Cupric Oxide (CuO)

It can act as a strong flux. Generally additions of copper to a glaze will reduce crazing.

2.1.1.4.5. Nickel Oxide (NiO)

Nickel oxide is most often used to modify and soften the color of other metallic oxides and thus small amounts are normally employed. It is not normally used in low fire glazes due to the refractory nature of nickel oxide powder. In lithium glazes nickel can produce yellow.

2.1.1.5. Additional Oxides

The ingredients of dental ceramic powders may vary according to the manufacturer. Additional oxides can be used to get more strong and translucent ceramics.

2.1.1.5.1. Lithium Oxide (Li_2O, Lithia)

Lithium is the lightest, smallest, and most reactive flux. Adding small amounts by weight introduces disproportionately large amounts to the glaze formula because of its low molecular weight. It is known that molten lithia is mobile and diffuses into the surrounding matrix because of its small ionic radius and low charge. It can also diffuse into the body and create a low expansion glaze interface. In small amounts it acts as a powerful auxiliary alkaline flux with thermal expansion lowering effects. However in large amounts lithia can drastically increase the thermal expansion of a glass.

Together with boron and sodium, it acts as a melter at lower temperatures. In frits and glazes, lithia is used to reduce the viscosity and thereby increase the fluidity of the coatings. This reduces maturing times and lowers firing temperatures. When used as a partial substitute for sodium and potassium oxides, it produces glazes of lower expansion.

Lithia gives the most intense colors in low alumina high alkali glazes. It can promote textural or variegated effects in the glaze surface because it promotes devitrifaction in glass systems (WEB_1 2006).

2.1.1.5.2. Magnesium Oxide (MgO, Magnesia)

Like CaO, MgO is refractory at lower temperatures, so much so that it can be used to increase opacity, to perform as a matting agent and act as a check to glaze fluidity in a manner similar to alumina (e.g. to prevent devitrification or the tendency to produce crystalline surfaces). When mixed with CaO, it is not as refractory.

It is valuable for its lower expansion and crazing resistance. When introduced it should preferentially replace calcia, baria, and zinc before the alkalis to maintain surface character. Adding too much will generally move the surface texture toward matte or dry.

2.1.1.5.3. Phosphorus Pentoxide (P_2O_5)

Phosphoric oxide is normally present in only trace amounts in ceramic materials. It is known to influence the rate of nucleation and/or crystallization in Li_2O and MgO low expansion glaze systems. It can act as a melter in middle to high fire. (WEB_1 2006). Phosphorus pentoxide is sometimes added to induce opalescence (McLean 1979).

2.1.1.5.4. Zinc Oxide (ZnO)

In smalls amounts zinc helps in the development of glossy and brilliant surfaces. It can improve durability in some glazes and exhibits refractory properties. However, in larger amounts ZnO can produce opacity or whiteness in glazes.

2.1.1.5.5. Barium Oxide (BaO, Baria)

Baria is the heaviest of the divalent fluxing oxides. As a flux it can be very active in small amounts but not active at low temperatures. For example, it can improve gloss, elasticity, mechanical strength and corrosion resistance, and acid resistance. Barium does not reduce in the melt and therefore does not discolor.

It acts as a flux if decomposed and can assist in the formation of a matte structure. Barium forms silicates slowly, but when completely combined it is very active as a fluxing agent. Baria is more effective as a melter when associated with other

fluxing oxides with which it can combine. The mechanism may well be better accomplished by another oxide. For example, SrO and CaO can both be employed to produce crystal mattes in saturation.

It can produce better translucency in porcelain bodies. In enamels its acts as a strong flux. Baria is used for surface modifier to cause the growth of a fine mesh of micro crystals to produce a silky matte texture (WEB_1 2006).

2.1.1.5.6. Strontium Oxide (SrO, Strontia)

Strontium oxide has matting and crystallizing properties similar to barium although it produces brighter and more fusible glazes with fewer surface defects. It has a lower dissociation temperature and reacts earlier and is potentially able to produce a more perfect surface unmarred by the bubbles and pits associated with higher temperature decomposition. If BaO is replaced in whole or in part with SrO, glazes can develop better interface and have a lower expansion. Even though it has a very high melting temperature, SrO is effective in combination with other fluxes at lower temperatures. Like calcia and baria, it will produce a fine crystalline mesh to give attractive satin matte surfaces (WEB_1 2006).

2.1.2. Production of Dental Ceramics

The porcelain powder used by the dental technician is not a simple mixture of the ingredients in table. In the production of dental ceramic powders, the manufacturer mixes the raw materials and additional metal oxides and heats at high temperatures then quenches the molten mass. The resultant products is known as a frit, and the process is known as fritting. This material can be ground very easily to produce a fine powder for use by the dental technician (Crispin 1994 and Van Noort 2002).

The production of a porcelain dental material involves three technical stages (Van Noort 2002):

- Compaction
- Firing
- Glazing

2.1.2.1. Compaction (Condensation)

Porcelain powder is built to shape using liquid binder to hold the particles together. The process of packing the particles together and of removing the liquid binder is known as condensation. Distilled water is the most common and probably the most useful liquid binder to use, but additions of glycerine, propylene glycol or alcohol have been tried by some manufacturers.

The usual procedure of the construction of a porcelain dental material is to mix the dry porcelain powder with water to a thick and creamy consistensy and then can be applied to the die in a number of ways, such as spatulation, brush application, whipping or vibrating, all of which are aimed at compacting the powder (McLean 1979). The binder helps to hold the particles together and a ceramic body which is formed as a particulate aggregate that has been dried but not fired forms which is called as green body (Callister 2001).

2.1.2.2. Firing

During the firing of a porcelain there is no chemical reaction taking place; the glass is simply melted above its glass transition temperature, when the particles fuse together by liquid phase sintering, and cooled down again. Thus, all that has happened is that the individual particles have fused together by sintering to produce a coherent solid.

The conversion of powder from a mass of individual particles loosely held together by a water binder to a coherent solid relies on a process known as sintering. In this process, the points at which the individual particles are in contact fuse at sufficiently high temperatures. The process relies on diffusion, which is greatly accelerated by elevated temperatures. Ceramics are sintered by raising them to a high temperature. This process consolidates the material, increases its strength, and usually causes it to shrink.

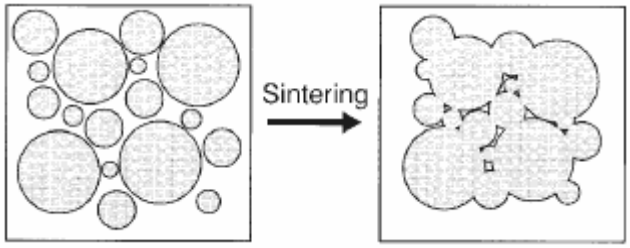

Figure 2.3. Sintering of Ceramic Particles
(Source: Van Noort 2002)

During the firing of porcelain there is always the danger of excessive pyroplastic flow, which may result in rounding of the edges and loss of tooth form. It is important that the correct amount of potash is present to prevent this.

Initially, the sample is heated slowly in the open entrance to the furnace. This is carried out in order to drive off excess water before it has a chance to form steam. If the water in the mix was allowed to turn into steam, it would cause the fragile powder-compact to crack as the steam tried to escape to the surface. Once the compact has been dried, it is placed in the furnace and the binders are burnt out. Some contraction occurs during this stage.

When the porcelain begins to fuse, continuity is only achieved at points of contact between the powder particles. The material is still porous, and is usually referred to as being at the low bisque stage. At this stage the grains of porcelain will have started to soften and dense at their contact points. Shrinkage will be minimal and the fired body is extremely weak and friable. As the exposure to the elevated temperature continues, more fusion takes place as the molten glass flows between the particles, drawing them closer together and filling the voids. A large contraction takes place during this phase (~20%), and the resultant material is virtually non-porous. This stage is called as medium bisque stage. The cause of the high shrinkage of porcelain on firing is therefore due to the fusion of the particles during sintering, as the powder particles are brought into close contact. At high bisque stage the surface of the porcelain will be completely sealed and present much smoother surface, the porcelain is strong and any corrections by grinding can be made prior to final glazing (McLean 1979).

The firing of the porcelain must be carried out exactly according to the manufacturer's instructions. If the crown should remain in the furnace for too long it

will lose form, due to pyroplastic flow (flow of the molten glass), and will become highly glazed.

A very slow cooling rate is essential in order to avoid the possibility of cracking or crazing. The furnaces available usually offer a considerable degree of automation, and can be used for air- or vacuum-firing. Vacuum-firing produces a denser porcelain than air-firing, as air is withdrawn during the firing process. Fewer voids are formed, resulting in a stronger crown with a more predictable shade. Areas of porosity in air-fired porcelain alter the translucency of the crown, as they cause light to scatter. An additional problem is that air voids will become exposed if grinding of the superficial layer should be necessary, giving rise to an unsightly appearance and a rough surface finish (Van Noort 2002). Due to the rapid action of vacuum sintering, the firing schedule for the porcelains can be reduced in comparison with the longer period recommended for air-fired porcelain (McLean 1979).

2.1.2.2.1. Firing on Ceramic Quality

The problems are with thermal shock, strength, and chemical reactions with the ware. Fine powders exhibit higher firing shrinkages for the following two reasons: these powders sinter to higher densities, and as the particle size becomes increasingly fine, surface forces between particles prevent packing to a high green density and result in a larger volume change upon densification.

Thermal shock is caused by uneven heating or cooling. Fine-grained, dense ceramics are susceptible to thermal shock, which can usually be prevented by slow heating and cooling. When a porcelain is removed from the furnace and cooled in air, the surface will be losing heat more rapidly than the interior, the surface will contract faster than the interior. The sample that is moved into the furnace rapidly will receive the full force of the heat and the surface will tend to expand faster than the interior so that the thermal cracks will develop from the inner surface and break through the outer skin. The ceramists are therefore strongly advised to insert the sample very slowly into the hot zone of the furnace muffle so that all sections of the porcelain are evenly heated (McLean 1979).

Thermal expansion and conductivity are important properties. Low expansion and high thermal conductivity result in better thermal shock resistance.

2.1.1.3. Glazing

There will always be some porosity in the porcelain, with small air voids being exposed at the surface. These will allow the ingress of bacteria and oral fluids and act as potential sites for the build-up of plaque. To avoid this, the surface is glazed to produce a smooth, shiny and impervious outer layer. There are two ways in which this can be achieved (Aksoy et al. 2006, Van Noort 2002):

1. Over-glazing: A thin layer of glasses fuses at low temperatures are applied to the crown after construction, and a short period at a relatively low temperature is sufficient to fuse the glaze.

2. Auto-glazing: The surface of the ceramic itself fuses the superficial layer to an impervious surface glaze at high temperatures.

2.1.2. Properties of Dental Porcelain

Dental porcelain is chemically very stable, and provides excellent aesthetics that do not deteriorate with time. The thermal conductivity and the coefficient of thermal expansion are similar to those of enamel and dentine.

Although the compressive strength of dental porcelain is high (350 – 550 MPa), its tensile strength is very low (20 – 60 MPa), which is a typical of a brittle solid. Fracture in brittle solids is nearly always initiated at a small internal or surface defect, such as a microcrack, that acts as a stress raiser. Glasses are extremely sensitive to the presence of surface microcracks, and this represents one of the major drawbacks in the use of dental porcelain. On cooling from the furnace temperature, the outside of the porcelain will cool more rapidly than the interior, particularly as the porcelain has a low thermal conductivity. The outside surface contracts more than the inside initially, resulting in a compressive load on the outside and a residual tensile stres on the inside, as the interior is being prevented from shrinking by the outside skin.

The application of a glaze with a slightly lower coefficient of expansion would potentially fill in the cracks and also place the surface under compression. Unfortunately, this is not possible on the fitting surface of the crown, as it may result in

the crown not seating properly. The tiny surface flaws in the interior of the crown act as initiating sites for catastrophic failure. The inherently low tensile strength of feldspathic porcelains (<60MPa) restricted their use to very low stress bearing anterior applications. The answer is to provide a high strength support for the porcelain.

Dental materials should:

a) be non-toxic; this is important not only for patients, but also for dental surgeons and ancillary staff.

b) be non-irritant to the oral or other tissues.

c) not produce allergic reactions, and,

d) not be mutagenic or carcinogenic. (Van Noort 2002)

2.1.3. Classification of Dental Ceramics

There are different types of dental ceramics available and they can be classified according to their structure and chemical composition or their construction techniques. Generally dental ceramics can be divided into two general categories as metal-ceramic restorations (porcelain-fused-to-metal systems) and all-ceramic restorations (full-ceramics). In each case the philosophy is to provide a high strength supporting structure for the ceramic providing the aesthetic finish. Obviously, the ideal ceramic would have both the strength and the aesthetics to perform both functions.

2.1.3.1. Metal-Ceramic Restorations (Porcelain-Fused-to-Metal)

In metal–ceramic restorations, the aesthetic ceramic is supported by a strong and tough metal to increase resistance to fracture. However, it is almost impossible to imitate the natural tooth to the finest detail with metal-ceramic materials. The colour of the natural tooth comes from within the tooth, in other words, from enamel and dentin, which demonstrate different optical absorption spectra. In dental restorations, however, a metal framework is simply coated with opaquer and a thin layer of dentin and enamel materials. This metal base can affect the aesthetics of the porcelain and cause to appear unnatural due to decreasing the light transmission, particularly in the interior region and creating metal ion discolorations. In addition, some patients may have allergic reactions or sensitivities to various metals (McCabe 1990, Rosenblum and Schulman 1997,

Heintze 1998). A large number of metal-ceramic systems have been developed for use in dentistry and they may be classified as follows (McLean 1979):

- Noble-Metal Alloy Systems
  - High gold 1. Gold – platinum – palladium alloys
    2. Gold – platinum – tantalum alloys
  - Low gold 3. Gold – platinum – silver alloys
  - Gold – free 4. Palladium – silver alloys
- Base – Metal Alloy Systems
  - Nickel – chromium alloys
  - Cobalt – chromium alloys

2.1.3.2. All-Ceramic Restorations (Full-Ceramics)

The drawbacks of metal-ceramic restorations together with the material and labor costs associated with metal substrate fabrication and high aesthetic requirements have prompted the development of new metal-free restorations, all-ceramic systems, that do not require metal, but have the high strength and precision fit of metal-ceramic systems (Rosenblum and Schulman 1997).

All-ceramic restorations can be classified in four groups based on construction techniques (Crispin 1994, Rosenblum and Schulman 1997):

- Castable Ceramic Systems: They are modelled in a wax (Dicor, Cerapearl).
- Infiltrated Ceramic Systems: They are based on the principle of two infiltrated phases, Al_2O_3 and a glass (In-Ceram).
- Machinable Ceramic Systems: They are based on taking an optical impression of a patient's oral situation and have a restoration milled from a ceramic block chairside with CAD/CAM and copy-milling systems (Cerec Vitablocks, Procera AllCeram, Dicor MGC, Celay).
- Pressable Ceramic Systems: They are produced by molding under pressure and heat (IPS Empress, Optec)

All-ceramic restorations can be divided into two categories based on their supporting structure (Van Noort 2002):

- Reinforced ceramic core systems: The support for the aesthetic ceramic is provided by another ceramic material, which has the necessary high strength and

toughness but may lack the desired aesthetics (In-Ceram, Cerec, Celay, Procera All-Ceram).

• Resin-bonded ceramic systems: The support of the ceramic is provided by the tooth structure itself, by bonding the aesthetic ceramic directly to the enamel and dentine. In this instance the ceramic provides the necessary aesthetics and the strength is provided by the ability to bond to the tooth tissues. The materials available for resin-bonded ceramic restorations are varieties of glass –ceramics.

2.1.4. Glass – Ceramics

Glass ceramics were first developed in 1950s by Stookey with controlling the crystallization of special glasses. These materials may possess certain characteristics found in both glasses and ceramics (Höland and Frank 1994, Van Noort 2002).

In principle, an article is formed with liquid, and a metastable glass results on cooling. During a subsequent heat treatment, controlled crystallisation occurs, with the nucleation and growth of internal crystals. This conversion process from a glass to a partially crystalline glass is called ceraming. Thus, a glass ceramic is a multiphase solid containing a residual glass phase with a finely dispersed crystalline phase. The controlled crystallisation of the glass results in the formation of tiny crystals that are evenly distributed throughout the glass. The number of crystals, their growth rate and thus their size are regulated by the time and temperature of the ceraming heat treatment. There are two important aspects to the formation of the crystalline phase: crystal nucleation and crystal growth. The schematic in Figure 2.4. shows that the rate of crystal nucleation and the rate of crystal growth are at a maximum at different temperatures. The ceraming process consequently involves a two-stage heat treatment. The first heat treatment is carried out at the temperature for maximum nucleation of crystals, to maximize the number of crystals formed. The material temperature is then raised, after a suitable period of time, to the higher temperature to allow crystal growth. It is held at the higher temperature until the optimum crystal size is formed. To ensure a high strength for the glass ceramic it is important that the crystals are numerous and are uniformly distributed throughout the glassy phase. The crystalline phase will grow during ceraming, and can eventually occupy from 50% to nearly 100% of the material.

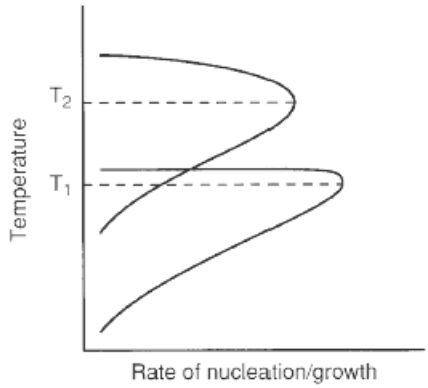

Figure 2.4. Rate of Nucleation (T_1) and Growth (T_2) of Crystals in a Glass Ceramic (Source: Van Noort 2002)

2.1.4.2. IPS Empress 2

IPS Empress 2 is a glass-ceramic recommended for aesthetic inlays, onlays and veneers. It is suitable for veneering because of providing restorations less than 0.8 mm thick which ensures look of natural tooth. Ceramic veneers are considered superior to composites because of their superior aesthetics, colour stability, surface finish, abrasion resistance and tissue compatibility. They are also chemically very stable and have a coefficient of expansion similar to that of enamel. The ceramic veneers have the distinct advantages that improved aesthetics can be achieved with minimal tooth reduction, and the palatal surface of the tooth is unchanged. These new materials have allowed the extension of the use of all-ceramic restorations from veneers to anterior and posterior crowns and inlays (Van Noort 2002)

2.2. Rheology

Rheology is the science of the change in form and flow of matter, encloses elasticity, viscosity and plasticity. Rheology is important in many industries such as food, paint, rubber, textiles. Rheological behaviour is also of major importance in biology and medicine (Shaw 1992).

Viscosity is a measure of the resistance of a slip to flow, the internal friction of a fluid. This friction becomes apparent when a layer of fluid is made to move in relation to another layer. The greater the friction, the grater the amount of force required to

cause this movement, which is called *shear*. Shearing occurs whenever the fluid is physically moved or distributed, as in pouring, spreading, spraying, mixing, etc. Highly viscous fluids, therefore, require more force to move than less viscous materials.

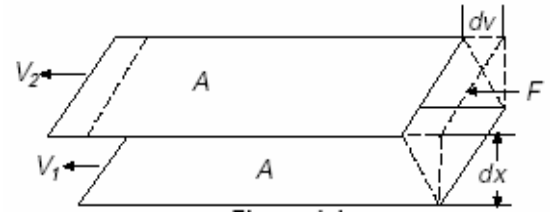

Figure 2.5. Viscosity Model

Two paralel flat areas of fluid of the same size A are separated by a distance dx and are moving in the same direction at different velocities V_1 and V_2. Newton assumed that the force required to maintain this difference in speed was proportional to the difference in speed through the liquid, or the velocity gradient.

$$\frac{F}{A} = \eta \frac{dv}{dx} \tag{2.1}$$

Where η is a constant for a given material and is called its viscosity. The velocity gradient, dv/dx, is a measure of change in speed at which the intermediate layers move with respect to each other. It describes the shearing the liquid experiences and is thus called shear rate. This is symbolized as γ and its unit of measure is called the reciprocal second (sec^{-1}). Plotting shear rate against viscosity determines the rheology of the slip.

The term F/A indicates the force per unit area required to produce shearing action. It is referred to as shear stress and is symbolized as τ. Its unit of measurement is "dynes per square centimeter" (dynes/cm^2) or "Newtons per square meter" (N/m^2).

Viscosity may be defined mathematically by Equation 2.2:

$$\eta = \text{viscosity} = \frac{\tau}{\gamma} = \frac{\text{shear stress}}{\text{shear rate}} \tag{2.2}$$

The fundamental unit of viscosity measurement is “poise”. Sometimes “Pascal-seconds” (Pa.s) or “milliPascal-seconds” (mPa.s) are used.

Fluids have different rheological characteristics. Generally fluids are divided into two classes as Newtonian and Non-Newtonian (Brookfield Engineering 2005).

2.2.1. Newtonian Fluids

Newton assumed that all materials have, at a constant temperature and pressure, a viscosity that is independent of the shear rate. In other words, the shear viscosity does not vary with shear rate and viscosity remains same at different shear rates (different rpm’s). Newtonian behavior is more typical of nonpolar liquids such as hydrocarbons, thin motor oils or water. Newtonian fluids have proportional relationship between shear stress (τ) and shear rate (γ) as shown in Figure 2.6.

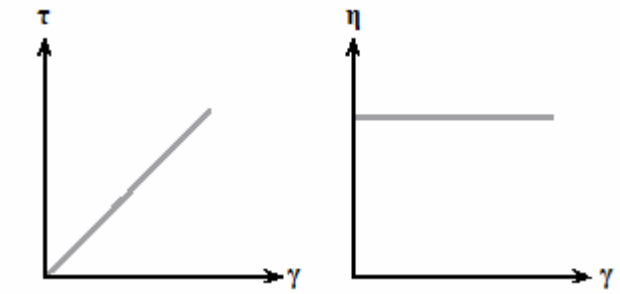

Figure 2.6. Diagram for Newtonian Behaviour

2.2.2. Non-Newtonian Fluids

These fluids have different viscosities at different shear rates (different rpm’s). When the shear rate is varied, the shear stress does not vary in the same proportion. The viscosity of such fluids will therefore change as the shear rate is varied. This measured viscosity is called the apparent viscosity of the fluid.

Non-Newtonian flow can be envisioned by thinking of any fluid as a mixtures of molecules with different shapes and sizes. As they pass by each other, as happens during flow, their size, shape, and cohesiveness will determine how much force is required to move them. At each specific rate of shear, the alignment may be different

and more or less force may be required to maintain motion (Brookfield Engineering 2005).

There are several types of non-Newtonian flow behavior, characterized by a fluid's viscosity changes in response to variations in shear rate. Flow behaviour may depend only on shear rate and not on the duration of shear that is time-independent, or may depend also on the duration of shear, time-dependent.

2.2.2.1. Time Independent Non-Newtonian Fluids

Time independency is also called as steady-state phenomena. There are three types of time-independent fluids.

2.2.2.1.1 Shear-Thinning

Shear-thinning fluids are popularly called pseudoplastic, include paints, emulsions, and dispersions of many types. This type of fluid will display a decreasing viscosity with an increasing shear rate. The faster the rotation, the more the structure is destroyed and the less structure of molecules slide in together therefore viscosity will be lower.

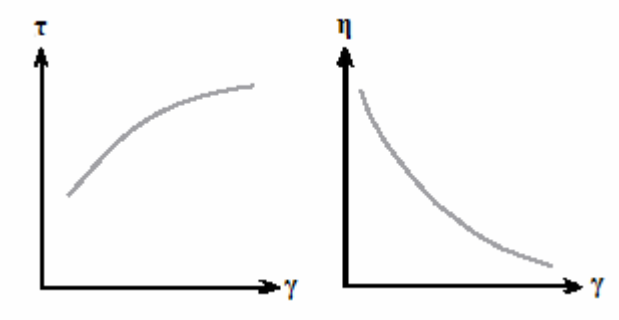

Figure 2.7. Diagram for Shear-Thinning Behaviour

If particle aggregation occurs in a colloidal system, then an increase in the shear rate will tend to break down the aggregates, which will result in a reduction of the amount of solvent immobilised by the particles, thus lowering the apparent viscosity of the system.

Shear-thinning is particularly common to systems containing asymmetric particles. Asymmetric particles disturb the flow lines to a greater extent when they are randomly orientated at low-velocity gradients than when they have been aligned at high-velocity gradients. In addition, particle interaction and solvent immobilisation are favoured when conditions of random orientation prevail. The apparent viscosity of a system which thins on shearing is most susceptible to changes in the shear rate in the intermediate range where there is a balance between randomness and alignment, and between aggregation and dispersion (Shaw 1992).

2.2.2.1.2. Shear-Thickening

Shear-thickening, dilatancy, is characterized by increasing viscosity with an increase in shear rate. Dilatancy is frequently observed in fluids containing high levels of deflocculated solids, such as clay slurries, candy compounds, and sand/water mixtures.

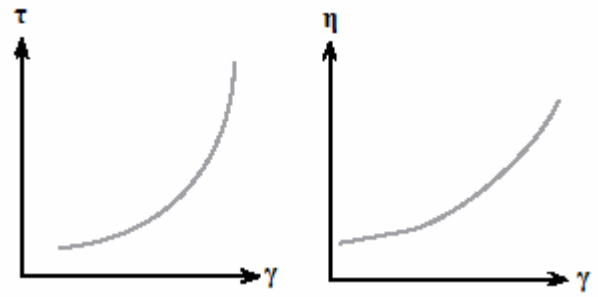

Figure 2.8. Diagrams for Shear-Thickening Behaviour

2.2.2.1.3. Plasticity

This type of fluid will behave as a solid under static conditions. A certain amount of stress must be applied to the fluid before any flow is induced; this stress is called yield stress or yield value (f´). Plasticity is due to a continuous structural network which imparts rigidity to the sample and which must be broken before flow can occur. Tomato catsup is a good example for this type of fluid. Once the yield value is exceeded

and flow begins, plastic fluids may display Newtonian, or dilatant flow characteristics (Shaw 1992, Brookfield Engineering 2005).

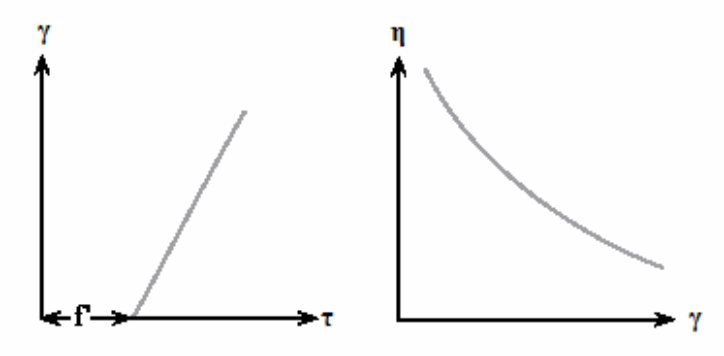

Figure 2.9. Diagrams for Plastic Behaviour

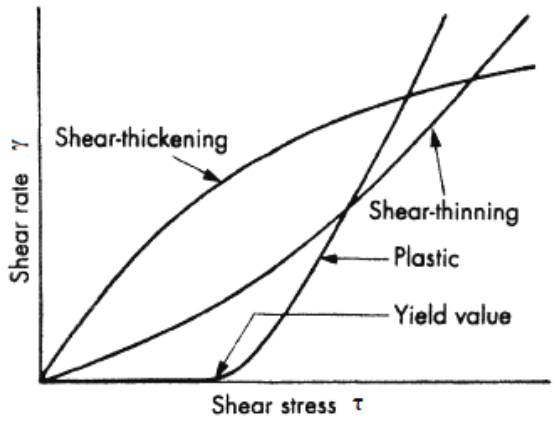

Figure 2.10. Types of Time Independent Non-Newtonian Flow

2.2.2.2. Time Dependent Non-Newtonian Fluids

Some fluids will display a change in viscosity with time under conditions of constant shear rate. There are two categories to consider: Thixotropy and Rheopexy.

2.2.2.2.1. Thixotropy

Thixotropy is the time-dependent analogue of shear-thinning and plastic behaviour. A thixotropic fluid undergoes a decrease in viscosity with time, while it is

subjected to a constant shear rate. The classical examples of thixotropic behaviour are the weak gel systems, such as flocculated sols of iron(III) oxide, alumina and many clays, which can be liquefied on shaking and solidify on standing (Shaw 1992).

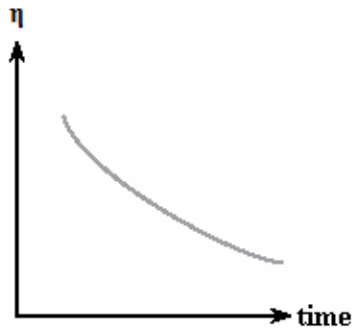

Figure 2.11. Diagram of Thixotropic Flow

2.2.2.2.2. Rheopexy

This is time-dependent shear-thickening, the opposite of thixotropic behavior, in that the fluid's viscosity increases with time as it is sheared at a constant rate.

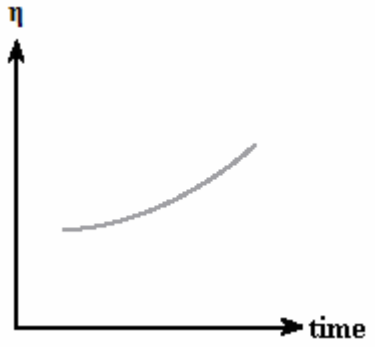

Figure 2.12. Diagram of Rheopectic Flow

2.2.3. Rheology of Ceramics

Rheology is important in ceramic processing and the rheological behaviour of colloidal suspensions depends mainly on the following factors (Shaw 1992, Funk and Dinger 1994, King 2002):

- viscosity of the dispersion medium
- particle concentration (volume percentage of solids)
- particle size distribution and shape
- deflocculant concentration
- pH
- ionic strength
- particle – particle and particle – dispersion medium interactions.

Measured viscosities and rheologies directly correlate to the behaviours of bodies and suspensions during processing. All particle/fluid suspensions, abroad category which includes all ceramic suspensions and forming bodies, are non-Newtonian fluids. For this reason it is important to characterize each suspension and forming body by measuring its viscosities at each shear rate and its rheology. Viscosity behaviour over a range of imposed shear rates defines a body's rheological properties (Funk and Dinger 1994).

2.3. Interparticle Relations

2.3.1. Theory of Surface Charge, Electrokinetic Phenomena and Zeta Potential

All powders exhibit electrostatically charged surfaces in liquid medium. The development of a net charge at the particle surface affects the distribution of ions in the surrounding interfacial region, resulting in an increased concentration of counter ions (opposite charged ions to that of the particle) close to the surface. Thus an electrical double layer exists around each particle (Figure 2.13). The overall effect of the ionic atmosphere is to shield the surface charge. The liquid layer surrounding the particle exists as two parts; an inner region called Stern layer, where the ions are strongly bound, and outer (diffuse) region where they are less firmly attached.

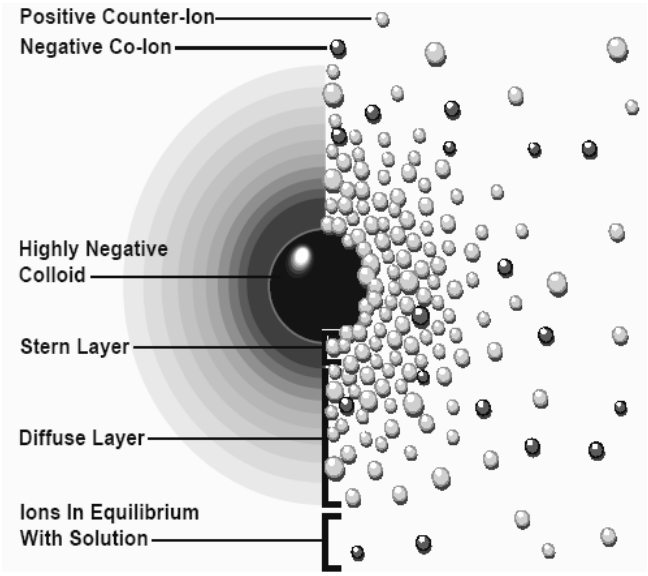

Figure 2.13. Electrical Double Layer Around Particle
(Source: Zeta-Meter Inc.)

The ions or charged molecules on the particle or within the diffuse layer surrounding the particle moves in respond to the electric field, this phenomena is called as electrophoresis. As a result of the opposing effects of the drag of the water molecules and the electrostatic pull by the moving particle, within the diffuse layer a notional boundary forms inside which the ions and particles form a stable entity. When a particle moves, ions within the boundary move with it, but any ions beyond the boundary do not travel with the particle. This boundary is called shear layer, shear plane or slipping plane. The potential that exists at this boundary is known as the Zeta Potential, ζ (Figure 2.14). (Zetasizer Nano Series User Manual 2004).

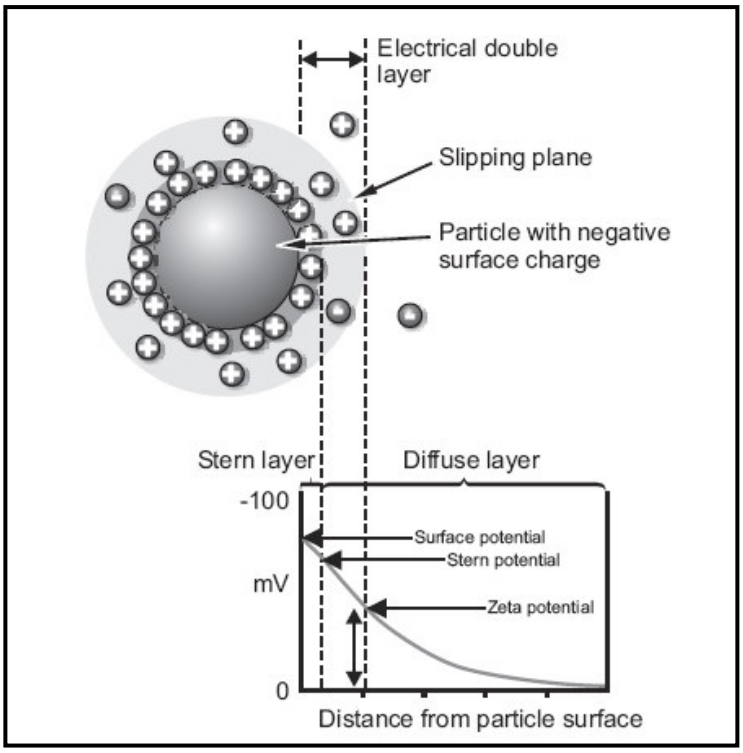

Figure 2.14. Electrical Double Layer around particle and Zeta Potential
(Source: Zetasizer Nano Series User Manual 2004)

The first theory for the electrical double layer was given by Helmholtz proposed that oppositely charged ions in solution are attached at the surface. However, Helmholtz double layer model is insufficient in terms of effect of electrolyte concentration and valency on the double layer. Gouy and Chapman proposed new double layer model independently named as Gouy-Chapman model which assumes that ions at solution side of double layer diffuse. At low electrolyte concentrations large thickness of solution may occur to accumulate ions in order to balance the surface charge. As a result of thermal motion, the electric charge extends over a certain distance from the particle surface and diminishes gradually with increasing distance into the bulk liquid phase. In this theory potential function have been related on the Poisson-Boltzman equation. For the solution contains a single and symmetrical electrolyte potential profile in the diffuse layer can be described by Equation 2.3 (Verwey and Overbeek 1948, Polat 1999, Liang et al. 2007).

$$\psi(x) = \frac{2RT}{zF} ln\left[\frac{1+\gamma e^{-\kappa H}}{1-\gamma e^{-\kappa H}}\right] \tag{2.3}$$

$$\gamma = [e^{\frac{zF\psi_0}{2RT}} - 1][e^{\frac{zF\psi_0}{2RT}} + 1]^{-1} \tag{2.4}$$

$$\kappa = \sqrt{\frac{2z^2F^2C_0}{RT\varepsilon\varepsilon_0}} \tag{2.5}$$

where ψ : Surface potential of the particle

R : Gas constant (8.314 J/mol.K)

T : Temperature (K)

z : Valency of electrolyte

F : Faraday constant (96484.5 C/mol)

κ : Reciprocal thickness of double layer (Debye-Hückel parameter, m^{-1})

H : Length of gap separating two particles

C_0 Concentration of electrolyte

ε : Relative permittivity of water (78.5)

ε_0 : Relative permittivity of vacuum (8.854×10^{-12} $C^2/J.m$)

The higher the ionic strength of the medium the more compact the diffuse region becomes due to the strong inter-ionic attraction. The more compact the diffuse layer, the greater the shielding effect. The potential field around the particle affect its interactions with the neighboring particles and therefore has far reaching implications in the stability of colloid. The magnitude of the zeta potential gives an indication of the potential stability of the colloid system. A colloid system is when one of the three states of matter; gas, liquid and solid, are finely dispersed in one of the others. For zeta potential measurements two states are important; a solid dispersed in a liquid and a liquid dispersed in a liquid (emulsion). If all the particles in suspension have a large negative or positive zeta potential then they will tend to repel each other and there is no tendency to flocculate. On the other hand, if the particles have low zeta potential values then there is no force to prevent the particles coming together and flocculating. The general dividing line between stable and unstable suspensions is generally taken at either +30

mV or -30 mV. Particles with zeta potentials more positive than +30 mV or more negative than -30 mV are normally considered stable.

The most important factor that affects zeta potential is pH. When zeta potential versus pH plot is drawn the point where the plot passes through zero zeta potential is called as Isoelectric Point where the colloidal system is least stable (Zetasizer Nano Series User Manual 2004).

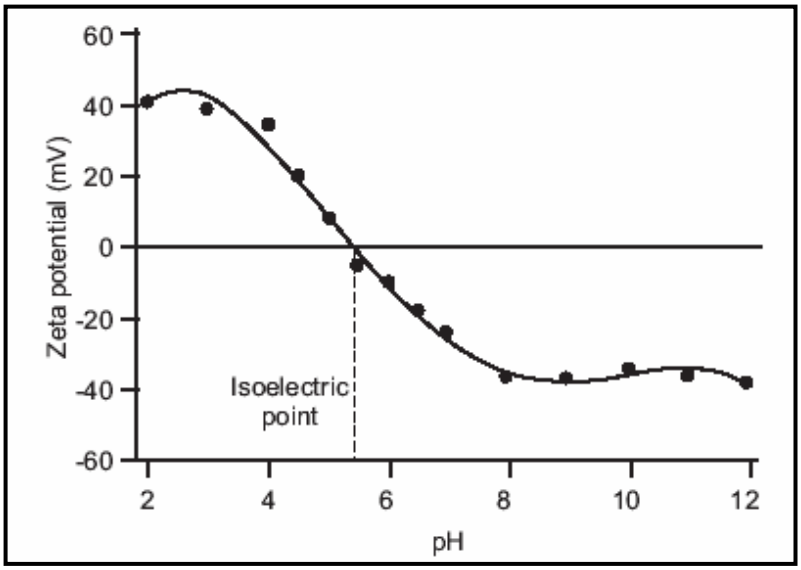

Figure 2.15. Zeta Potential versus pH Plot
(Source: Zetasizer Nano Series User Manual 2004)

As long as the interactions among the particles are considered the zeta potential by far the most important property since it is the potential which affects particles' interactions with the surrounding particles therefore, it is the most commonly used quantity in the calculation of the energy of interaction between colloidal particles about their stability.

2.3.2. Electrostatic Interactions

Electrostatic repulsion becomes significant when two like-charged colloids approach each other and their electrical double layers begin to overlap, resulting in a repulsive force that opposes further approach. The repulsive interaction between the electrical double layers of two particles is caused by the free energy change and involved when overlap occurs and the osmotic pressure generated by the accumulation

of ions between the particles. Therefore, energy is required to overcome this repulsion. It has a maximum value when they are almost touching and decreases to zero outside the double layer. The maximum energy is related to the surface potential. The repulsive interaction (V_{el}) decreases exponentially with increase in the distance between the particles (Burgess 2002, Zeta-Meter Inc.).

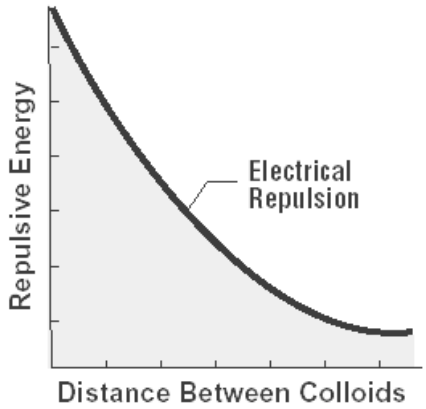

Figure 2.16. Electrostatic repulsion between particles
(Source Zeta-Meter Inc.)

In order to calculate the interaction between double layers on spherical particles Hogg et al. used Derjaguin's approximation which assumes the thickness of the double layer is small compared to the particle size. For two spherical particles electrostatic interactions can be computed by using Equation 2.6 which expresses the interaction between the electrical double layer surrounding any dissimilar colloidal particles (Hogg et al. 1966, Polat and Polat 2000).

$$V_{el} = \frac{\pi\varepsilon\varepsilon_0 d_1 d_2}{2(d_1 + d_2)}\left[2\psi_1\psi_2\, ln\left(\frac{1+e^{-\kappa H}}{1-e^{-\kappa H}}\right) + \left(\psi_1^2 + \psi_2^2\right) ln\left(1 - e^{-2\kappa H}\right)\right] \qquad (2.6)$$

where ε : Relative permittivity of water (78.5)

ε_0 : Relative permittivity of vacuum (8.854×10^{-12} C^2/J.m)

d : Diameter of particle

ψ_1, ψ_2 : Surface potentials of particle 1 and 2

κ : Reciprocal thickness of double layer (Debye-Hückel parameter, m^{-1})

H : Length of gap separating two particles

2.3.3. Attractive (Van der Waals) Interactions

The existence of attractive interaction between the particles was first asserted by Van der Waals in 1873, to account for certain anomalous phenomena occuring in non-ideal gases and liquids. By the end of 1930s it was suggested that Van der Waals forces consist of three major categories.

1. Keesom interactions: They describe randomly oriented permanent dipole – permanent dipole interactions. The perturbation creates attraction.

2. Debye interactions: A permanent dipole induces a dipole in another molecule randomly oriented permanent dipole – induced dipole interactions. The direction of the induce dipole is to create attraction.

3. London interactions: They describe induced dipole – induced dipole (dispersion) interactions.

Of the three forces, Keesom and Debye interactions are only found between molecules which have permanent dipole moments, dominant for polar molecules. Whereas, the London interaction is always present, because it does not require existence of permanent polarity or charge-induced polarity in the molecules (Van Oss 1994, Hiemenz and Rajagopalan 1997, Parsegian 2006).

Hamaker investigated the properties of Van der Waals interaction between large bodies. The coefficient of interaction between them is termed as Hamaker constant. The interaction potential is inversely dependent on particle separation but directly proportional to Hamaker constant (Hamaker 1937). The Hamaker constant occurs in an equation for approximating the attractive forces between two spheres:

$$V_{vdw} = -\frac{Ad_1d_2}{12(d_1 + d_2)H} \tag{2.7}$$

Where V_{vdw} is the potential energy, d is the diameter of the spheres, H is the distance between the surfaces of the spheres, and A is the Hamaker constant, which can be calculated from refractive index data and has a value between 10^{-19} and 10^{-20} joule for various materials (Mutsuddy and Ford 1995).

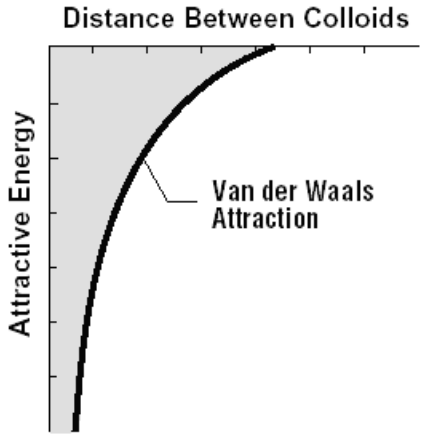

Figure 2.17. Van der Waals Attraction between particles
(Source: Zeta-Meter Inc.)

The van der Waals energy of attraction is due to interatomic electrical forces within particles. The Hamaker constant sums all these interatomic energies as a function of the volume of a particle of any material. The van der Waals energy is calculated from the Hamaker constant, the size of the respective particles, and the interparticle separation distance, H. So attraction of particles is fundamentally a bulk volume (a mass) effect which is intrinsic and cannot be changed by any outside effort. The Hamaker constants, hence the magnitude of the vdW interaction energy, changes significantly depending on whether the gap separating the macroscopic bodies is simply vacuum or contain another phase such as water. Therefore, an effective Hamaker constant A_{132} must be utilized for two bodies 1 and 2 separated by a gap containing medium 3. The most commonly used method to determine A_{132} is to assume that two particles interact through a pseudo-chemical reaction where the two particle-medium pairs (1-3 and 2-3) produces one particle-particle (1-2) and one medium-medium (3-3) pairs (Polat and Polat 2000).

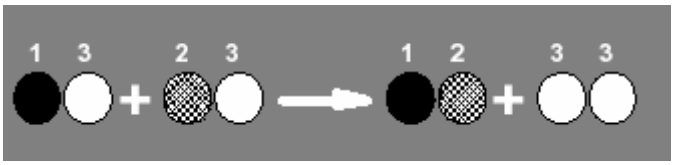

Figure 2.18. The Thermodynamic Path Taken for Calculating the Effective Hamaker Constants

Effective Hamaker constant is calculated with Equation 2.5 for dissimilar particles.

$$A_{132} = \left(\sqrt{A_{22}} - \sqrt{A_{33}}\right)\left(\sqrt{A_{11}} - \sqrt{A_{33}}\right) \tag{2.8}$$

For two identical particles *(A_{11}=A_{22})*, the effective Hamaker constant becomes A_{131} and is equal to

$$A_{131} = \left(\sqrt{A_{11}} - \sqrt{A_{33}}\right)^2 \tag{2.9}$$

Table 2.2. Hamaker Constants of Some Materials (x10-20 J)

Material	**Hamaker Constant**	**Reference**
Water	5.47 (in vacuum)	Visser 1975
	4.38 (in vacuum)	Krupp et al. 1972
	4.35 (in vacuum)	Bargeman and Voorst Vader 1972
	3.70 (in vacuum)	Hunter 1992
Al_2O_3	17.91 (in vacuum)	Visser 1975
	4.44 (in water)	Visser 1975
	15.4 (in vacuum)	Bargeman and Voorst Vader 1972
	4.17 (in water)	Krupp et al. 1972
SiO_2	8.55 (in vacuum)	Büttner and Gerlach 1970
	16.4 (in vacuum)	Fowkes 1967
	1.7 (in water)	Fowkes 1967
MgO	11.6 (in vacuum)	Visser 1975
	1.8 (in water)	Visser 1975
	1.76 (in water)	Krupp et al. 1972

2.3.4. DLVO Theory and Stability

The stabilization of aqueous suspensions of particles is explained on the basis of coulombic repulsions between the charged surfaces of particles, by the DLVO theory proposed by Derjaguin and Landau (1941) and Verwey and Overbeek (1946)

independently. DLVO theory is concerned with estimating the energy due to the overlap of electric double layers (repulsive) and London-van der Waals forces (attractive) in terms of interparticle distances and their summation to give the total interaction energy (Mutsuddy and Ford 1995).

$$V_{tot} = V_{el} + V_{vdw} \tag{2.10}$$

$$V_{tot} = \frac{\pi \varepsilon \varepsilon_0 d_1 d_2}{2(d_1 + d_2)} \left[2\psi_1 \psi_2 \ln\left(\frac{1 + e^{-\kappa H}}{1 - e^{-\kappa H}} \right) + \left(\psi_1^2 + \psi_2^2 \right) \ln\left(1 - e^{-2\kappa H} \right) \right] - \frac{A d_1 d_2}{12(d_1 + d_2) H} \tag{2.11}$$

The DLVO theory explains the tendency of colloids to agglomerate or remain discrete by combining the van der Waals attraction curve with the electrostatic repulsion curve to form the net interaction energy curve. At each distance, the smaller value is subtracted from the larger to get the net energy. The net value is then plotted (above if repulsive and below if attractive) and a curve is formed. If there is a repulsive section, then the point of maximum repulsive energy is called the energy barrier.

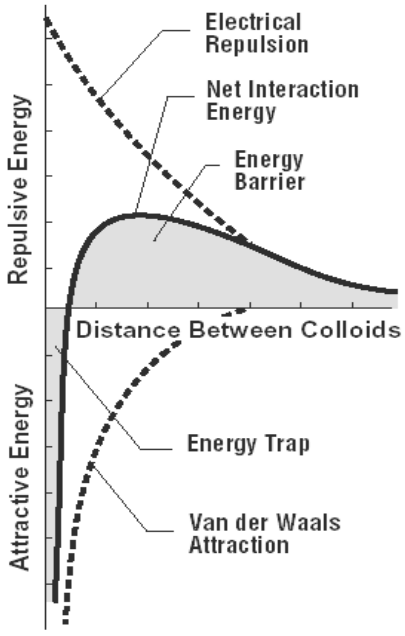

Figure 2.19. DLVO curve for a system
(Source: Zeta-Meter Inc.)

The height of the barrier indicates how stable the system is. In order to agglomerate, two particles on a collision course must have sufficient kinetic energy due to their velocity and mass, to jump over this barrier. If the barrier is cleared, then the net interaction is all attractive, and as a result the particles agglomerate.

CHAPTER 3

MATERIALS AND METHODS

3.1. Materials

The all-ceramic system selected in this study was IPS Empress 2 veneer, obtained from Ivoclar Vivadent AG, Schaan, Lichtenstein, which is a sintered glass-ceramic. The properties of this veneer is given in Table 3.1.

Table 3.1. Properties of the IPS Empress 2 Sintered Glass-Ceramic
(Source: Höland 1998)

Properties	**Parameters**
Mechanical:	
• Flexural Strength	80 ± 25 MPa
• Abrasion Behaviour	similar to that of natural teeth
Optical:	
• Translucency	similar to that of natural teeth
Thermal:	
• Coefficient of linear thermal expansion (α)	$9.7 \pm 0.5 \times 10^{-6}$ K^{-1} m/m
Chemical:	
• Solubility	< 100 μg/cm^2
Technical	
• Sintering Temperature	800°C

IPS Empress 2 ceramic powder consists of different oxides as shown in Table 3.2.

Table 3.2. Composition of the Glass-Ceramic IPS Empress 2 powder
(Source: Höland 1998)

Components	**Wt%**
SiO_2	45 – 70
Al_2O_3	5 – 22
P_2O_5	0.5 – 6.5
K_2O	3 – 9
Na_2O	4 – 13
CaO	1 – 11
F	0.1 – 2.5
Additional Components: B_2O_3, La_2O_3, Li_2O, BaO, MgO, ZnO, SrO, TiO_2, ZrO_2, CeO_2, approx. 10 wt%	

3.2. Methods

3.2.1. Preparation of Samples

Double distilled water which was passed through Barnstead Easypure UV-Compact ultrapure water system (18.3 ohm) was used to prepare electrolyte solutions, NaCl and $CaCl_2$ obtained from Sigma, at different concentrations (0.1M, 0.25M, 0.5M, 0.75M, and 1M).

Four disc-shaped specimens (d: 10 mm, h: 5 mm) of IPS Empress 2 veneering porcelain were fabricated by mixing veneer powder with distilled water and electrolyte solutions on a glass with a spatula until porcelain paste was formed. Then porcelain slurry was condensed into a plastic cylindrical mould with 10-mm internal diameter and 5-mm height. The excess of liquid was blotted from the slurry with an absorbent paper. The porcelain pastes in green body was removed from the mould and placed on a refractory tray. All specimens were fired in a programmable and calibrated porcelain furnace (Programat P90, Ivoclar-Vivadent, Schaan, Liechtenstein) with the firing cycle set for a 6-min climb to 840^{o}C at 60^{o}C/min. increments. A vacuum was turned on at 450^{o}C and samples were fired at 840^{o}C with 2-min holding time. After 2 minutes

vacuum was turned off at 839°C and samples remain in the furnace as it cools down. (IPS Empress 2 Catalogue 2004)

After sintering, specimens were cleaned by ultrasonic treatment for 10 min (Ceia CP 102 Ultrasonic Cleaner, Italy) and used for surface analyses without any surface techniques. The procedure for preparation of the samples was shown in Figure 3.1.

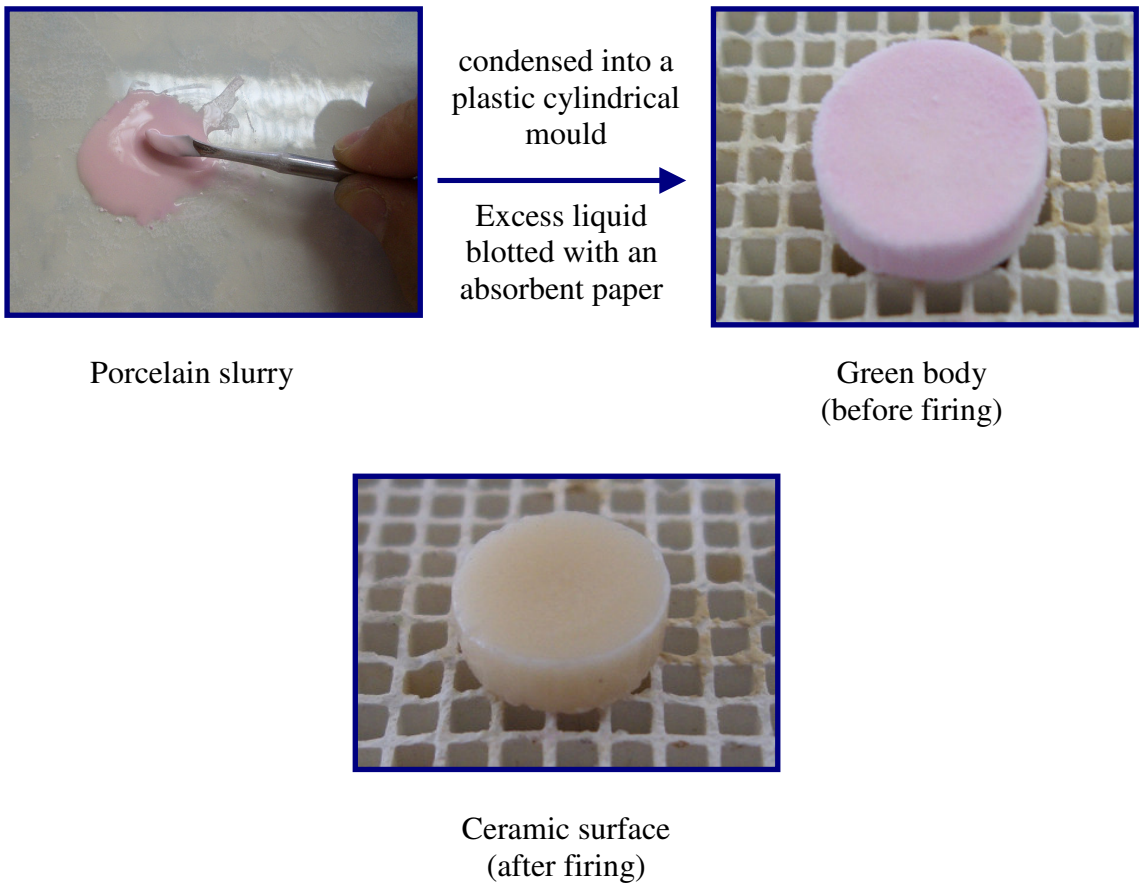

Figure 3.1. Preparation of Dental Ceramics

3.2.2. Rheology Measurements

In this study, Brookfield DV III+ rheometer was used with ULA adapter in order to understand the rheological behaviour of the particles in 60% (w/v) solutions in their natural pH. Solutions were prepared with ultra pure water which was passed through Barnstead Easypure UV- Compact ultra pure water system (18.3 ohm) and pH measurements were conducted with ORION 420A pH- meter.

Viscositites of the suspensions were measured at different speeds by using the following set conditions:

- Speed was set at minimum 10 rpm
- It was incresed to 100 rpm by 10rpm in every 10 sec
- Speed was then again decreased by 10 rpm to 10 rpm

The shear rate range was varied between $0s^{-1}$ to 140 s^{-1}. The most effective parameter in defining the shear rate range was the applied torque.

3.2.3. Zeta Potential Analysis

Zeta-potential and isoelectric point (point of zero charge) determination of the ceramic powder in distilled water and different concentrations of NaCl and $CaCl_2$ were performed using a Malvern Zetasizer Nano ZS model zeta potential apparatus. 0.1 wt% ceramic suspensions were prepared and pH was adjusted using H_2SO_4 or NaOH. After the pH stabilized, required amount of the solutions transferred to the measuring cell and about three measurements were done at each pH at room temperature.

Table 3.3. Isoelectric Points of Some Oxides in IPS Empress 2 Veneer Powder

Material	IEP	Reference
α-Al_2O_3	9.4	Johnson et al. 1999, Sverjensky 2005
Amorphous SiO_2	2.2	Sonnefeld et al. 2001, Franks 2002, Sverjensky 2005
MgO	12.4	Robinson et al. 1964, Parks 1965, Sverjensky 2005
CeO_2 (hydrous)	6.75	Mattson and Pugh 1934, Parks 1965
La_2O_3 (hydrous)	10.4	Mattson and Pugh 1934, Parks 1965
ZnO	9.0 ± 0.3	Herczynska and Prozynska 1962, Parks 1965
ZrO_2	4.0	Verwey 1941, Parks 1965
α-TiO_2	5.4	Johansen and Buchanan 1957, Machesky et al. 1998, Sverjensky 2005

3.2.4. Surface Area Analysis

Surface area analyzers measure the total exposed surface area (m^2) present in powder samples. Surface area values are usually reported as either Specific Surface Area (SSA) which is the surface area in a fixed mass of particles (m^2/g) or as Volume specific Surface Area (VSA) which is the surface area in a fixed volume of particles (m^2/cm^3). Surface area analysis requires small samples of dry powders (several grams) or particulate suspensions (several ml).

Specific surface area measurements include the total external and open, internal surface areas of the powders analyzed. This includes the surface areas of all powder particles, even those that are too coarse and too fine.

The most common automatic instruments measure SSA of powders using Nitrogen Adsorption Technique or more generally BET technique. Other measurement gases can also be used, but nitrogen is most common. Adsorption of measurement gases takes place at cryogenic temperatures, and desorption occurs as sample powders return to room temperature. The goal of the BET technique is to determine the amount of gas adsorbed when powder surfaces are covered by a monolayer of gas molecules. Each adsobed nitrogen molecule covers a known area of particle surface then the volume of adsorbed gas is measured as a function of pressure in the sample cell. By knowing the volume of a monolayer of adsobed nitrogen gas and the mass of the powder sample, SSA can be accurately and precisely measured. (Dinger 2005) The equation is ;

$$\frac{x}{V(1-x)} = \frac{1}{V_m} + \frac{(C-1)x}{V_m} \tag{3.1}$$

Where x is the relative pressure, P/P_0 , at which a gas volume V (m^3 at S.T.P.) is adsorbed, P is the pressure of the gas, and P_0 is the saturated vapor pressure at the temperature of the vessel holding the adsorbent.

V_m is the volume of gas required to form a monolayer on the adsorbent at the system temperature, and C is a constant. Therefore, a plot of [x/V(1-x)] against x should be linear, with slope [(C-1)/V_m] and intercept (C-1). Determination of these values from the plot gives two simultaneous equations, enabling the calculation of V_m. Linear plots

of [x/V(1-x)] against x are usually observed over the relative pressure range 0.05 P/P_0, although expections to this are known.

Equation 3.1 is a generalization of the Langmuir adsorption isotherm applied to multilayer adsorption. The theory based is based on the establisment of an equilibrium between gas and adsorbed material involving the dynamic transfer of molecules betwwen the gas phase and the surface.

The B.E.T. method yields a value for the volume of a monolayer of adsorbed gas on the solid surface. The surface area of one molecule of adsorbed gas (adsorbate) may be calculated from its density and molecular weight. Using this datun the total surface area of the solid may be calculated (McKay 1996).

The B.E.T. and Langmuir surface area, and pore size of IPS Empress 2 veneer powder were determined by Micromeritics Gemini 2380 model surface area analyzer. The sample was degassed at 200 ± 1 °C in a vacuum and then the adsorption measurements of nitrogen were carried out at 77 ± 1 K. In this method, the average pore diameter of the composite adsorbents can be calculated from the surface area and the pore volume by assuming cylindrical pores.

3.2.5. X-Ray Diffraction (XRD)

X- ray diffraction is a versatile analytical technique to identify crystalline solids which include ceramics, metals, electronic materials, geological materials, organics, and polymers. These materials may be powders, single crystals, multilayer thin films, sheets, fibers, or irregular shapes, depending on the desired measurement. XRD can be used both qualitatively and quantitatively. When a precise percentage of a standard powder is added to the sample powder to be analyzed, phases can be quantitatively determined (Loehman 1993, Dinger 2005).

X-Ray diffractometers fall broadly into two classes: single-crystal and powder. Single-crystal diffractometers are most often used to determine the molecular structure of new materials. Powder diffractometers are routinely used to identify mineralogical compositions and crystal structures. Since this technique only identifies crystalline structures, it cannot be used to analyze amorphous materials and to identify elemental compositions. Each crystalline material has a unique XRD pattern which corresponds to the crytal structure, but also correspond to the precise compositions and number of

atoms and ions and their sizes that sit on each site in the crystal structure. The theoretical basis of X-Ray diffraction stands on Bragg's equation given by;

$$n\lambda = 2d\sin\theta \tag{3.2}$$

Where n is the order of reflection n =(1, 2, 3, ……), λ, the wavelength, d the distance between parallel lattice planes, and θ the angle the incident beam and a lattice plane, known as the Bragg angle.

Powders are dispersed randomly onto a sample holder, inserted into position in the diffractometer. Incident, collimated, monochromatic X-radiation from a source arrives at precise angles to the surface plane of the powder samples. This incident radiation then diffracts off of lon-range ordered, crystalline arrays of atoms in the particle structures. X-rays diffract off all atoms, but only the planes that are paralel to the sample holder will be directed at the precise angle to enter the detector.

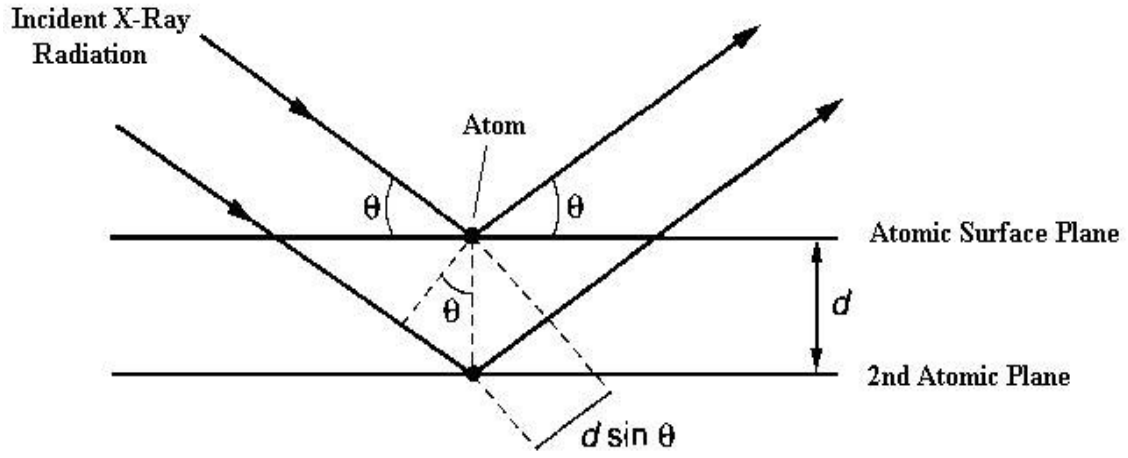

Figure 3.2. Illustration of Bragg's Law
(Source: Dinger 2005)

The radiation used in a typical diffraction measurement contains several wavelengths, denoted $K_{\alpha 1}$, $K_{\alpha 2}$, K_{β}, which are characteristic of the material producing the X rays (Settle 1997). Common anode materials and their specific wavelengths are shown in Table 3.4.

Table 3.4. X-ray Wavelengths (in Å) for Common Anode Materials
(Source: Settle 1997)

Anode	$K_{\alpha 1}$	$K_{\alpha 2}$	K_{β}
Chromium(Cr)	2.28970	2.29361	2.08487
Cobalt (Cu)	1.78897	1.79285	1.62079
Copper (Cu)	1.54056	1.54439	1.39222
Molybdenum (Mo)	0.70930	0.71359	0.63229

X-ray powder diffraction (XRD) data were collected on a Philipps X'Pert Pro diffractometer using Cu $K_{\alpha 1}$ radiation (λ=0.154056nm) in 5-70 θ values. Diffractograms for IPS Empress 2 veneer powders were collected before and after firing process.

3.2.6. Profilometry

Profilometry is used to study the topography of a material surface. Surface roughness is a critical parameter in various fields of materials science (Seitavuopio et al. 2005). The basic principle of all instruments for physical profile measurement is based on a sensitive detection stylus that scans the substrate surface. The stylus consists of a fine tip that is fixed to a lever. (Sinzinger and Jahns 2003). Profilometry is accurate, quantitative, flexible method and it can be used to study areas with diameters up to several centimeters. (Seitavuopio et al. 2005). All profilometers measure the physical depth of surface irregularities using some form of diamond or brush-type stylus attached to an arm that travels in a straight line for a specified cutoff or sampling length, typically 0.08 cm. Most profilometers allow for various cutoff lengths. The profilometer transforms the information from the stylus into an electrical signal and converts that signal into usable data.

Profilometry can be divided into two groups as stylus and optical. The stylus profilometer (SP), a powerful microscopic technique, has been developed to study the surface roughness of materials (Williamson 1967, Guenther et al. 1984, Wiesendanger 1994). The stylus in the SP is used to scan surface, sense the variations of the sample. The stylus in the profilometer is carried by a cantilever beam and it rides on the sample

surface. This means that a rough surface can be plastically deformed. (Davis and Stout 1982)**.** It is a technique in which a diamond stylus brought into contact with a sample and scanned over the surface. The surface profile causes an up-and-down movement of the lever which is detected (Sinzinger and Jahns 2003).

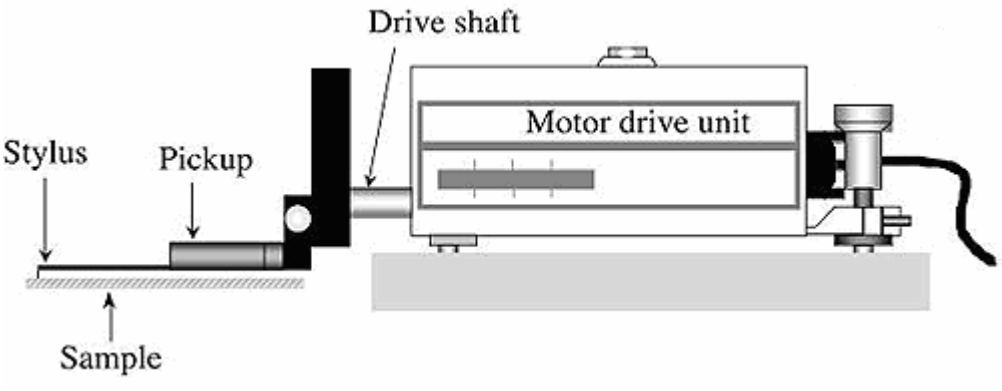

Figure 3.3. Schematic Configuration of a Profilometer and Its Units
(Source: Johnson 2000)

One well-established method for surface roughness measurement is non-contact laser profilometry or optical profilometry. (Podczek 1998, Riippi et al. 1998, Salako et al. 1998, Ruotsalainen et al. 2002, Seitavuopio et al. 2003). The advantages of profilometry using a laser are the absence of contact, higher measurement speed, higher lateral resolution and greater depth range. Profilometry using a diamond stylus produces far better depth resolution. Laser profilometry has also been used in many different fields of material research like paper coating, dental materials and surgical prothesis. (Wagberg et al. 1993, Cho et al. 2002, Chauvy et al. 1998).

Roughness is commonly calculated using one of four methods: Ra (roughness average), RMS (root mean square), Rz (a 10 point average), and Rt or Rmax (maximum between peak and valley). Surface roughness is calculated by a profilometer using any of four common methods: Ra, RMS, Rz, and Rt (Rmax).

a) Ra or roughness average is the average of peak and valley distances measured along the centerline of one cutoff length (usually 0.08 cm).

b) RMS or root mean square is an older method, not common today, averaging only the heights of all points measured in one cutoff length. Readings are similar to Ra but about 10% higher.

c) Rz, a 10-point average, is an average of the five highest peaks and the five lowest valleys measured in one cutoff length.

d) Rt (Rmax), maximum height between peak and valley, is the value of the vertical distance between the highest peak and lowest valley measured along one cutoff length.

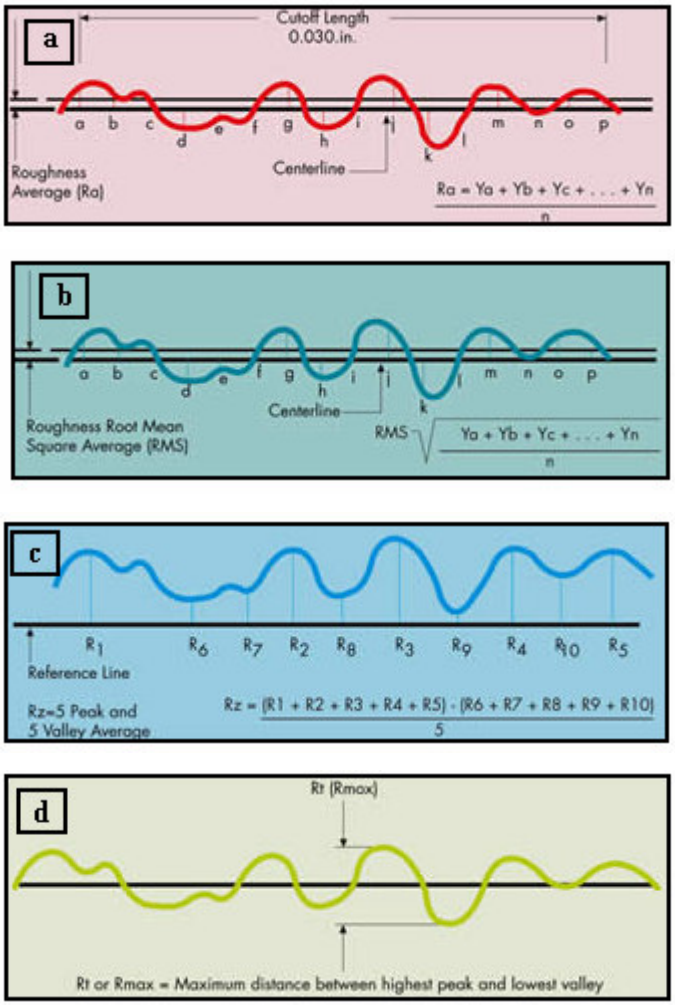

Figure 3.4. Four Ways to Calculate Roughness

(Source: WEB_2 2007)

In the study surface roughness of the dental porcelain discs was measured with a stylus profilometer (Mitutoyo Surftest SJ-201P, Japan) which scans surface roughness between 0.01 – 100 µm with 2µm-diameter diamond stylus and 0.01µm resolution. The roughness of the surfaces, R_a, was determined with 0.8 mm sampling length and three sampling scans. For each porcelain disc at least ten measurements were done.

3.2.7. Atomic Force Microscopy (AFM)

The potential of physical profilometers is limited mainly by the size and shape of the sensor tip. If very step trenches are to be characterized, the tip cannot reach deep enough to measure the exact depth (Sinzinger and Jahns 2003).

Throughout the last decades a number of more sophisticated techniques have been developed to measure surface roughness. One of these techniques is force microscopy which is based on the measurement of forces between a sharp tip, which serves as a force sensor, and a sample surface (Meyer and Bennewitz 2004, Sinzinger and Jahns 2003). AFM is a system wherein the STM is used to measure the motion of a cantilever beam with an ultrasmall mass. AFM is a new tool used to investigate both conductors and insulators on an atomic scale (Binnig et al., 1986)

In the AFM, the sample is scanned by a tip, which is mounted to a cantilever spring. While scanning, the force between the tip and the sample is measured by monitoring the deflection of the cantilever. The AFM sample is connected to a three-dimensional piezoelectric drive, i.e., the x,y,z scanner. A feedback loop is used to keep the force acting on the stylus at a constant level. A topographic image of the sample is obtained by plotting the deflection of the cantilever versus its position on the sample (Binnig et al. 1986 and Butt et al. 2005). The AFM generates a real-space topographic image of a surface by feeling rather than looking at the specimens and small samples can be used due to its high lateral and high vertical resolution (Morris et al. 1999).

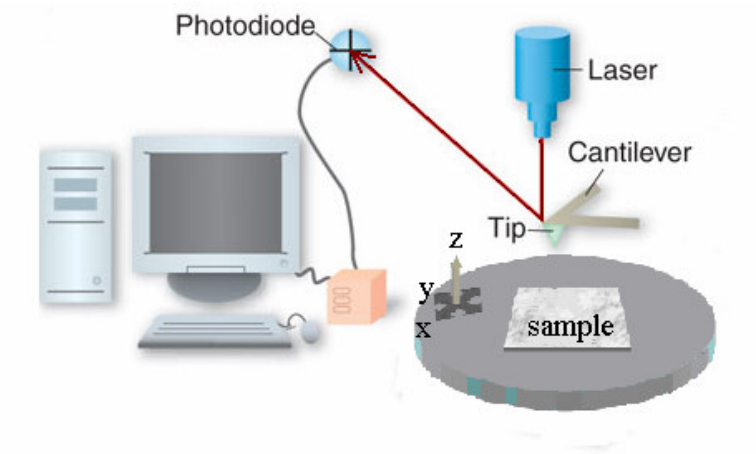

Figure 3.5. Schematic Illustration of AFM

(Source: WEB_3 2007)

AFM images are obtained by measurement of the force on a sharp tip (insulating or not) created by the proximity to the surface of the sample. This force is kept small and at a constant level using a feedback mechanism. When the tip is moved sideways it will follow the surface contours such as the trace in the Figure 3.5 (Bai 2000, Binnig et al. 2005).

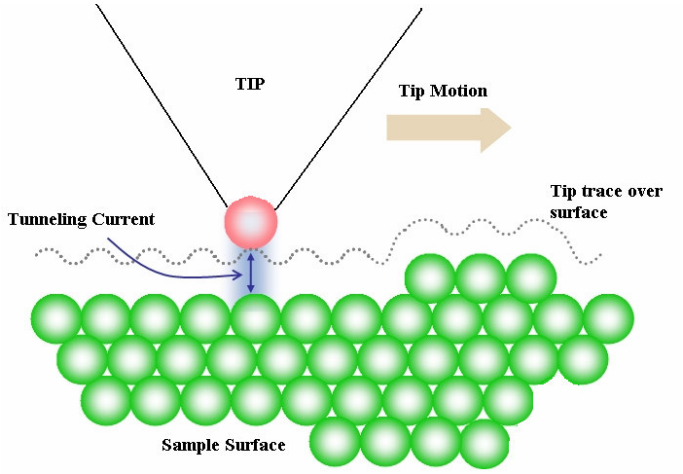

Figure 3.6. Description of the Principle Operation of an STM and AFM (Source: WEB_4 2007)

The cantilever in the AFM is a key element and its mechanical properties are responsible for the performance. For a given force maximum deflection is needed and this requires a cantilever that is as soft as possible (Binnig et al. 1986). Commercial cantilevers are typically made of silicon or silicon nitride (Butt et al. 2005).

Atomic force microscopes have the ability to operate on a scale from microns down to nanometers and can image clusters of atoms and molecules. AFM can be operated in air, different gases, vacuum, or liquid. Different environmental cells, in which the kind of gas and the temperature can be adjusted, are commercially available. AFM is used for studies of non-conductors and more commonly used for studies of macromolecules and biological specimen. The operation of the AFM in a liquid environments is facilitated by using a liquid cell. Imaging in liquid can be advantageous for biological samples (Ricci and Braga 2004, Butt et al. 2005). Some application areas are given in Table 3.5.

Table 3.5. Application Areas of AFM

(Source: WEB_5 2006)

Physical Science	Biological Structures	High Technology	Industrial
Polymers Phase transitions Surface texture Nanoparticles Carbon nanotubes	Cells Biomolecules • DNA • Proteins • Living cells	Semiconductor Data storage • DVD • CD-R/W Advanced Optics • Cameras • LCD display	Health Care Paper Automotive Cosmetic Aerospace

AFM is a device measure any type of force; not only the interatomic forces, but electromagnetic forces as well (Binnig et al. 1986). Depending on whether the cantilever is sensing repulsive or attractive forces, different imaging modes can be applied (Morris et al. 1999). The three main classes of interaction are contact mode, tapping mode and non-contact mode.

Contact mode is the most common method of operation of AFM. The tip scans sample remain in close contact as the scanning proceeds. Contact AFM provides 3D images nondestructively, operates in air and fluid environments, analyzes insulators and conductors easily, provides information about physical properties such as elasticity, adhesion, hardness, etc. Contact mode is most useful for hard surfaces because it can damage fragile surfaces.

Tapping mode or intermittent-contact mode is the next most common mode used in AFM. When operated in air or other gases, the cantilever is oscillated and positioned above the surface so that it only taps the surface for a very small fraction. This is stil contact with the sample but the very short time means that lateral forces are reduced as the tip scans over the surface. Tapping mode is better choice than contact mode for imaging of soft samples because of its less damaging.

Non-contact mode is amother method for imaging by AFM. The cantilever must be oscillated above the surface of the sample at such a distance that is not in the repulsive region of the intermolecular force curve and tip does not touch to the sample

(Ricci and Braga 2004). This is a very difficult mode to operate in ambient conditions because thin water layer exists on the sample surface will form a small capillary bridge between tip and the sample and cause the tip to jump to contact mode. Even under liquids and in vacuum, jump to contact is extremely likely so imaging is most probably occuring using tapping mode.

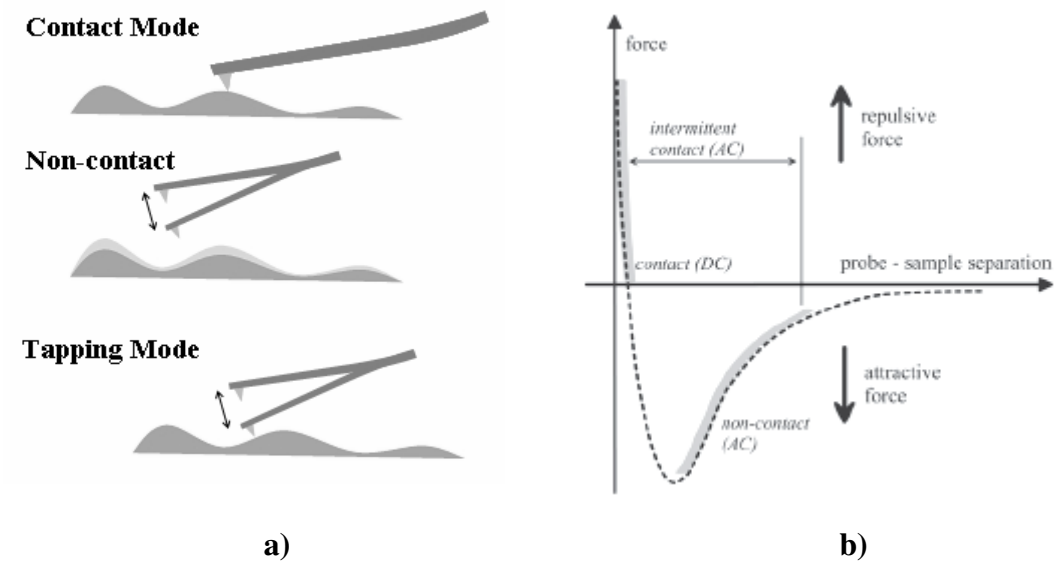

Figure 3.7. a) Illustration of modes used in AFM b) Idealized Plot of the Forces Between Tip and Sample, Highlights where imaging modes are operative (Source: WEB_4 2007 and Ricci and Braga 2004)

Table 3.6. Comparison of Surface Roughness Measurement Methods
(Source: Loehman 1993)

	Stylus Profilometer	**Optical Profilometer**	**Atomic Force Microscopy**
Dimension	2D	3D	3D
Maximum Vertical Range	150 microns	15 microns	50 microns
Vertical (Depth) Resolution	0.5 nm	0.1 nm	0.01 nm
Lateral Resolution	0.1 – 25 μm depending on stylus radius	0.35 – 9 μm depending on optical system	Atomic to 1 nm
Method	Contact Stylus	Non-contact Optical	Tapping, Contact and non-contact
Field of View	50 microns – 1cm	Microns to 1 cm	Atoms to >250 microns
Speed of Data Acquisition	Fast/Slow	Fast	Slow

In the study Digital Instruments – MMSPM Nanoscope IV Scanning Probe Microscobe was used to determine the surface roughness. For each porcelain sample five measurements were done in contact mode with 20μ x 20μ scanning area in air medium.

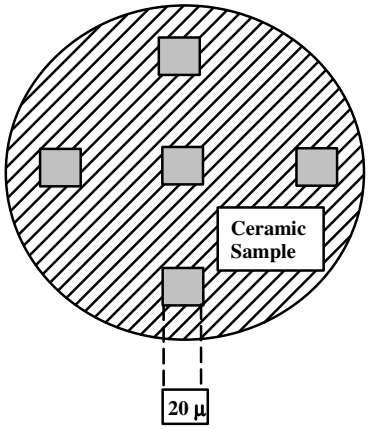

Figure 3.8. Measurement of surface roughness of ceramic pastes in AFM

3.2.8. Scanning Electron Microscopy (SEM)

The scanning electron microscope (SEM) is often used when a quick look at a material is required to study surfaces, structures, morphologies and forms of materials. In the SEM an electron beam is focused into a fine probe and subsequently raster scanned over a small rectangular area. As the beam interacts with the sample it creates various signals (secondary electrons, internal currents, photon emission, etc.). These signals are highly localized to the area directly under the beam. By using these signals to modulate the brightness of a cathode ray tube, an image s formed on the screen. This image is highly magnified and usually has the look of a traditional microscope image but with a much greater depth of field. SEM analyses are conducted in vacuum environments (Loehman 1993, Dinger 2005).

SEM characterization was carried out using a Philips XL-30S FEG type instrument in vacuum environment. Prior to analysis the powder and ceramic samples were attached onto adhesive C tapes supported on metallic disks but they were not coated with Au.

SEM was used in order to obtain a large and accurate view of the porcelain discs. The SEM pictures were also used as a reference for the profilometer measurements. For each porcelain disc specimen prepared at different electrolyte concentrations SEM pictures were collected at ten different places on the samples at 2500x magnification.

3.2.9. Energy-Dispersive X-Ray Spectroscopy (EDS)

EDS is sometimes referred to also as EDX or EDAX analysis. It is a non-destructive technique used for identifying the elemental composition of the specimen. This technique is used in conjunction with SEM with ancillary detectors such as lithium-drifted silicon, Si (Li) (Loehman 1993).

During EDX Analysis, the specimen is bombarded with an electron beam inside the scanning electron microscope. The bombarding electrons collide with the specimen atoms' own electrons, knocking some of them off in the process. A position vacated by an ejected inner shell electron is eventually occupied by a higher-energy electron from an outer shell. To be able to do so, however, the transferring outer electron must give up

some of its energy by emitting an X-ray. The amount of energy released by the transferring electron depends on which shell it is transferring from, as well as which shell it is transferring to. Furthermore, the atom of every element releases X-rays with unique amounts of energy during the transferring process. Thus, by measuring the amounts of energy present in the X-rays being released by a specimen during electron beam bombardment, the identity of the atom from which the X-ray was emitted can be established.

The output of an EDX analysis is an EDX spectrum. It is just a plot of how frequently an X-ray is received for each energy level. An EDX spectrum normally displays peaks corresponding to the energy levels for which the most X-rays had been received. Each of these peaks are unique to an atom, and therefore corresponds to a single element. The higher a peak in a spectrum, the more concentrated the element is in the specimen. The number of counts in each peak may be further converted into elemental weight concentration or oxide concentration.

An EDX spectrum plot not only identifies the element corresponding to each of its peaks, but the type of X-ray to which it corresponds as well. For example, a peak corresponding to the amount of energy possessed by X-rays emitted by an electron in the L-shell going down to the K-shell is identified as a K-Alpha peak. The peak corresponding to X-rays emitted by M-shell electrons going to the K-shell is identified as a K-Beta peak.

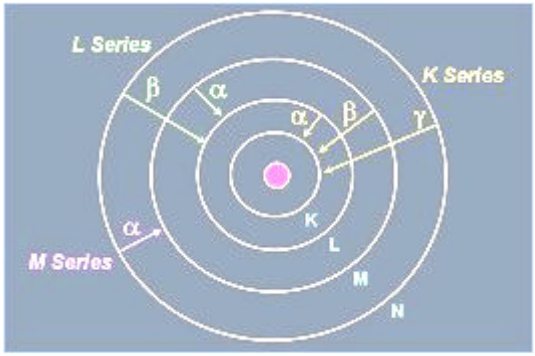

Figure 3.9. Elements in an EDX spectrum are identified based on the energy content of the X-rays emitted by their electrons as these electrons transfer from a higher-energy shell to a lower-energy one (Source: WEB_6 2007).

In the study, EDX analyses were performed for both veneer powder and porcelain discs and oxide composition was determined at five random points on the sample for each specimen.

3.2.9. Contact Angle

The contact angle is often defined as the angle between the liquid – vapour and solid – liquid interfaces of a solid – liquid – vapour system. The contact angle of a liquid is given by Young's equation. (Hiemenz and Rajagopalan, 1997)

$$\gamma_{LV} \cos\theta = \gamma_{SV} - \gamma_{SL} \tag{3.3}$$

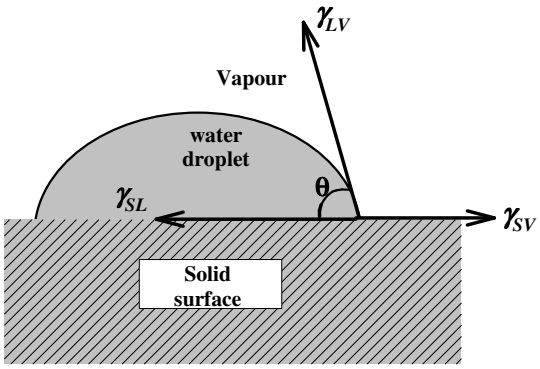

Figure 3.10. Contact angle measurement by Sessile drop method
(Source: Aksoy et al. 2006)

Contact angle is the angle at the three-point contact at a solid–liquid–gas interface and gives a measure of the wettability of the solid by the liquid. A smaller contact angle means a more wettable, hydrophilic ceramic surface. Though it is an intrinsic thermodynamical property of the solid, mechanical factors such as roughness directly influence the angle at the three-point contact. In this study, contact angles were measured in ceramic/air/water system with a goniometer/microscope setup (Krüss GmbH, Germany model G10) using a modified sessile drop method suggested by Polat and Chander (Polat and Chander 1999). The ceramic surface was divided into a 4×4 grid for contact angle measurement and a micro-droplet of double-distilled water (~5µl)

was generated with a micrometer syringe and placed on a specific potion of the grid using a micro-positioning device and a micrometer-driven micropipette. The angle which developed at the three point air/water/ceramic interface was measured using a microscope–goniometer system for the droplet. The process was repeated for each grid point to obtain at least 16 measurements for each sample. This yielded 64 readings for each surface treatment procedure (4 samples times 16 readings per sample). Similar to the AFM Figure 3.8. A schematic view of modified micro-contact angle measurements using sessile drops. γ_{pw}, γ_{pa} and γ_{wa} are respective ceramic–water, ceramic–air and water–air interfacial tensions. The upper figure is drawn for illustration purposes and is not to the scale.

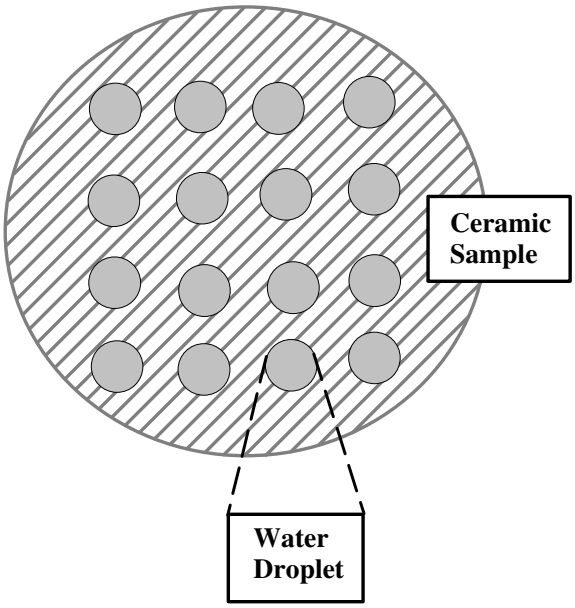

Figure 3.11. Measurement of Contact Angle of Ceramic Surfaces

CHAPTER 4

RESULTS AND DISCUSSION

4.1. Characterization of Material

4.1.1. Surface Area Analysis

Surface area is an important parameter for the processing of ceramic bodies. Chemical additives in ceramic suspensions and bodies interact with particle surfaces and affect interparticle repulsive and attractive forces in the interparticle fluid environment by changing the properties of the available powder surfaces. During processing, particles behave and interact according to the properties of their available surfaces. Therefore surface area measurements of Empress 2 was done and the results are presented in Table 4.1.

Table 4.1. Surface area of IPS Empress 2 veneer powder

Powder	BET Surface Area (m^2/g)	Langmuir Surface Area (m^2/g)	Pore Volume (cm^3/g)	Average Pore Size (Å)
IPS Empress 2 veneer	0.3326	1.2586	0.000237	28.5212

4.1.2. Particle Size Analysis

Particle size is important in dental applications to obtain smooth surfaces. Dental ceramic powders are desired to have different particle sizes (broad distributions) in order to provide better sintering to have smooth surfaces. SEM picture of IPS Empress 2 veneer shows that the particles have different sizes.

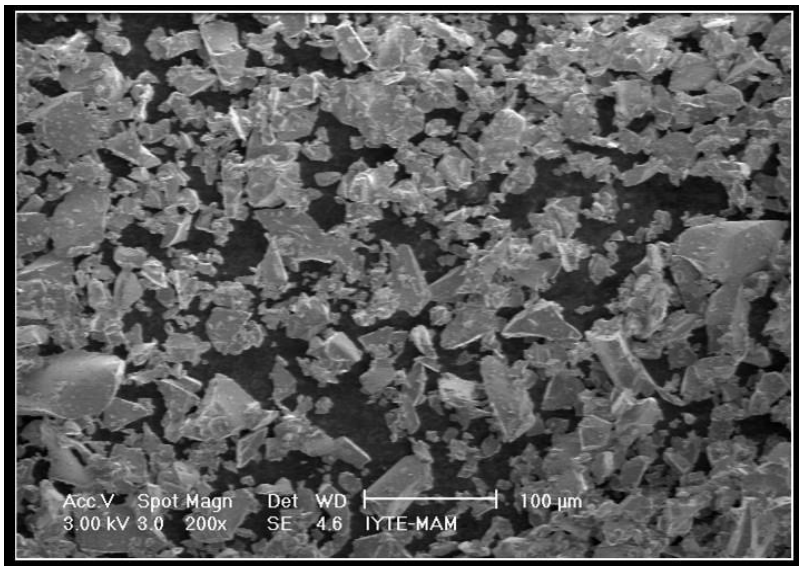

Figure 4.1. SEM Picture of IPS Empress 2 veneer powder (100x)

Particle size measurements were obtained as a function of pH (except PZC) without using any dispersent and the results were presented as size distribution plots from Figure 4.2 to Figure 4.12. As it is seen size of particles change as a function of pH. This is expected since the surface charge of particles change as a function of pH and therefore particles attract each other differently.

The average particle sizes were also given in Figure 4.14. The particle size at natural pH (6.86) was 1602 nm and changed between 500 nm and 2600 nm as a function of pH.

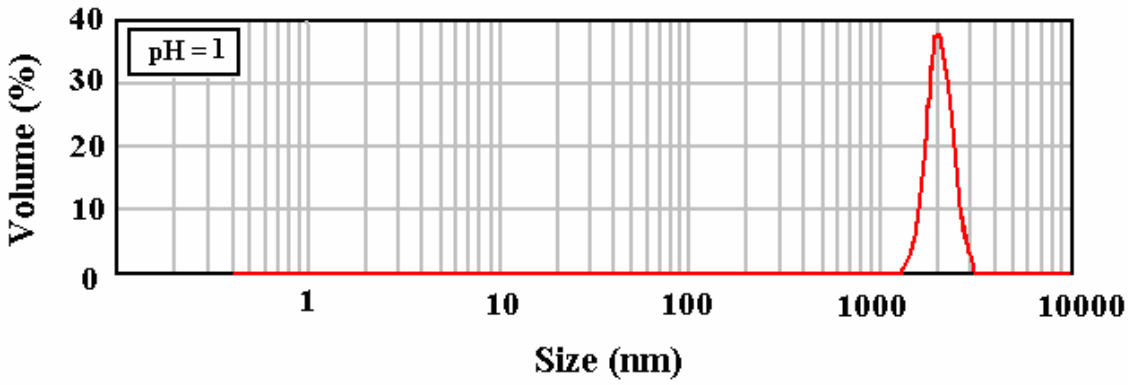

Figure 4.2. Particle size distribution of IPS Empress 2 veneer powder at pH 1 (2010 nm)

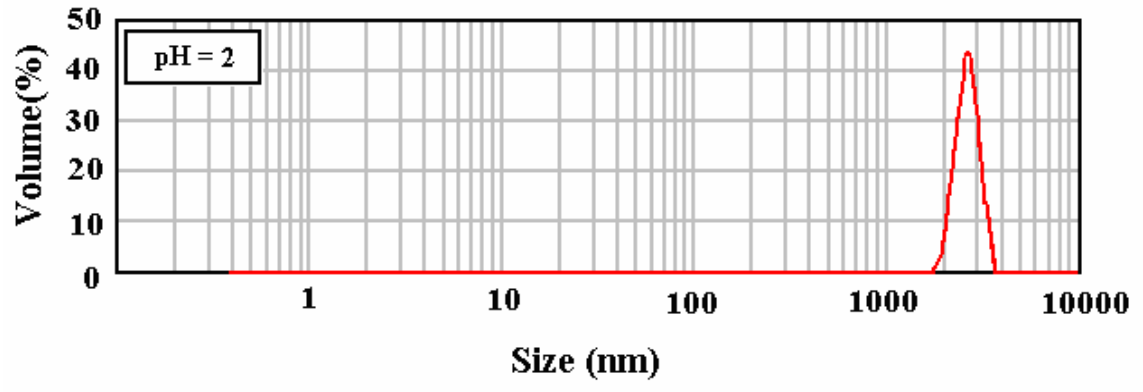

Figure 4.3. Particle size distribution of IPS Empress 2 veneer powder at pH 2 (2600 nm)

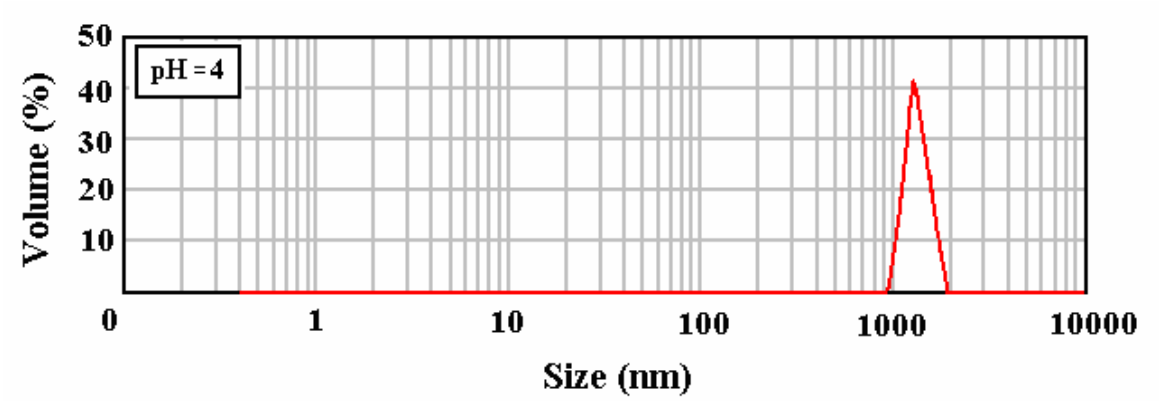

Figure 4.4. Particle size distribution of IPS Empress 2 veneer powder at pH 4 (1340 nm)

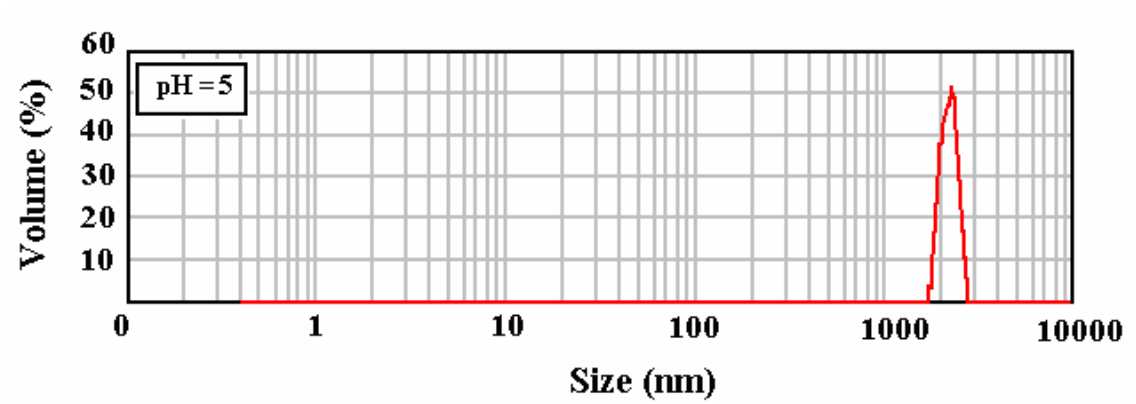

Figure 4.5. Particle size distribuiton of IPS Empress 2 veneer powder at pH 5 (2200 nm)

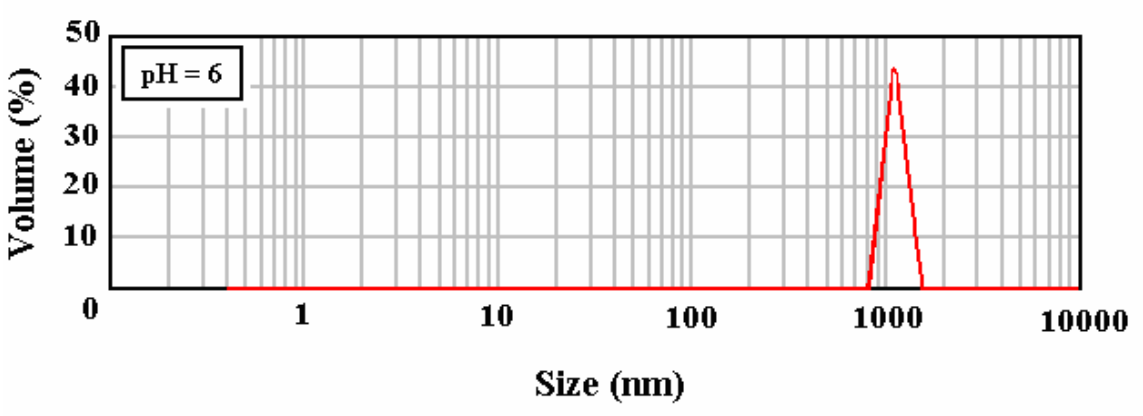

Figure 4.6. Particle size distribution of IPS Empress 2 veneer powder at pH 6 (1140 nm)

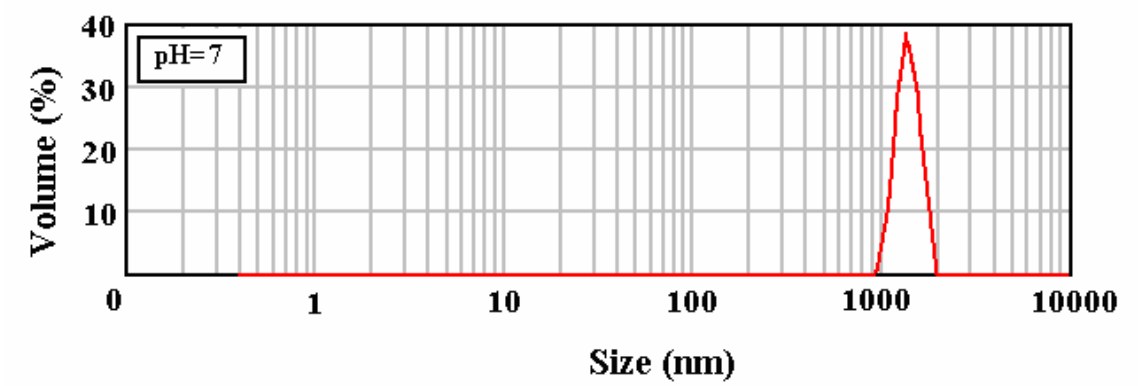

Figure 4.7. Particle size distribution of IPS Empress 2 veneer powder at pH 7 (1520 nm)

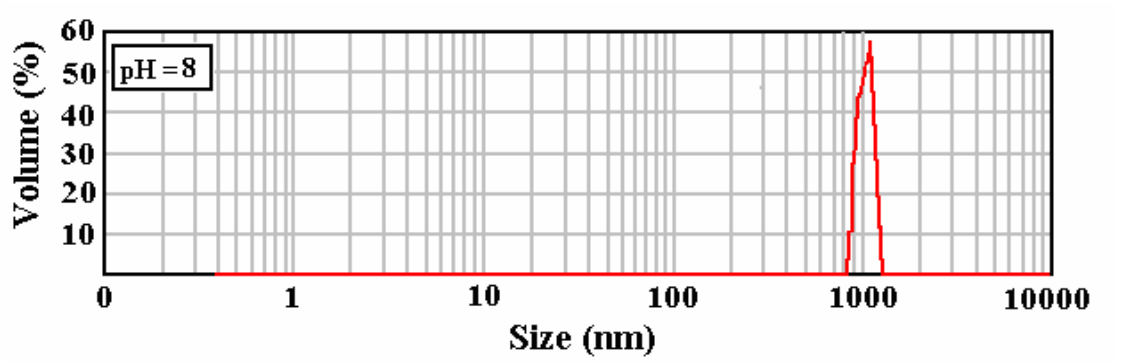

Figure 4.8. Particle size distribution of IPS Empress 2 veneer powder at pH 8 (1260 nm)

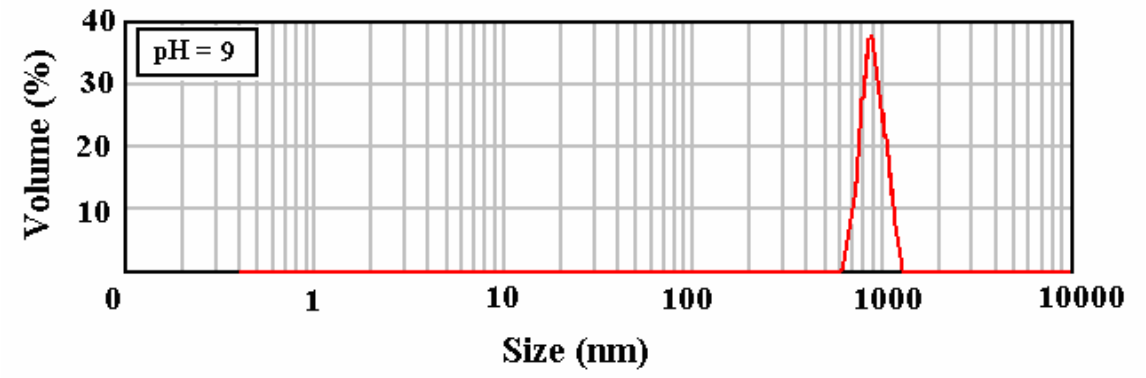

Figure 4.9. Particle size distribution of IPS Empress 2 veneer powder at pH 9 (920 nm)

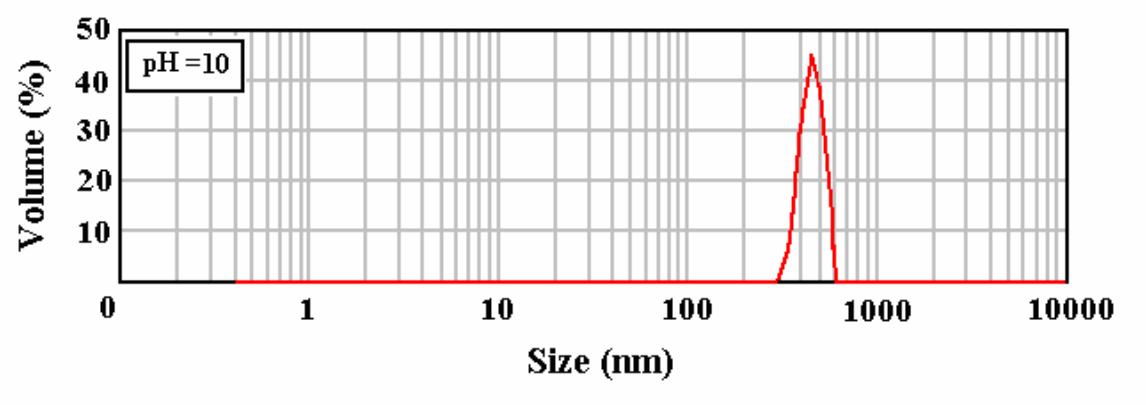

Figure 4.10. Particle size distribution of IPS Empress 2 veneer powder at pH 10 (350 nm)

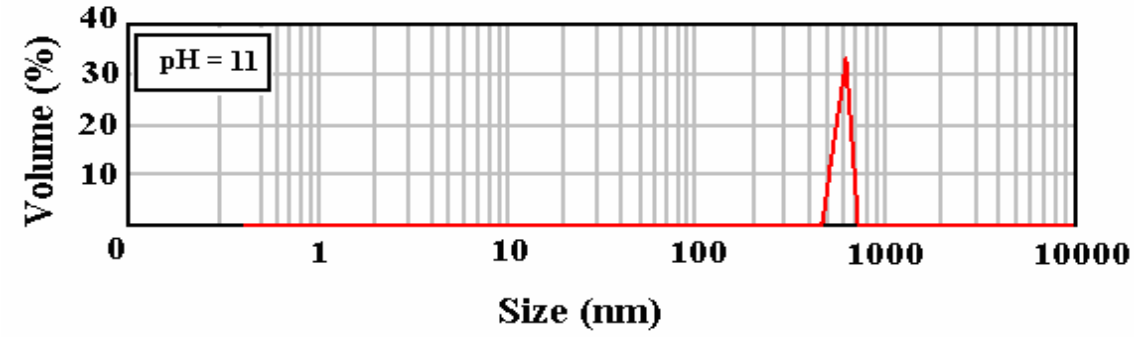

Figure 4.11. Particle size distribuion of IPS Empress 2 veneer powder at pH 11 (602 nm)

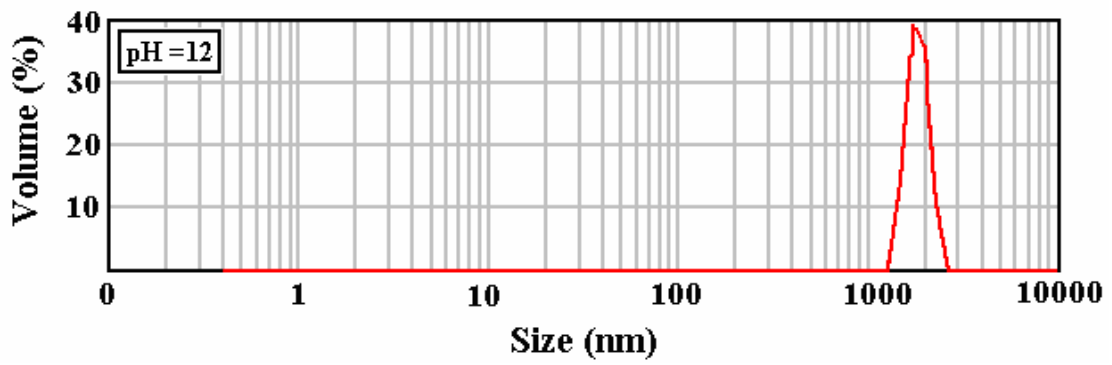

Figure 4.12. Particle size distribution of IPS Empress 2 veneer powder at pH 12 (985 nm)

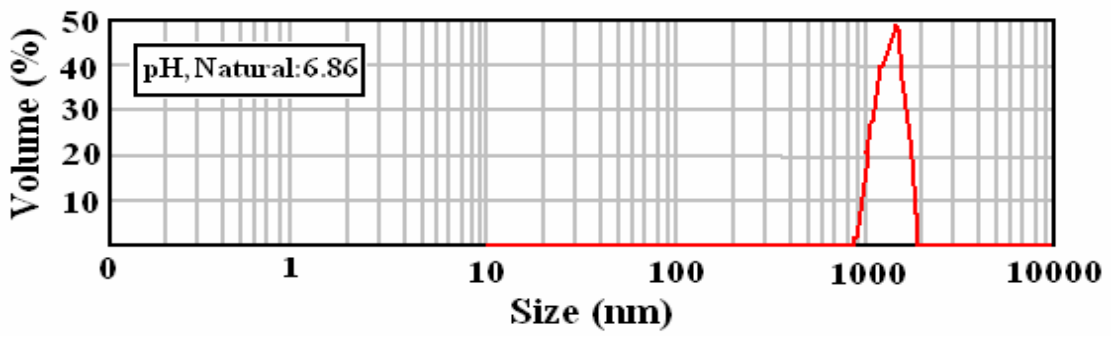

Figure 4.13. Particles size distribution of IPS Empress 2 veneer powder at natural pH 6.86 (1602 nm)

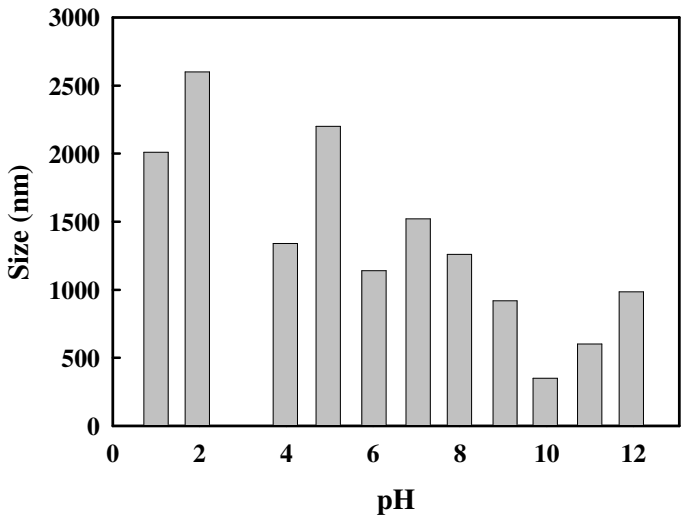

Figure 4.14. Particle size of IPS Empress 2 veneer powder as a function of pH

4.1.3. Surface Charge Analysis

Zeta potential measurements as a function of pH was conducted and the results are presented in Figure 4.15. It gives the mean zeta potential values for three measurements as a function of pH and shows the isoelectric point value.. As it is seen from the mean values, surface of Empress 2 particles carry positive charge before pH 3.0 and negative charge after pH 3.0. That is the pH where surface of sample particles have no charge.

The isoelectric point observed at pH 3 can be because of silica particles that veneer includes as dominant ingredient (~ 70%). Indeed the iep value of pure silica is known as 2.0. its shifting from 2 to 3 might be due to presence of alumina particles, which has iep at pH 9, that Empress 2 includes as second dominant ingredient . Also the sample has some oxides that have high pzc values. These are CaO (iep 7), MgO (iep 12.4), ZnO (iep 9-10) and La_2O_3 (iep 10).

The zeta potential distribution curves were also given in Figure 4.16 through Figure 4.28.

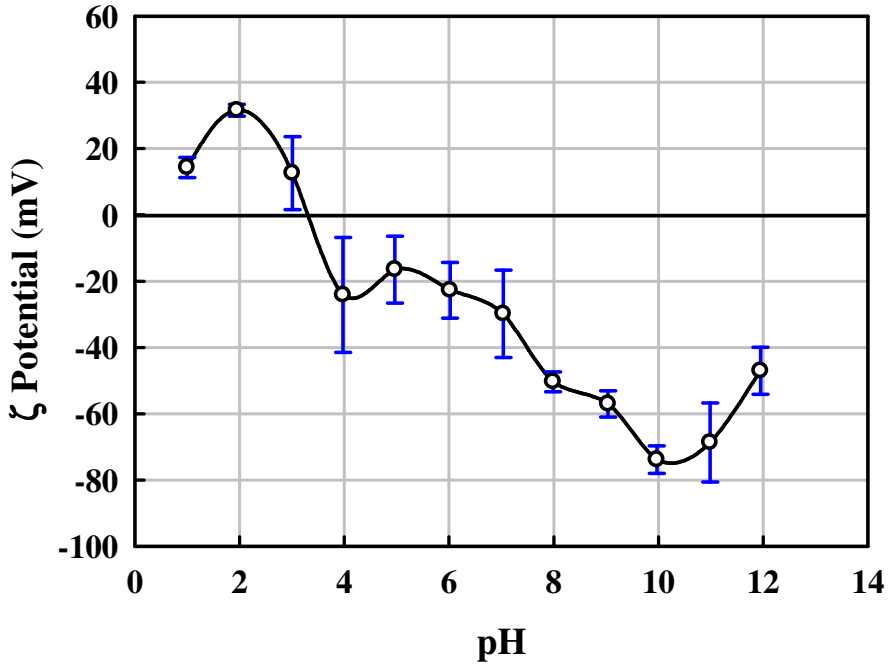

Figure 4.15. Zeta potential graph of IPS Empress 2 veneer powder

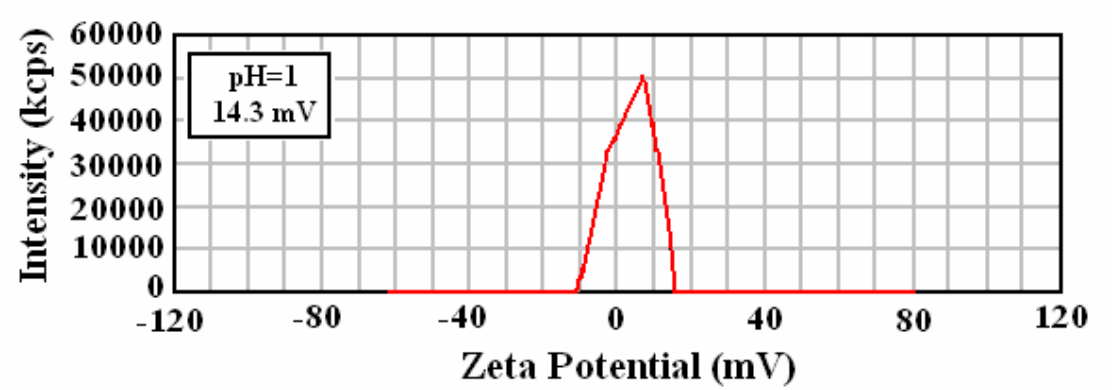

Figure 4.16. Zeta potential distribution curve of IPS Empress 2 veneer at pH 1

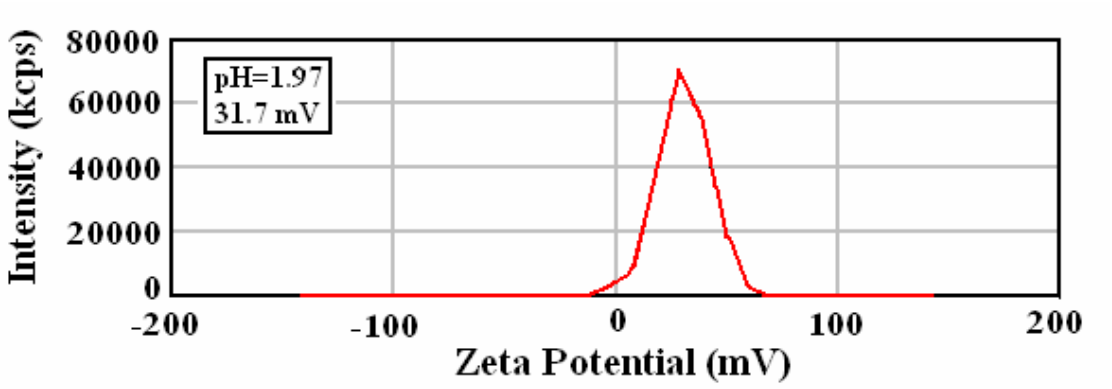

Figure 4.17. Zeta potential distribution curve of IPS Empress 2 veneer at pH 2

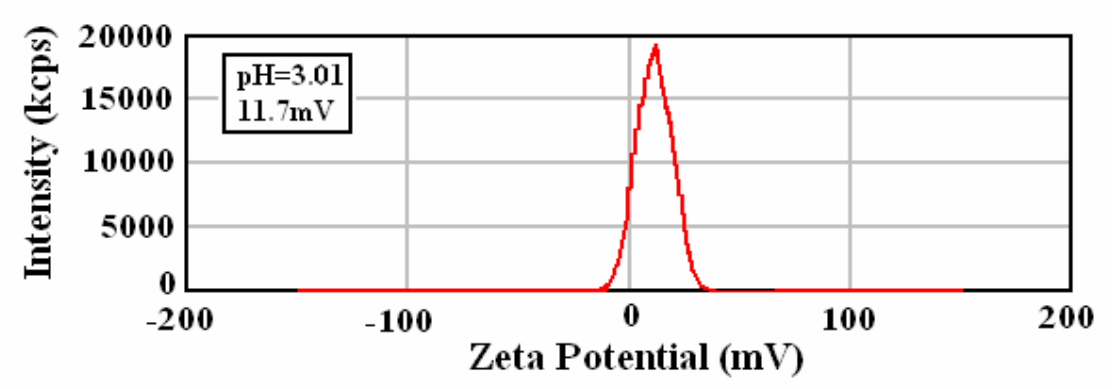

Figure 4.18. Zeta potential distribution curve of IPS Empress 2 veneer at pH 3

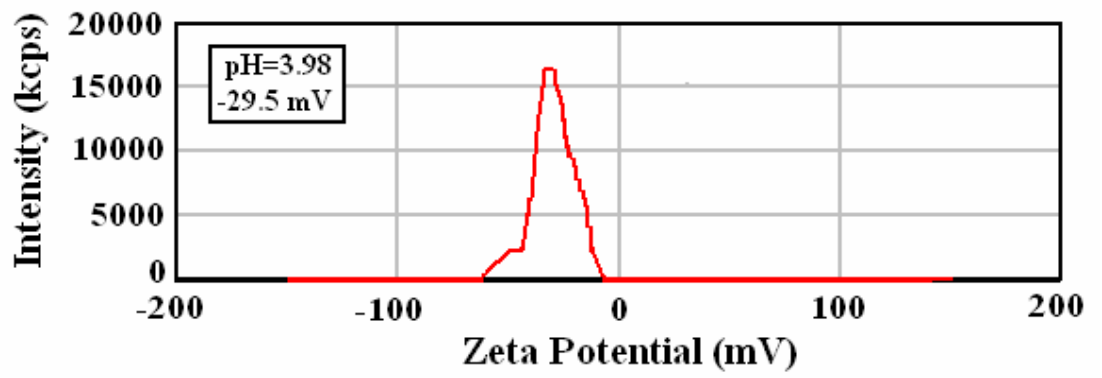

Figure 4.19. Zeta potential distribution curve of IPS Empress 2 veneer at pH 4

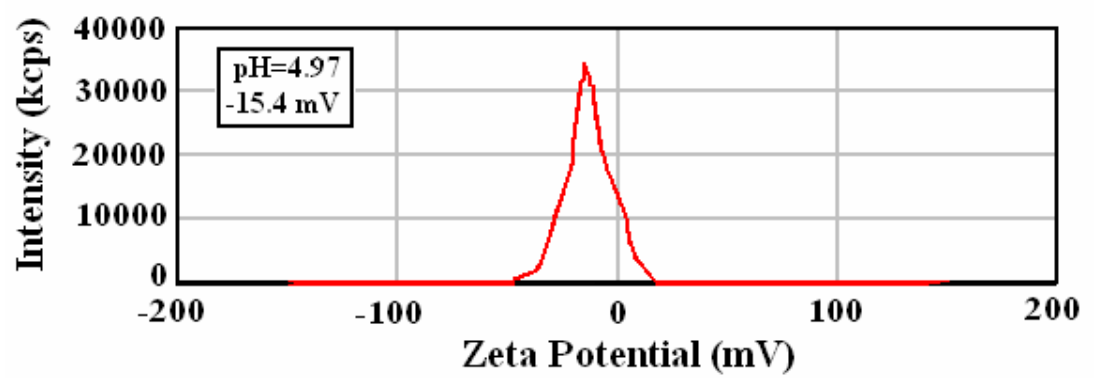

Figure 4.20. Zeta potential distribution curve of IPS Empress 2 veneer at pH 5

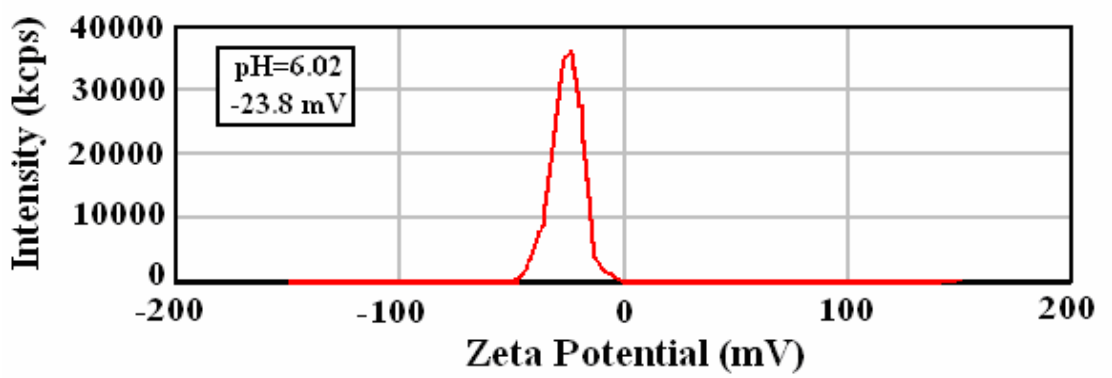

Figure 4.21. Zeta potential distribution curve of IPS Empress 2 veneer at pH 6

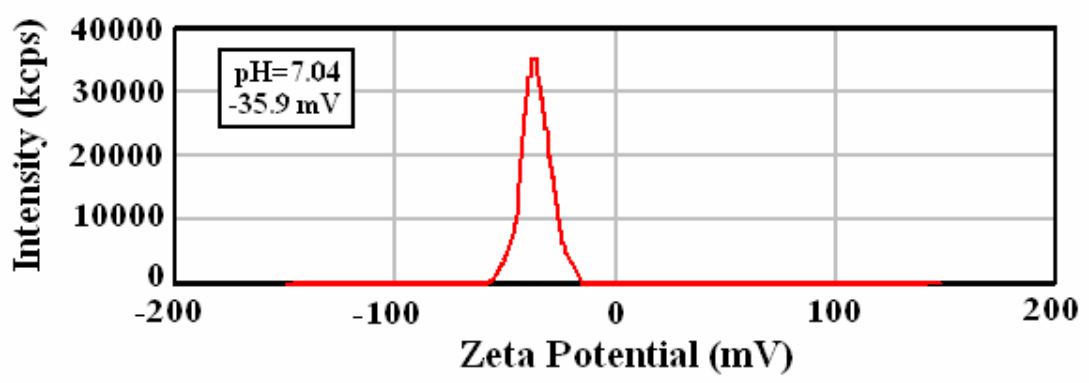

Figure 4.22. Zeta potential distribution curve of IPS Empress 2 veneer at pH 7

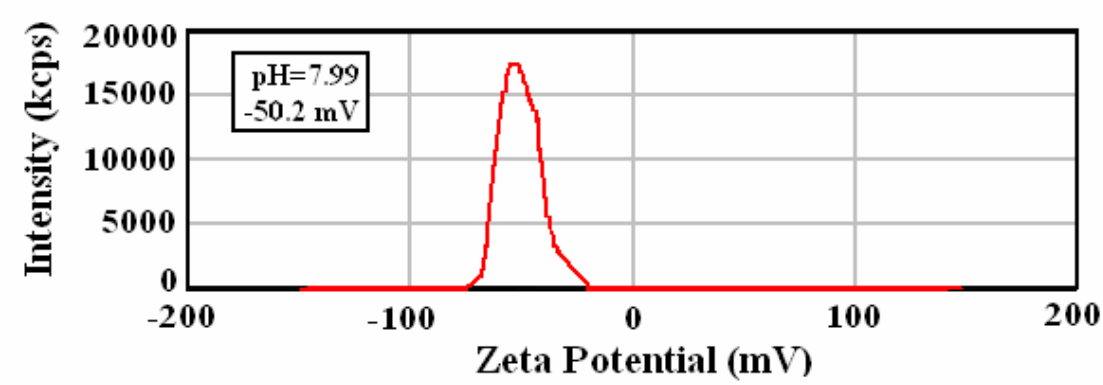

Figure 4.23. Zeta potential distribution curve of IPS Empress 2 veneer at pH 8

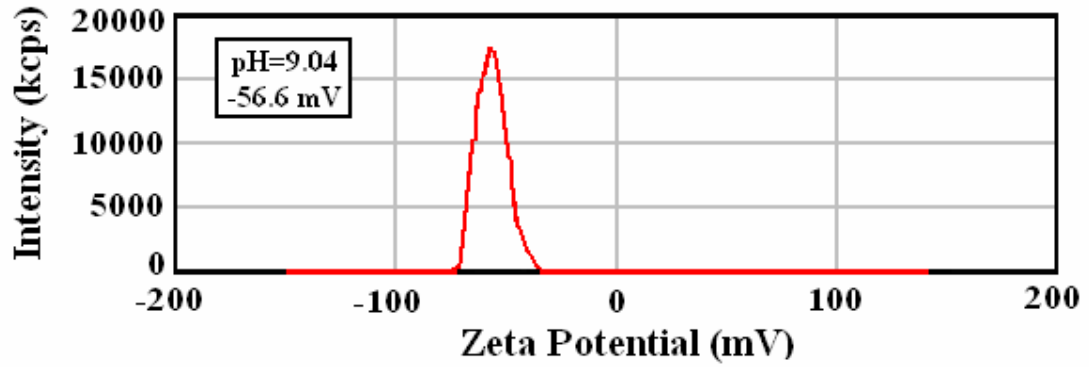

Figure 4.24. Zeta potential distribution curve of IPS Empress 2 veneer at pH 9

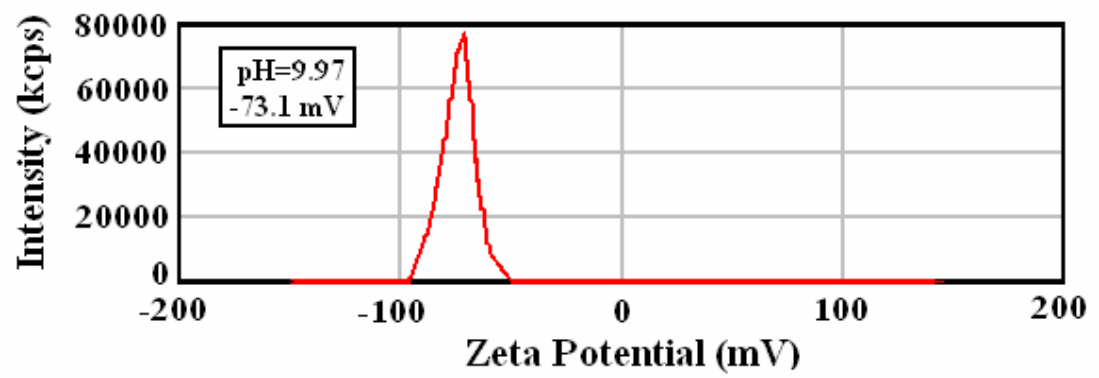

Figure 4.25. Zeta potential distribution curve of IPS Empress 2 veneer at pH 10

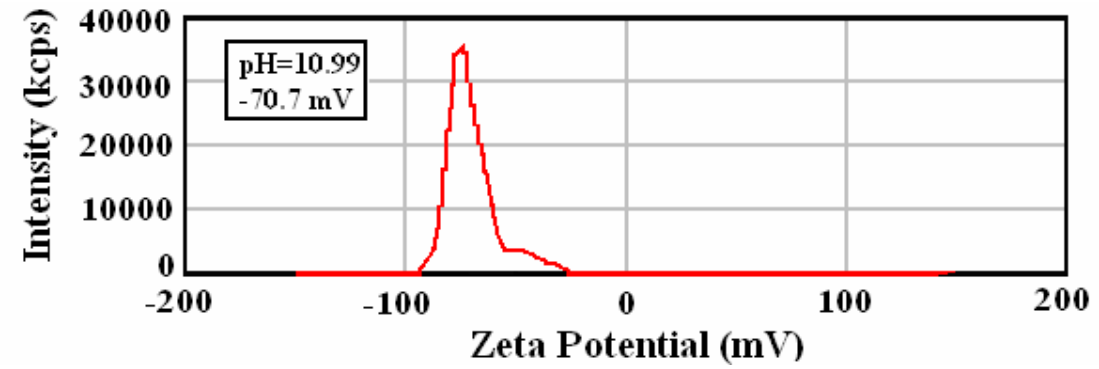

Figure 4.26. Zeta potential distribution curve of IPS Empress 2 veneer at pH 11

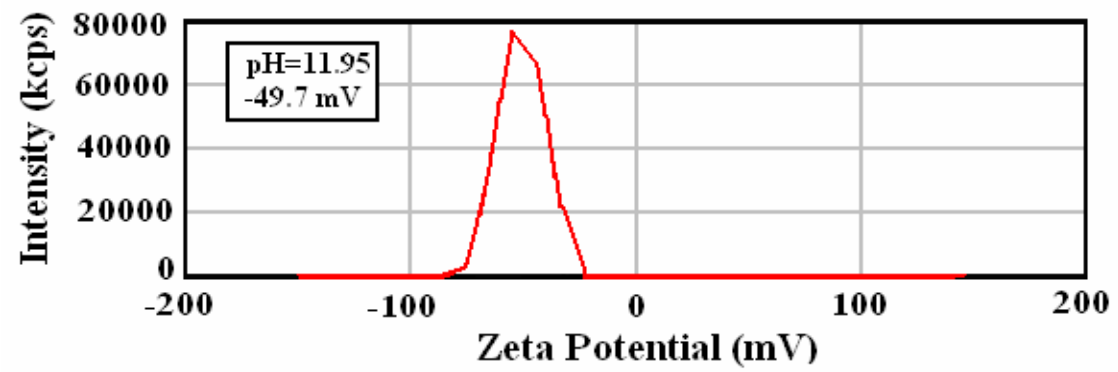

Figure 4.27. Zeta potential distribution curve of IPS Empress 2 veneer at pH 12

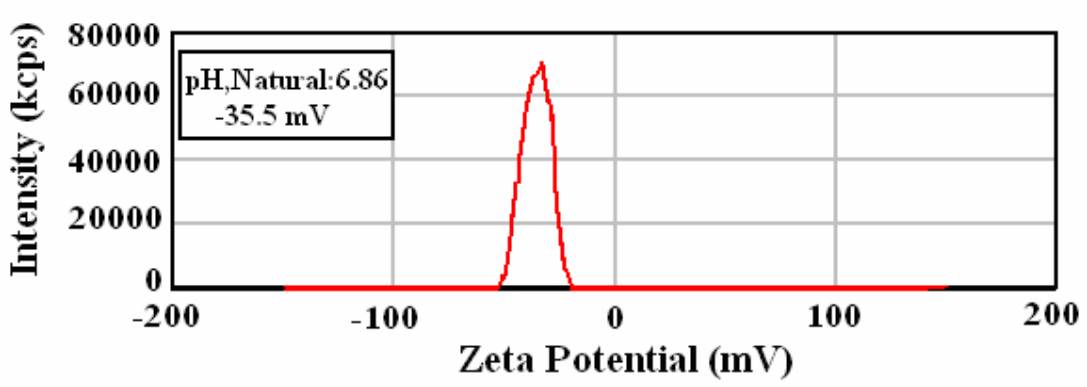

Figure 4.28. Zeta Potential distribution curve of IPs Empress 2 veneer powder at natural pH 6.86

In addition, the zeta potentials of particles were also determined in electrolyte solutions to observe the effect of electrolytes The system is mostly composed of silica particles and silica carries negative surface charge over the entire studied pH. This creates favorable electrostatic conditions for cation adsorption, while the ability of silica to adsorb anions is limited (Kosmulski 2006). As it is seen from the figures that the presence of NaCl makes surface less negatively charged. That is, it decreases the magnitute of surface charge but do not effect the sign of charge. This is expected since Na^+ , Ca^{++} and Cl^- ions are indifferent ions for this system. Indifferent ions effect the magnitute of charge but do not change the sign. As it is seen here it does not make surface positive. The presence of $CaCl_2$,however, affects both the magnitute and sign of the charge. It makes surface positive while it was negative. That is Ca^{++} ions behave like potential determining ions (PDI) similar to the H^+ ions for this surface. That is Ca^{++} ions may adsorb at the surface. Dinger 2005 says that multivalent cations such as Mg^{++} and Ca^{++} are frequently used as flocculants. Positively charged ions are attracted to negatively charged sites and as they adsorb onto the particles, they reduce negative zeta potentials towards zero. This situation can be seen in the zeta potential distribution graphs for NaCl from Figure 4.29 to Figure 4.33 and for $CaCl_2$ from Figure 4.34 to Figure 4.38.

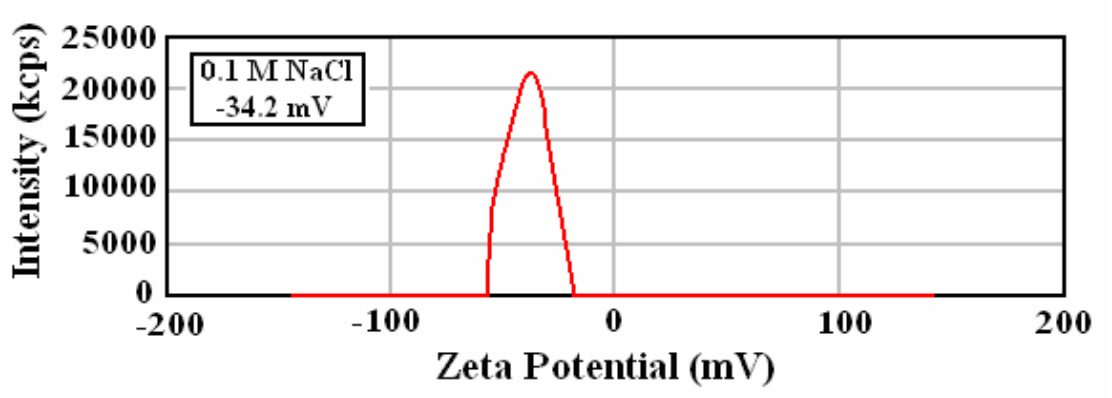

Figure 4.29. Zeta Potential distribution graph of IPS Empress 2 veneer powder in 0.1M NaCl

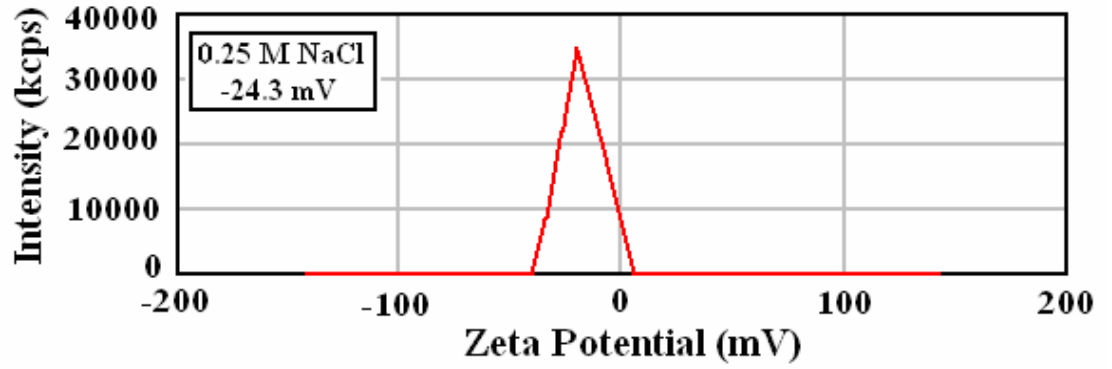

Figure 4.30. Zeta Potential distribution graph of IPS Empress 2 veneer powder in 0.25M NaCl

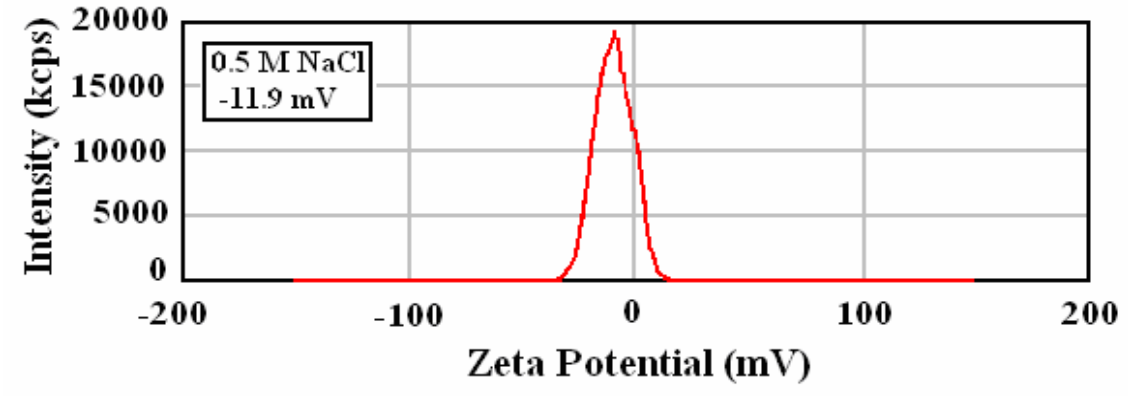

Figure 4.31. Zeta Potential distribution graph of IPS Empress 2 veneer powder in 0.5M NaCl

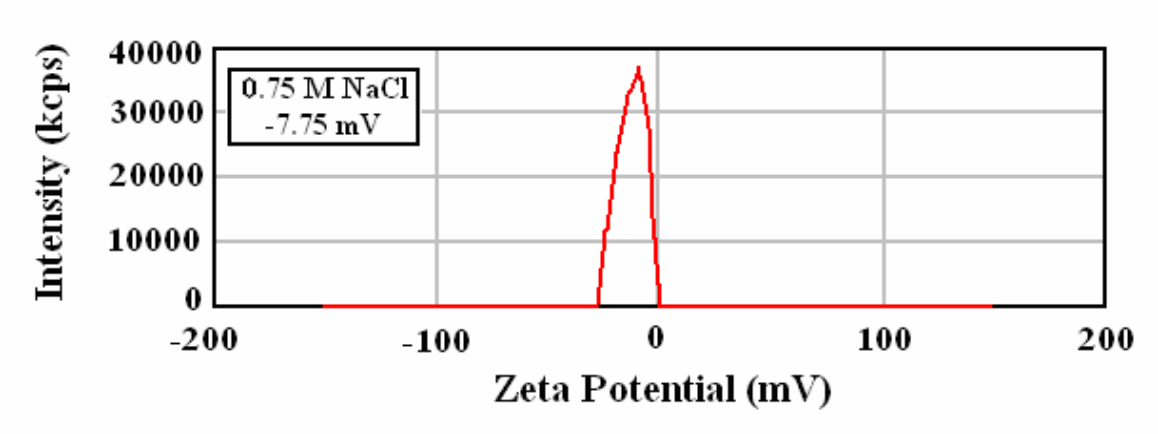

Figure 4.32. Zeta Potential distribution graph of IPS Empress 2 veneer powder in 0.75M NaCl

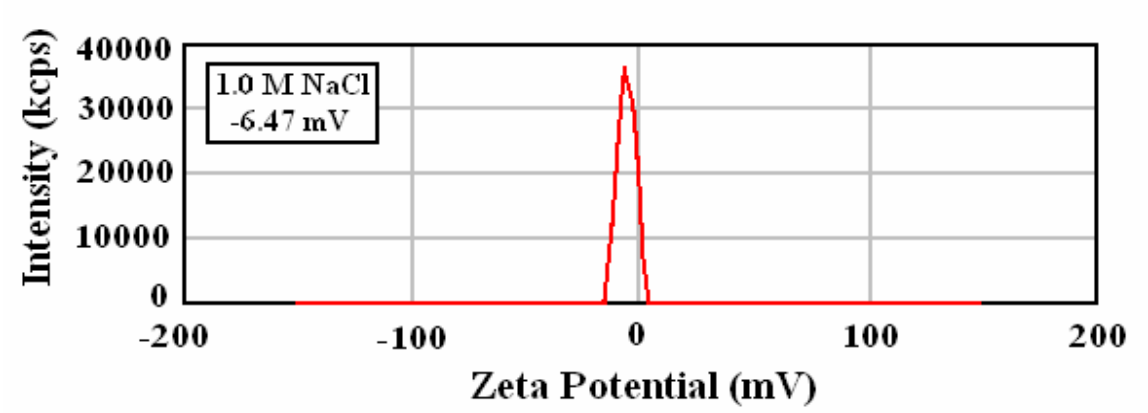

Figure 4.33. Zeta Potential distribution graph of IPS Empress 2 veneer powder in 1M NaCl

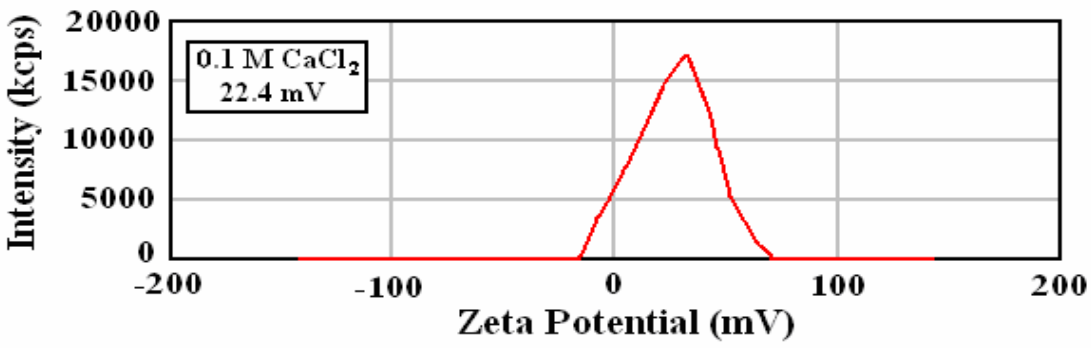

Figure 4.34. Zeta Potential distribution graph of IPS Empress 2 veneer powder in 0.1M $CaCl_2$

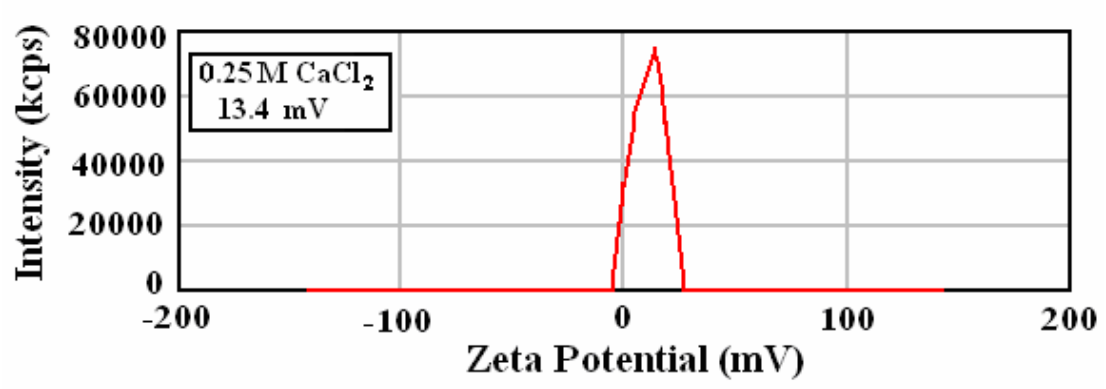

Figure 4.35. Zeta Potential distribution graph of IPS Empress 2 veneer powder in 0.25M $CaCl_2$

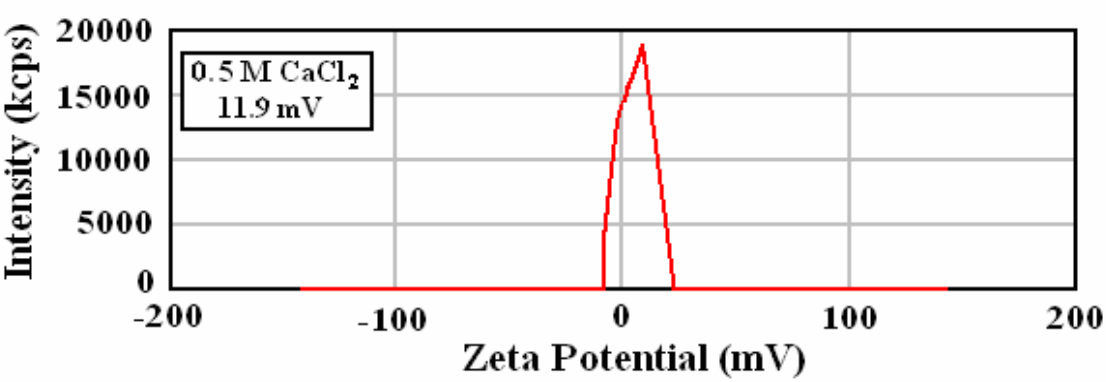

Figure 4.36. Zeta Potential distribution graph of IPS Empress 2 veneer powder in 0.5M $CaCl_2$

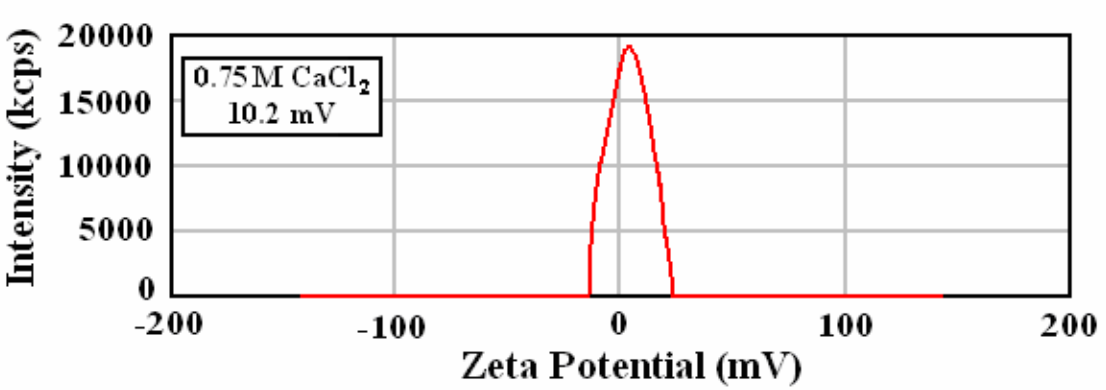

Figure 4.37. Zeta Potential distribution graph of IPS Empress 2 veneer powder in 0.75M $CaCl_2$

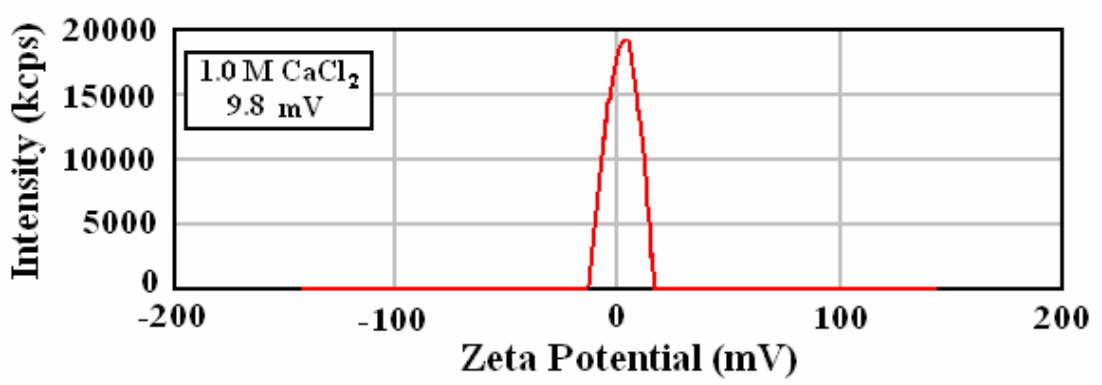

Figure 4.38. Zeta Potential distribution graph of IPS Empress 2 veneer powder in 1M $CaCl_2$

As an overall Figure 4.39 shows that both electrolyte decreases the potential of the surface as thier concentrations are increased.

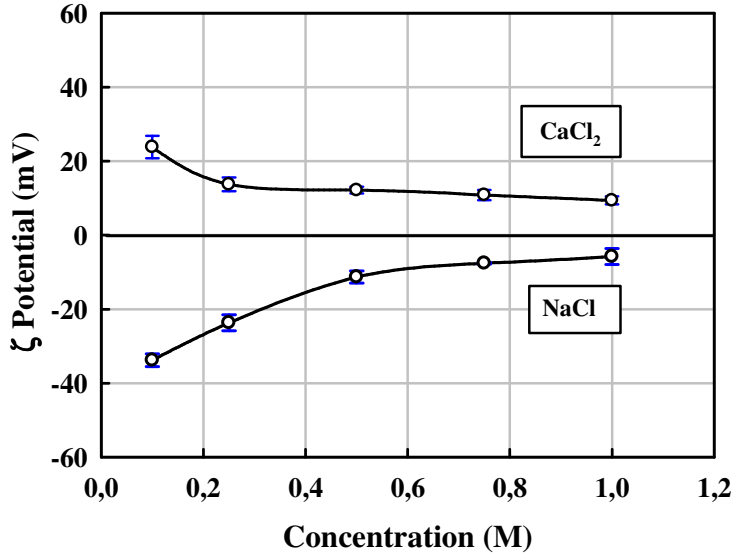

Figure 4.39. Zeta Potential graph of IPS Empress 2 veneer powder in different electrolyte concentrations

4.1.4. X-Ray Diffraction (XRD) Analyses

XRD is generally used to determine the composition and crystallization of materials. In the study XRD was used to observe whether crystallization takes place

after firing process. As shown in the Figure 4.40 there is no change in the structure of the powder after firing. This means that there is no crystallization during firing process.

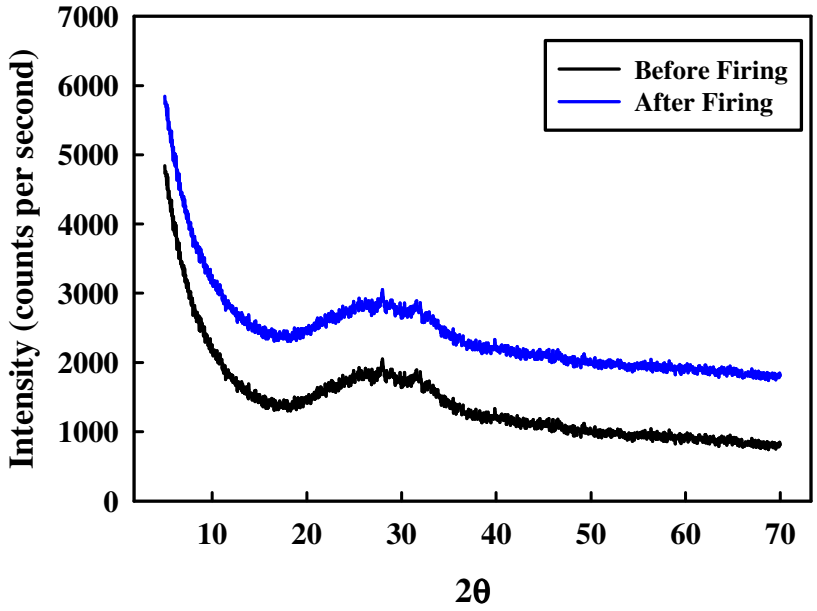

Figure 4.40. X-Ray Diffractogram for IPS Empress 2 veneer powder before and after firing

4.2. Particle-Particle Interactions: Potential Energy Curves

Particles of IPS Empress 2 veneer powder carry electrostatic charge as a function of pH. In this study the working pH was 10.01 and at this pH the charge of particle surface was -73.1 mV. As mentioned before, in response to the charging of a colloidal particle in liquid, an ionic environment spontaneously develops around it on the liquid side. These two charged regions (one on the particle and the other on the solution side) are called the Electrical Double Layer, EDL. That is an electrical double layer develops through solution side around particles. Accumulation of charge in solution side of the EDL requires a finite thickness because of an interplay between electrostatic interactions and the thermal disturbance. Therefore, while the charges on the particle are confined to the surface, charges on the solution side show a diffuse character. The change of potential in this layer is plotted assuming the zeta potential as the surface potential and using the general solution of the Poisson –Boltzmann equation suggested by electrical double layer model of Gouy-Chapman as shown in Equation 2.3.

Potential profiles and potential energy curves were drawn with Mathcad 2001 Professional software.

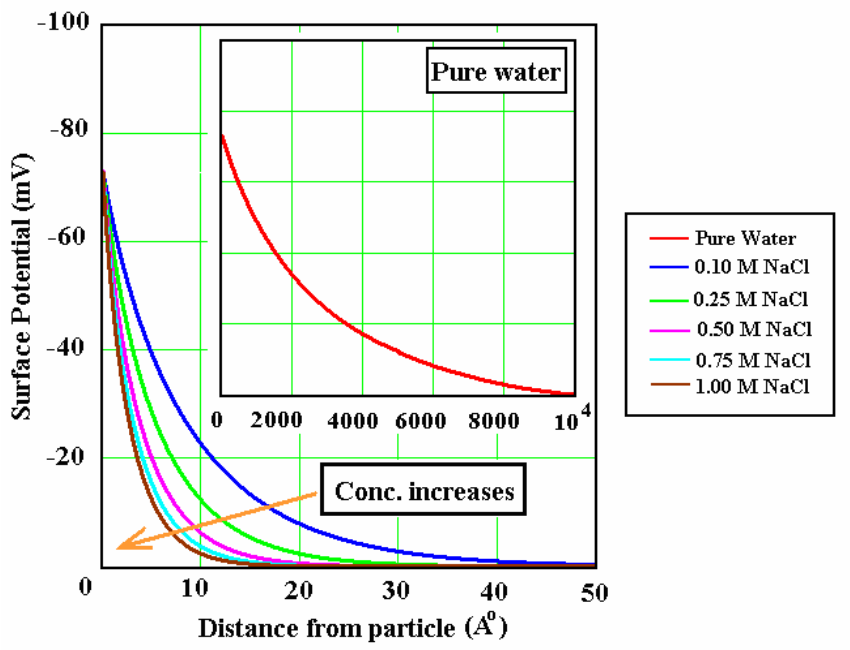

Figure 4.41. Potential profile of IPS Empress 2 veneer powder in pure water and NaCl solutions at different concentrations (Ψ_0= -73.1 mV)

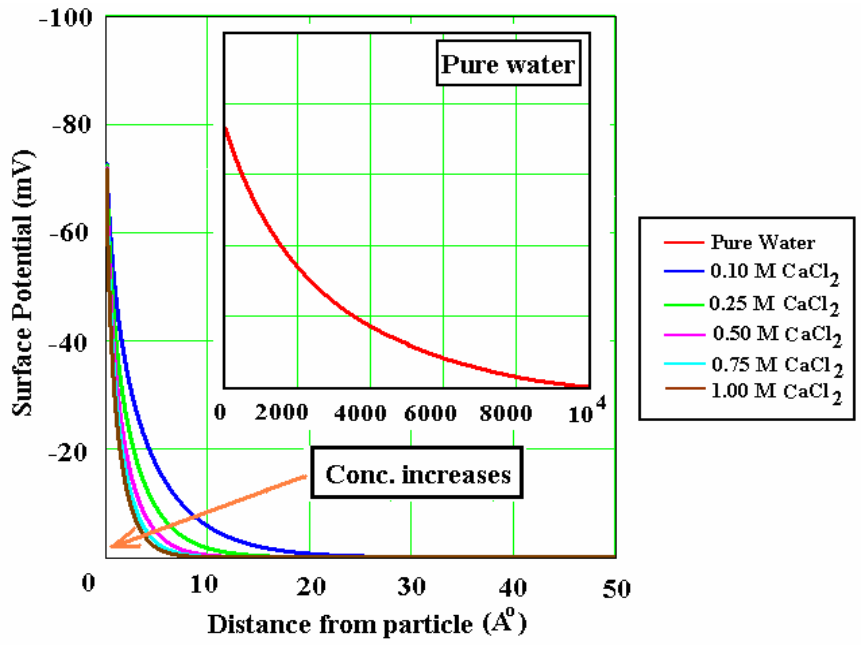

Figure 4.42. Potential profile of IPS Empress 2 veneer powder in $CaCl_2$ solutions at different concentrations (Ψ_0= -73.1 mV)

Figures 4.42 and 4.43 include the change of potential profile as a function of electrolyte concentration. As it is seen the ionic atmosphere around the particles decreases with increasing electrolyte concentration. Elctrical double layer thickness of suspension in distilled water was found 3032 Å. The electrical double layer thicknesses of suspensions in different electrolyte solutions were given in Table 4.2.

Table 4.2. Electrical Double Layer Thickness in Different Electrolytes (Å)

Electrolyte / Concentration	NaCl	$CaCl_2$
0.10 M	9.60	4.80
0.25 M	6.06	3.03
0.50 M	4.30	2.14
0.75 M	3.50	1.75
1.00 M	3.00	1.52

Effect of valency can be also seen from the Figure. 4.44 where Ca^{2+} ions are more effective due to their double positive charge.

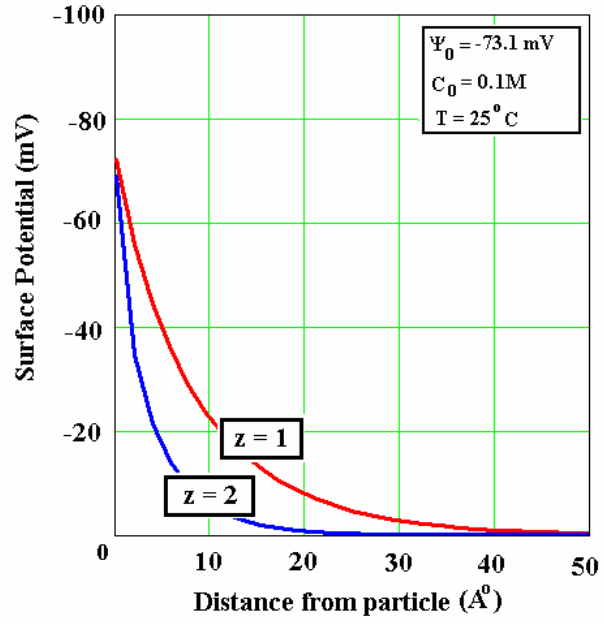

Figure 4.43. Effect of valency on electrical double layer for IPS Empress 2 veneer powder (Ψ_0= -73.1 mV)

The potential energy curves of sample were obtained using DLVO theory for all the electrolyte concentrations at pH 10. This the pH where potential profiles were obtained. As discussed earliear Derjaguin and Landau (1941) and Verwey and Overbeek (1948) were the first to develop independently the theory describing the interactions of two parallel, infinite, flat double layers. The theory is known as the DLVO theory in colloid science.

According to the DLVO theory, the total interaction energy is the sum of electrostatic and Van der Waals interactions, shown is Equations 2.6 and 2.7 respectively, for two particles of diameter d_1 and d_2, interacting through a distance of H.

The potential energy curves obtained by using Hamaker constant as 3.83×10^{-20} J calculated by using equation 2.6 for silica and water (Polat and Polat 2000).

The potential energy curves obtained for NaCl and $CaCl_2$ are presented in Figure 4.44 and Figure 4.45.. As it is seen form the figures that in the absence of any electrolyte (any ion), there is an energy barier for agglomeration of particles due to the repulsive electrostatic interactions of particles at natural pH and high surface charge (zeta potential=-73.1 mV). This shows that this powder will be well dispersed in water under this condition. Particles will not interact with each other and there will be distances among them due to the presence of repulsive forces. This is expected to effect the structure of porcelain ceramic pastes prepared and their surface roughness. Therefore in the next section the rheological behaviour of these systems will be analyzed and related to the particle-particle interactions.

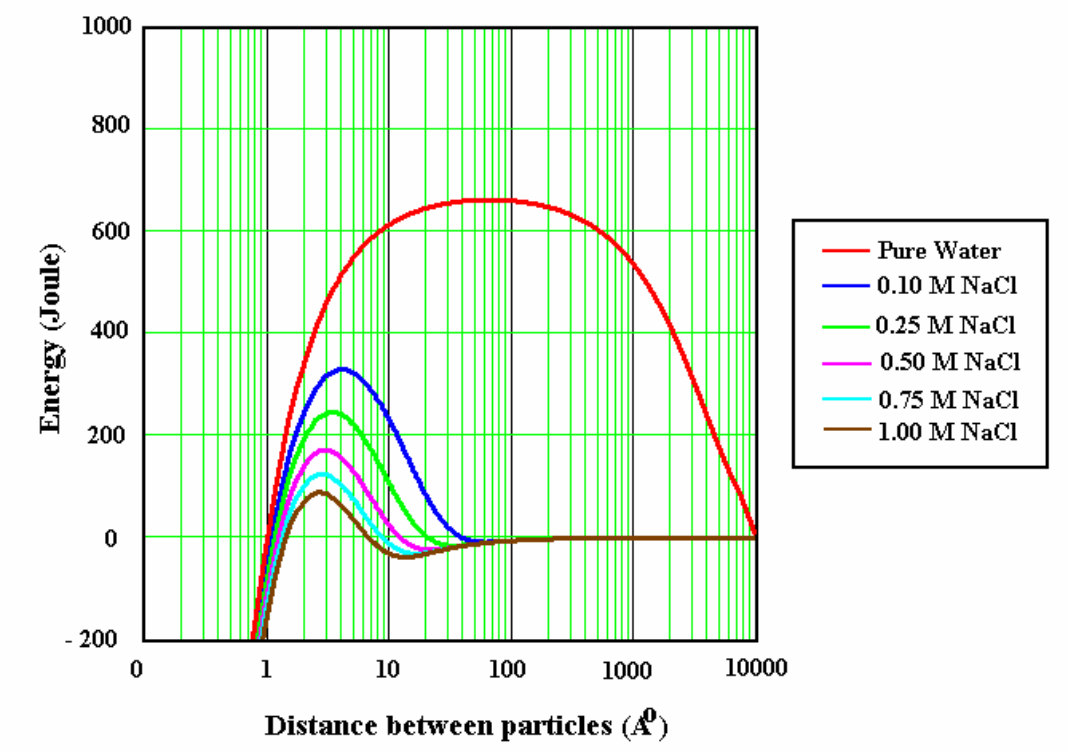

Figure 4.44. Effect of NaCl concentration on the Potential energy curve of IPS Empress2 veneer powder (size = 0.35μ, Ψ_0= -73.1 mV, A_{131}= 3.83 x 10^{-20} J, T=25^{o}C)

The potential energy curves in the presence of electrolytes are also obtained and given in the Figures 4.44 and 4.45. As it is seen from the figure that the presence of any indifferent ion in the system as counter ions (Na or Ca) effect the potential energy curves drastically decrease. Increasing both the NaCl and the $CaCl_2$ concentration decreases the energy barier height present due to their effect on repulsion interactions present among particles. This is the indication of agglomeration tendency among particles. As concentration increases particles will approch each other more and there will be smaller distances between them.

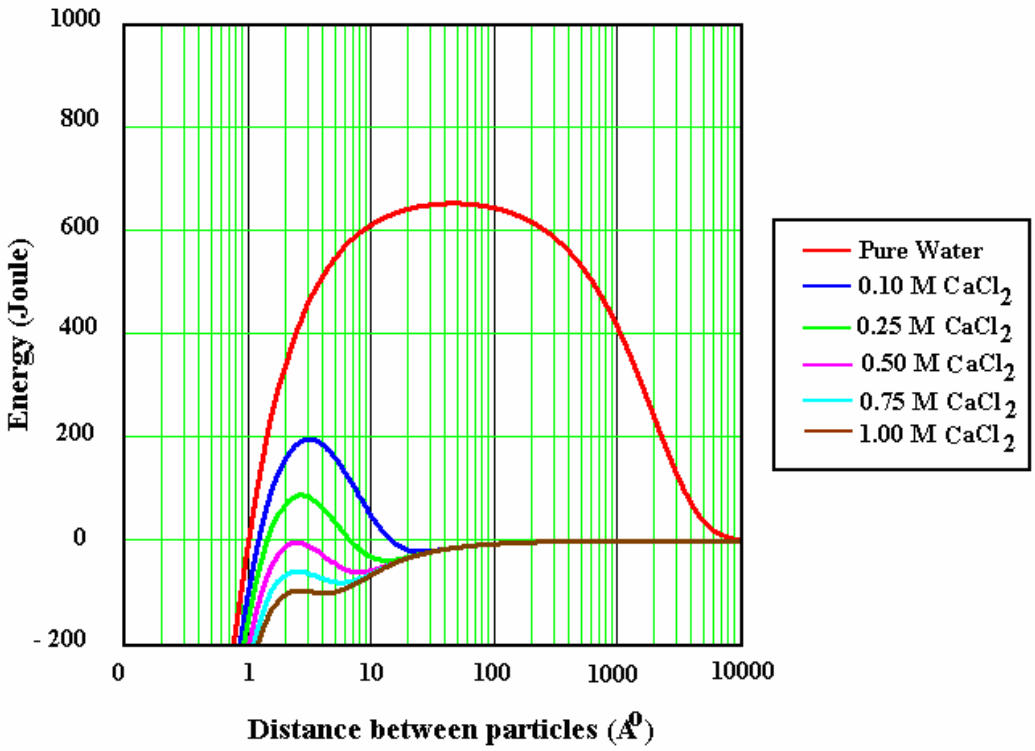

Figure 4.45. Effect of $CaCl_2$ concentration on the potential energy of IPS Empress 2 veneer powder (size = 0.35μ, Ψ_0= -73.1 mV, A_{131}= 3.83 x 10^{-20} J, T=25°C).

As seen is figure 4.47 electrolytes decreases energy barrier as their concentration increases and $CaCl_2$ is more effective than NaCl.

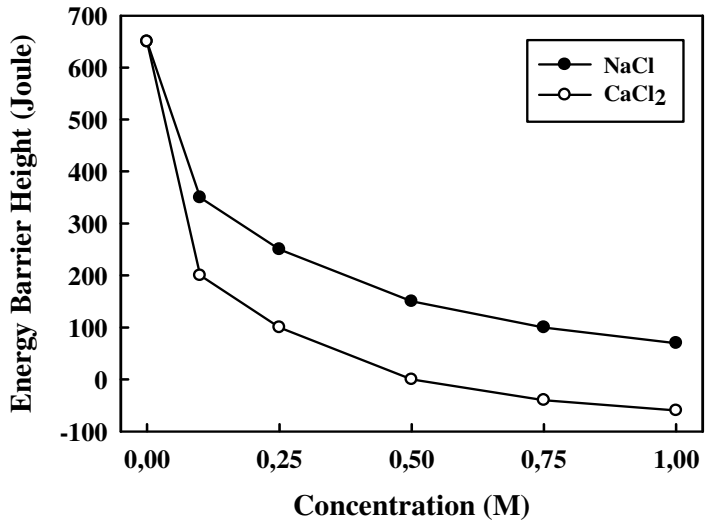

Figure 4.46. Effect of NaCl and $CaCl_2$ concentrations on the energy barrier height

4.4. Surface Roughness Analyses

The surface roughness were tested using R_a values obtained using Profilometer and AFM scans. In the case of profilometer, the whole sample surface (D= 0.7 cm) was scaned and an average R_a value was determined. In the case of AFM, however, only small areas (20 μm x 20 μm) on the surface was scanned and again an average Ra value was determined. Therefore the results obtained were quite different from each other. In this study the results of profilometer were used and related with other studies due to the possible representation problems will be faced in the case of AFM.

4.4.1. Profilometer Measurements

R_a values obtained are given as a function of NaCl and $CaCl_2$ concentrations in Figures 4.47 and 4.48. It is seen in the figures that the value of R_a was 2.3 μm in the absence of ions (distilled water only). For NaCl in Figure 4.47 initial increase in concentration increased the surface roughness little bit than decreased down to 1 μm. $CaCl_2$ also showed similar type of trend. There is an increase first and than a decrase in roughness as a function of concentration. The initial increase in the roughness may be explained with the presence of agglomeration in the system. Indeed this agglomeration is expected to increase with the increase in electrolyte concentration. Since the system becomes increasingly unstable with an increase in the electrolye concentration according to the DLVO theory. This is because of the reduced repulsive interactions between particles due to their reduced electrical surface charges as discussed in previous sections. However this process that is the increase in surface rougness is prevented by another process, gelation, besides agglomeration. The presence of gelation due to the ions was suggested based on the rheolgy measurements and discussed in the following section. Therefore the only concentration that is responsible from the increase for surface roughness due to agglomeration is the low concentrations since the gelation starts after this concentration.

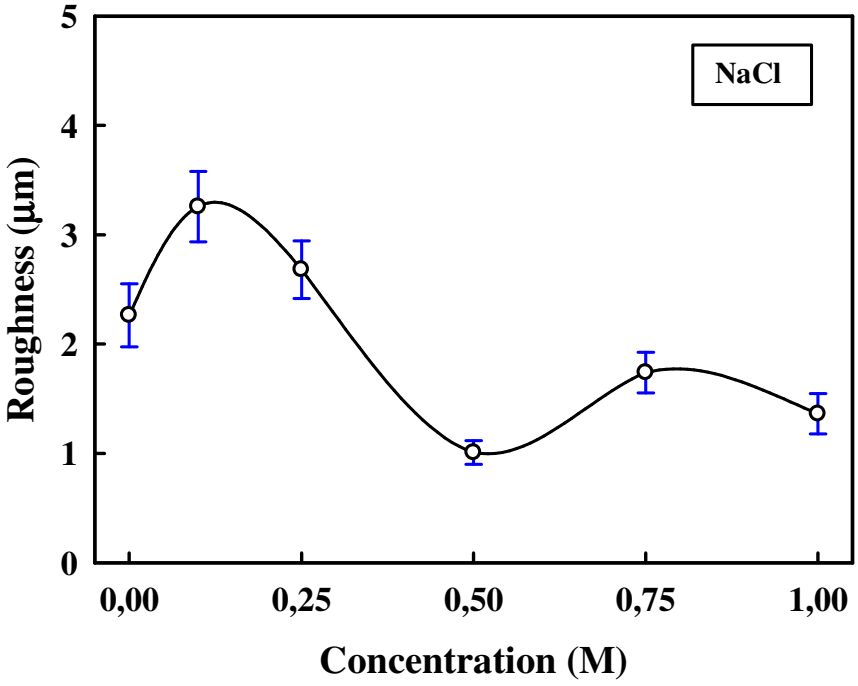

Figure 4.47. Profilometer surface roughness graph for IPS Empress 2 veneer pastes prepared with various NaCl concentrations

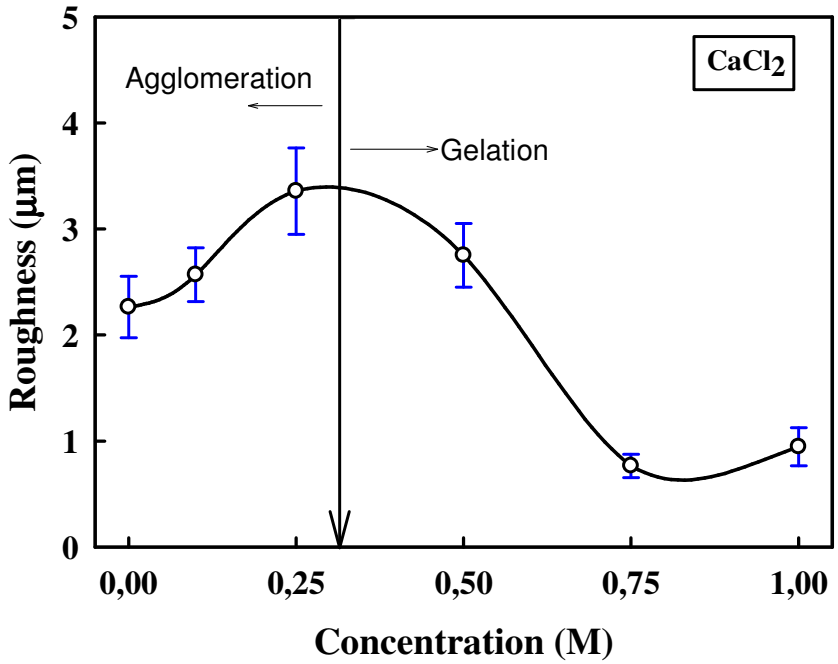

Figure 4.48. Profilometer surface roughness graph for IPS Empress 2 veneer pastes prepared with various $CaCl_2$ concentrations

4.4.2. Atomic Force Microscope (AFM) Measurements

In AFM studies R_a values were obtained by scanning 20µ x 20µ area. This scanning was chosen because samples are rough to scan at 100µ mx 100µm.area which is the largest scanning area in AFM. In the absence of ions surface roughness was 19 nm and changed as a function of electrolyte type and concentration. The change of surface roughness trend was similar to that of profilometer in case of $CaCl_2$, however, it is little different in case of NaCl. But there is still a decrease in the surface roughness in general even in case of NaCl.

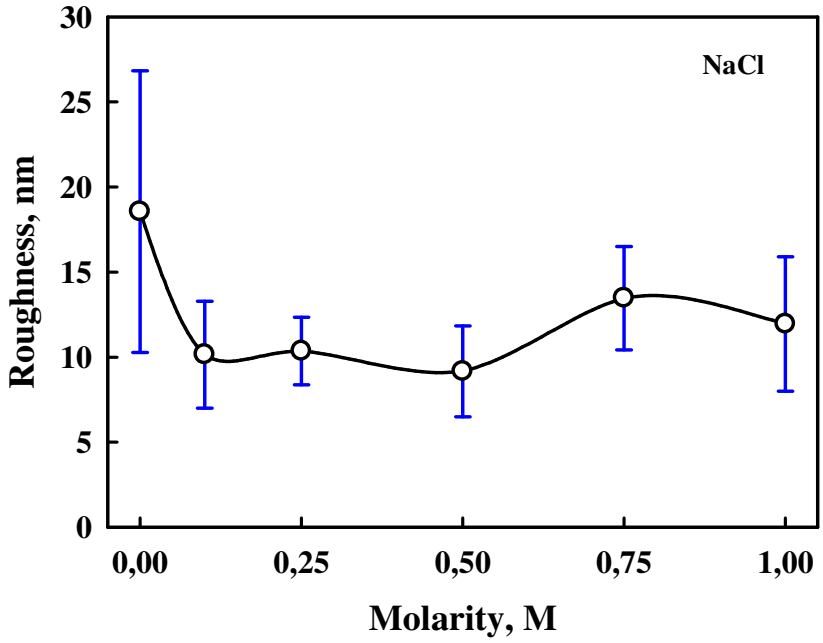

Figure 4.49. AFM surface roughness graph for IPS Empress 2 veneer pastes prepared with different NaCl concentrations

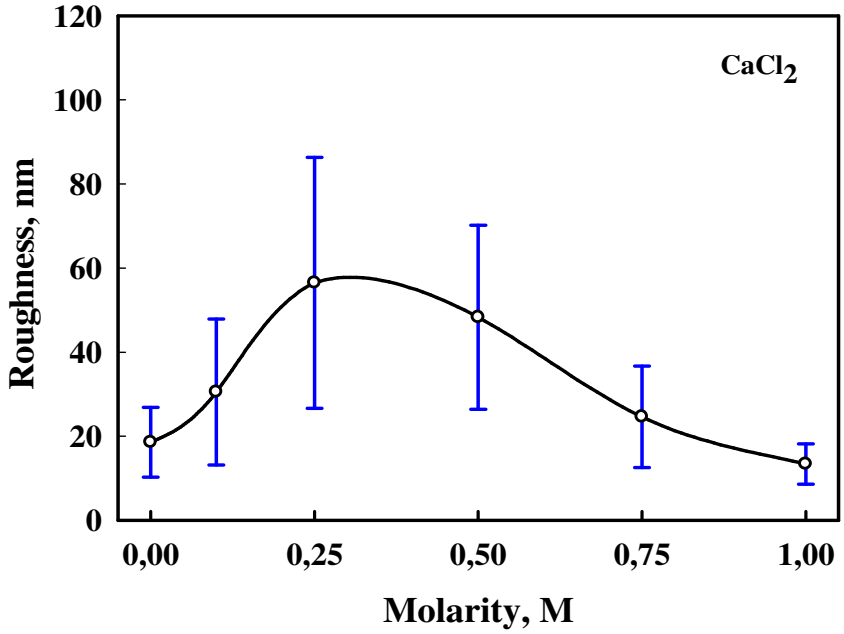

Figure 4.50. AFM surface roughness graph for IPS Empress 2 veneer pastes prepared with different $CaCl_2$ concentrations

This difference between AFM and profilometer can be because of small number (5 times for each sample) of scanning and small scanning area (20µ x 20µ) in AFM. The disadvantage of AFM is its low vertical range. The scanned areas are smaller when compared with the sample's diameter which is 7 mm. The number of scanning also is not enough to represent the whole sample surface. The number of scans must be really large to get a detailed idea about the surface roughness. But this is time consuming. On the other hand, profilometer scans the whole surface through a line. Each sample can be scaned so many times to represent sample. The procedure is easy and fast.

4.4.3. Scanning Electron Microscope (SEM) Analyses

In the study for each ceramic sample ten SEM images were collected randomly at 2500 magnification to have a detailed idea about the surface roughness**.**

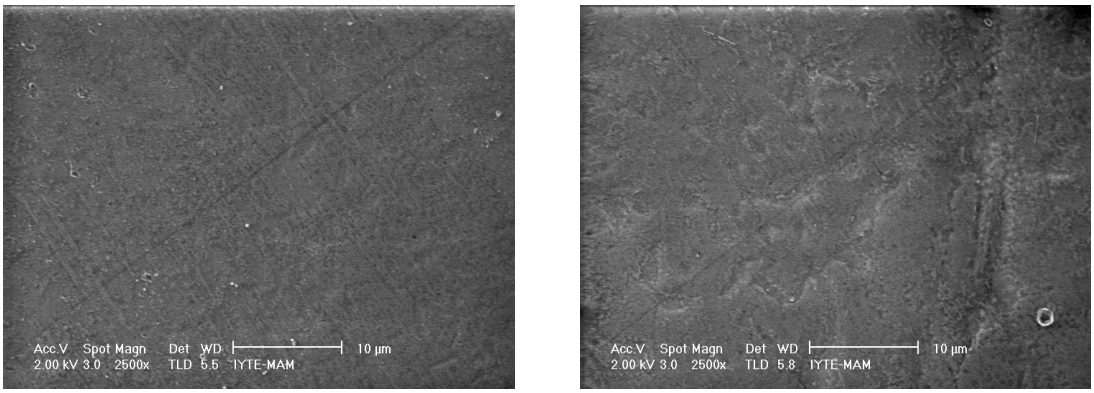

Figure 4.51. SEM images of IPS Empress 2 veneer in distilled water (2500x)

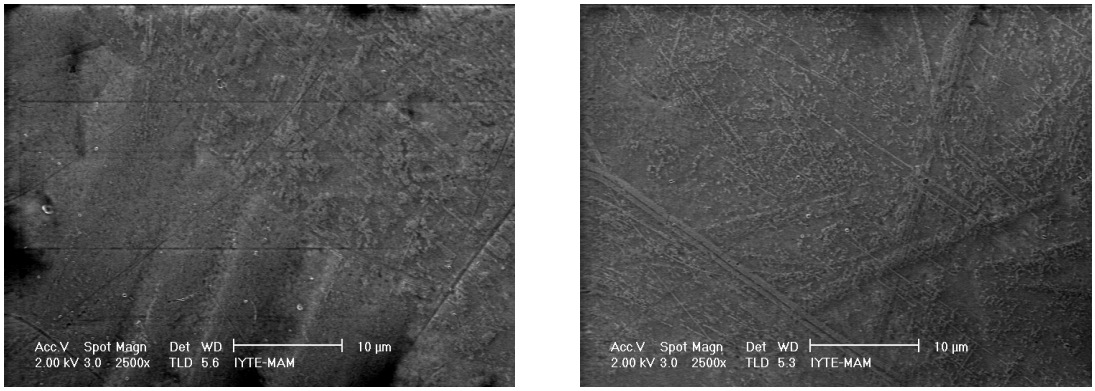

Figure 4.52. SEM image of IPS Empress 2 veneer in 0.1M NaCl

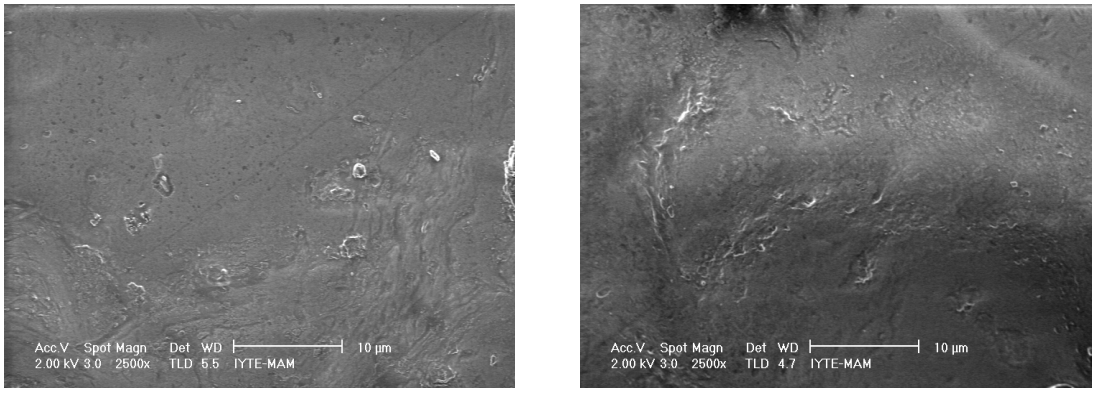

Figure 4.53. SEM image of IPS Empress 2 veneer in 0.25M NaCl

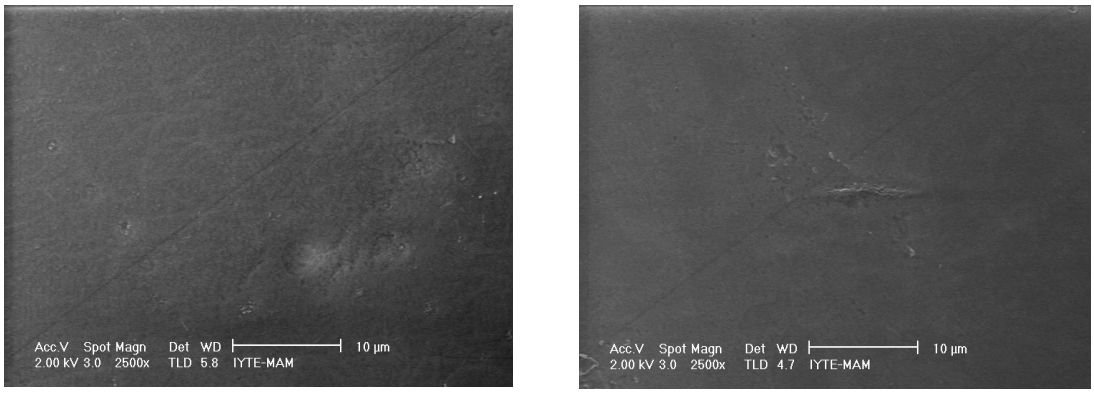

Figure 4.54. SEM image of IPS Empress 2 veneer in 0.5M NaCl

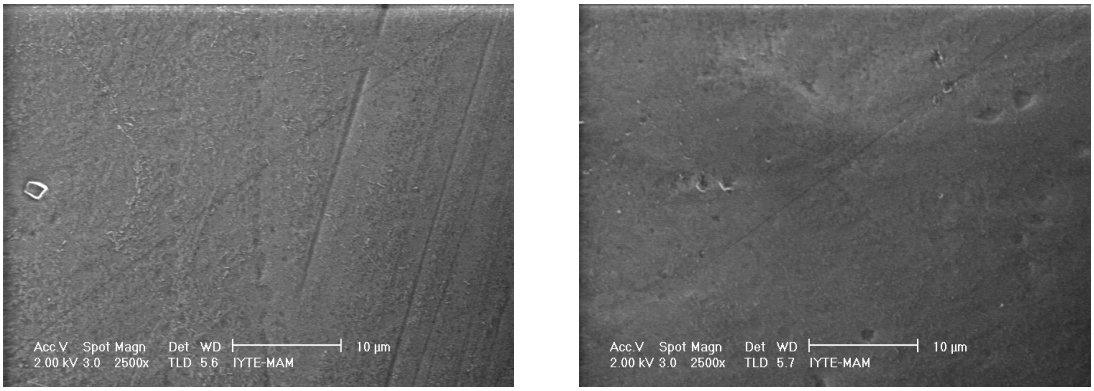

Figure 4.55. SEM image of IPS Empress 2 veneer in 0.75M NaCl

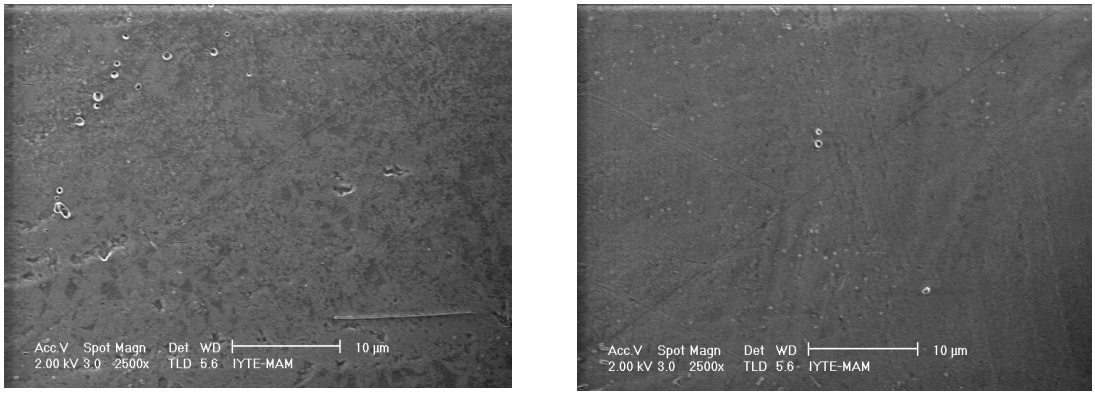

Figure 4.56. SEM image of IPS Empress 2 veneer in 1M NaCl

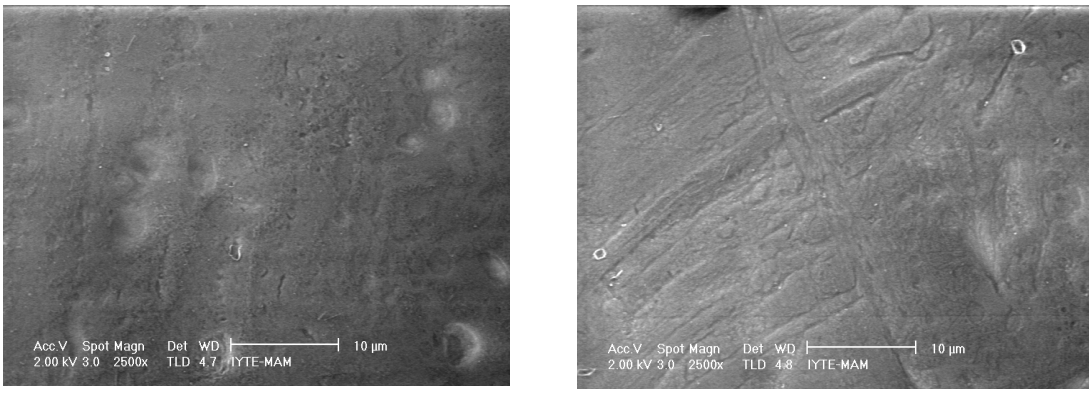

Figure 4.57. SEM image of IPS Empress 2 veneer in 0.1M $CaCl_2$

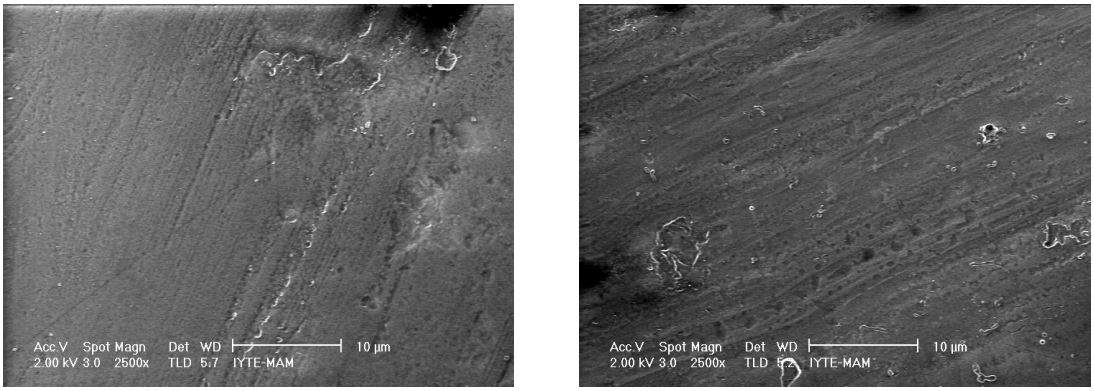

Figure 4.58. SEM image of IPS Empress 2 veneer in 0.25M $CaCl_2$

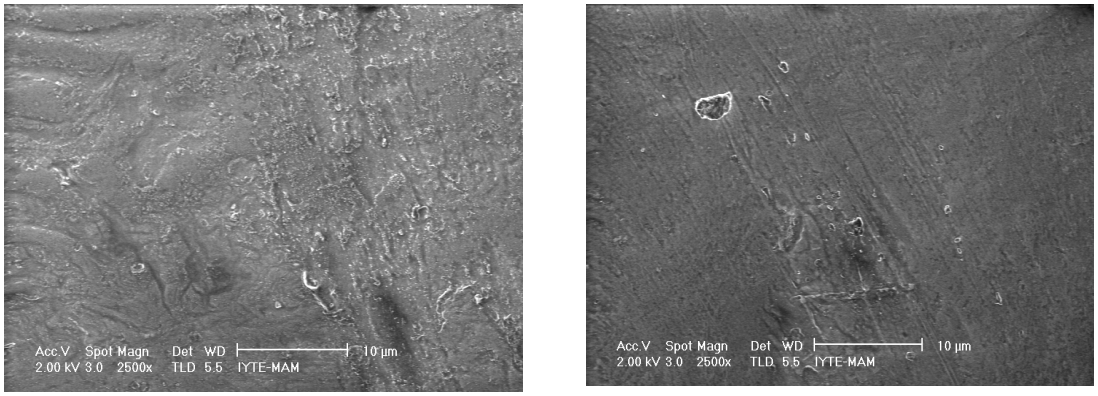

Figure 4.59. SEM image of IPS Empress 2 veneer in 0.5M $CaCl_2$

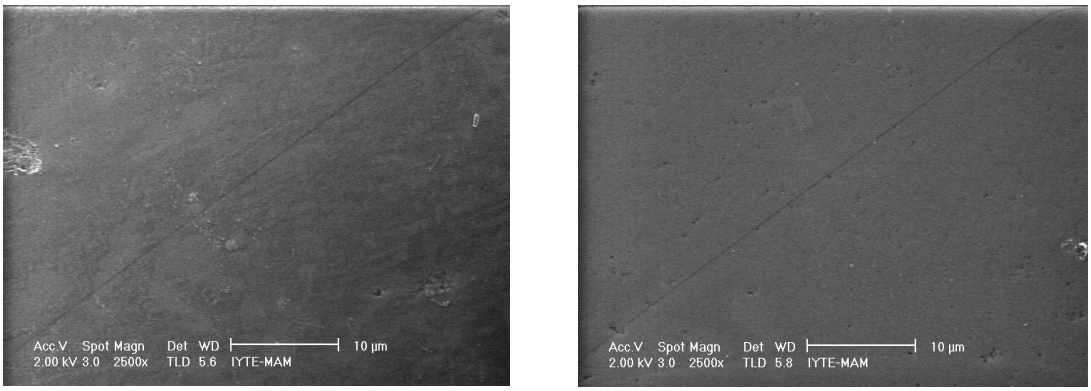

Figure 4.60. SEM image of IPS Empress 2 veneer in 0.75M $CaCl_2$

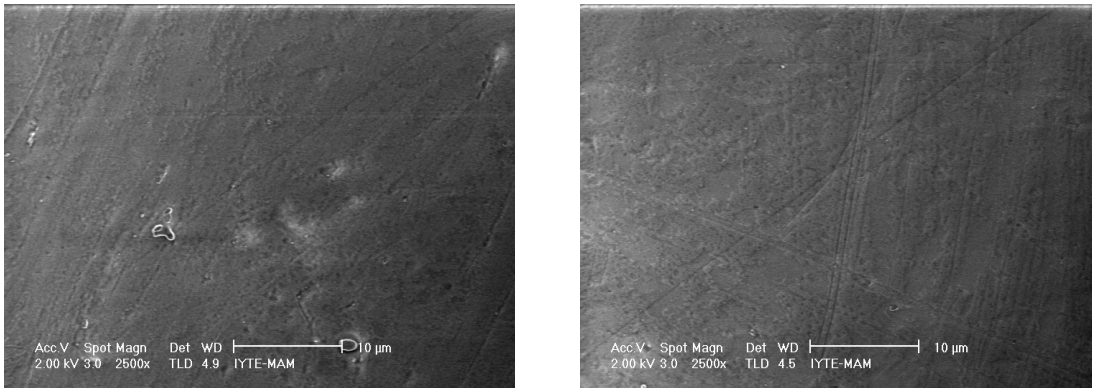

Figure 4.61. SEM image of IPS Empress 2 veneer in 1M $CaCl_2$

It can be seen in figures that the trend is same as obtained in profilometer measurements.

4.4.4. Energy Dispersive X-Ray Spectroscope (EDS) Analyses

EDS was studied for IPS Empress 2 veneer pastes to have an idea about which oxides were present at the surface after firing powder and whether the added electrolytes found in the interior part of the pastes or at the surface. The oxides found in rich amount were analyzed in EDS measurements because EDS analysis is not reliable for elements that are found less in the sample. EDS studies were repeated 5 times for each specimen and the average values are shown from Table 4.3 to 4.6.

Table 4.3. EDS analyses results of IPS Empress 2 veneer powder

Element	**Weight %**
SiO_2	62.57 ± 2.74
Al_2O_3	12.28 ± 1.79
Na_2O	9.95 ± 1.01
P_2O_5	3.40 ± 0.87
K_2O	7.84 ± 0.78
CaO	3.98 ± 1.07
Total	100.02 ± 0.02

Table 4.4. EDS analyses results of IPS Empress 2 veneer pastes prepared with distilled water

Element	**Weight %**
SiO_2	59.02 ± 1.42
Al_2O_3	12.42 ± 1.43
Na_2O	26.29 ± 3.89
P_2O_5	0.38 ± 0.64
K_2O	1.32 ± 1.39
CaO	0.58 ± 0.86
Total	100.01 ± 0.00

Table 4.5. EDS analyses results of IPS Empress 2 pastes prepared with NaCl

Elements	**0.1M NaCl (wt%)**	**0.25M NaCl (wt%)**	**0.5M NaCl (wt%)**	**0.75M NaCl (wt%)**	**1M NaCl (wt%)**
SiO_2	56.66 ± 2.99	58.66 ± 1.99	59.91 ± 1.57	60.57 ± 1.14	60.27 ± 2.29
Al_2O_3	13.07 ± 0.83	12.46 ± 0.93	12.18 ± 0.79	12.11 ± 0.65	11.91 ± 0.99
Na_2O	27.13 ± 3.54	22.82 ± 3.33	24.31 ± 4.39	23.60 ± 2.22	23.47 ± 3.61
P_2O_5	0.69 ± 0.98	1.77 ± 1.76	0.88 ± 0.85	0.76 ± 1.04	1.69 ± 1.77
K_2O	1.18 ± 1.38	2.53 ± 1.28	1.74 ± 1.59	1.84 ± 0.77	1.66 ± 1.49
CaO	1.27 ± 0.42	1.75 ± 1.02	0.99 ± 0.92	1.12 ± 0.59	0.99 ± 0.85
Total	100 ± 0.00	99.99 ± 0.00	100.01 ± 0.00	100 ± 0.00	99.99 ± 0.00

Table 4.6. EDS analyses results of IPS Empress 2 pastes prepared with $CaCl_2$

Elements	**0.1M $CaCl_2$ (wt%)**	**0.25M $CaCl_2$ (wt%)**	**0.5M $CaCl_2$ (wt%)**	**0.75M $CaCl_2$ (wt%)**	**1M $CaCl_2$ (wt%)**
SiO_2	58.61 ± 1.76	55.37 ± 5.06	66.51 ± 2.73	61.19 ± 2.12	55.82 ± 4.37
Al_2O_3	12.35 ± 1.79	13.96 ± 1.66	14.78 ± 0.95	13.82 ± 0.78	14.48 ± 2.60
Na_2O	25.99 ± 4.38	27.12 ± 2.53	12.36 ± 0.64	19.42 ± 4.36	24.73 ± 2.63
P_2O_5	1.75 ± 1.06	2.48 ± 3.23	4.84 ± 1.62	3.16 ± 1.52	3.94 ± 3.61
K_2O	0.91 ± 0.86	0.59 ± 0.66	1.20 ± 0.42	2.26 ± 1.73	0.58 ± 0.62
CaO	0.38 ± 0.39	0.49 ± 0.46	0.31 ± 0.22	0.16 ± 0.12	0.45 ± 0.48
Total	99.99 ± 0.01	100 ± 0.01	100 ± 0.01	100.01 ± 0.01	100 ± 0.00

EDS analyses show that Na_2O amount decreases whereas CaO amount increases. when compared with the values in Table 4.2. for IPS Empress 2 veneer paste prepared with distilled water. This means that Na^+ ions are not found on the surface but found in the interior of the pastes. However, as concentration increases its amount remains nearly same. In $CaCl_2$ case both amounts of Na^+ and Ca^{2+} ions are decreased and amounts of both ions decreases as concentration increases. This situation goes on up to a certain point, 0.75 and 1M. This means that both ions are found in the interior part and supposed to form agglomerates and yield smooth surfaces.

4.4.5. Contact Angle Measurements

The contact angles measured on the surfaces are presented in Figure 4.64. The symbols in the figure give the mean contact angles for 60 readings along with the error bars for 2-standard deviation spread around this mean. It is immediately clear that the contact angle values follow the trend of surface roughness values as a function of electrolyte concentration.

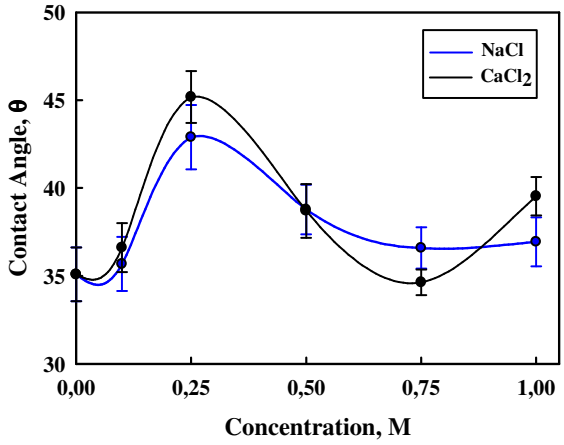

Figure 4.64. Comparison of Contact Angles of IPS Empress 2 Ceramic Surfaces as a function of Electrolyte

The mean contact angle values were 33 degrees in the absence of any electrolyte in the system. This value increased to 42 and 45 degrees with addition of NaCl and $CaCl_2$ respectively with an initial increase in concentration then decreased to 35 degrees with further increase in concentration. That is the roughest surface showed the highest contact angle. This finding is in agreement with the findings of some literature on the effect of surface roughness on contact angle value (Wolansky et al. 1999, Ponsonnet et al. 2003) on the other hand it is not in agreement with some other studies (Adamson 1967 and Feng et al. 1998).

The wetting behaviour of an ideal flat solid is fixed by its chemical composition (Young's relation) but real solids are rough which affects their wettability or non-wettability (Wenzel 1936, Wenzel 1949, Johnson and Dettre 1964, Netz and Andelman 1997, Bico et al. 2001). Wenzel proposed the first theoretical model describing the contact angle for a liquid drop at a rough solid in 1936 (Wenzel 1936). He extended Young's model for the contact angle on rough surfaces, by adding a roughness factor to Young's equation. The surface roughness factor (r) is given by Equation 4.1.

$$r = \frac{actual\ surface\ area}{geometric\ surface\ area} \tag{4.1}$$

The geometric surface area is also known as the projected surface area, since it can be seen as a 2D projection or shadow of the actual surface area.

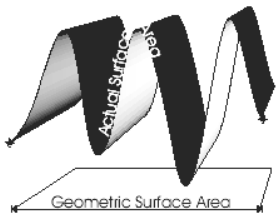

Figure 4.62 A schematic drawing of the actual surface area and the geometric surface area (Source: Van der Wal 2006)

For a perfectly smooth surface, r = 1, but for a rough surface the actual surface area is larger than the geometric surface area. A drop of liquid on a rough surface, compensates for this increased surface area by a change in its contact angle. The effect of the surface roughness on the contact angle is given by Wenzel's equation:

$$\cos\theta_a = r\cos\theta_Y \tag{4.2}$$

Where θ_a is apparent contact angle, r is the surface roughness ratio, $\cos\theta = (\gamma_{sv} - \gamma_{sl})/\gamma_{lv}$; γ_{sv}, γ_{sl}, γ_{lv} are the interfacial tensions at the liquid-vapor, solid-vapor, and the solid-liquid interfaces, respectively, and θ_Y is the Young's contact angle on a similar smooth surface.

It is well known that contact angle of a sessile drop on a surface of a solid depends largely on the roughness of the plane (Tamai and Aratani 1972, Miller et al. 1996). The surface roughness amplifies the wetting or de-wetting behaviour of the surface.

The theory of contact angles on rough surfaces involves difficult conceptual problems. There is a controversy in the literature about the effect of surface roughness on contact angle. According to Adamson 1967 and Feng et al. 1998 the contact angle values are approximately inversely proportional to the surface roughness values. They are indicated that if contact angle (θ) of a liquid is less than 90°, the surface roughness results in a lower contact while if θ is greater than 90°, it is increased by roughness (Adamson, 1967). But it should be noted that the surface roughness factor does not give any indication of the length scale of the roughness. On the other hand, Wolansky and Marmur 1999 and Ponsennet et al. 2003 say that contact angle increases as surface roughness increases. Wolansky et al. 1999 demonstrated by an example that Wenzel

equation may be incorrect for three- dimensional systems with no special symmetry, and the apparent contact angle may vary from point to point (Wolansky and Marmur 1998).

Figure 4.63. Apparent Contact Angle for an Asymmetric Rough Surface
(Source: Wolansky et al. 1998)

Apart from these conclusions of these studies surface type is also important in determining the contact angle. Wenzel 1936 and Adamson 1989 says that this relation changes depending on surface type whether it is hydrophobic or hydrophilic. That is low energy and high energy surfaces give different dependence on roughness when surface type is fixed. For smooth surfaces contact angles will be small because the only difference between rough and smooth surfaces is spreading of liquid on smooth surface when surface is hydrophilic.

Wolansky and Marmur proposed that Wenzel equation yields the apparent contact angle on sawtooth surfaces when the size of the drop is infinetely large compared with the scale of the roughness. In this study volume of the liquid was 5µl which equals to 0.21 cm in diameter. The scale is not infinetely larger than the scale of roughness obtained with profilometer which is in micrometers. When compared the diameter of the sample with that of drop it can be seen that number of contact angle measurements (16 measurements) is quite enough to get an idea about surface roughness. Because nearly all of the surface is scanned.

In addition there is ion concentration difference between the cases involved here. The only difference between the surfaces may not be because of the roughness of the surface. The presence of ions may affect the energy of the surface therefore contact angles may be different. This relation between the energy of surface and the contact angle can be shown with the relation given in Equation 4.3 (Girifalco and Good 1957).

$$\gamma_S = \gamma_l \left[\frac{(1+\cos\theta)^2}{4\Phi^2} \right] \qquad \Phi = \frac{4(V V_l)^{1/3}}{(V_S^{1/3} + V_l^{1/3})^2} \tag{4.3}$$

Where γ_S is the energy of surface, γ_l is the energy of liquid surface, V_s is the volume of solid and V_l is the volume of solution. This part of the study, however, requires more studies to clarify the discussion on the relationship between surface roughness and contact angle.

Figures 4.65 and 4.66 give the distributions of contact angle values. They actually show the change in the homogeneity of the surface as a function of electrolyte concentration change.

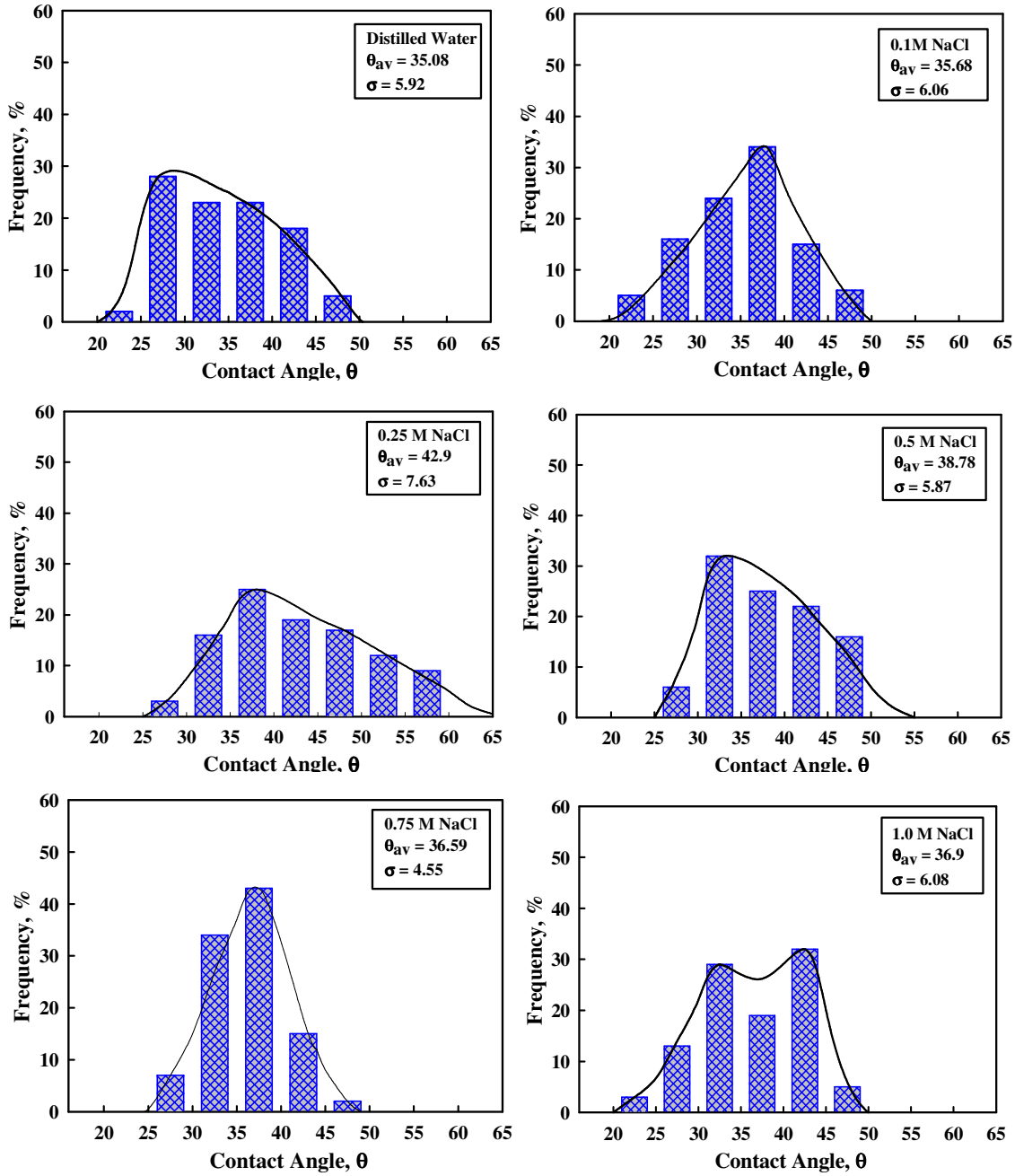

Figure 4.65. Contact Angle Graphs for Samples Prepared with NaCl

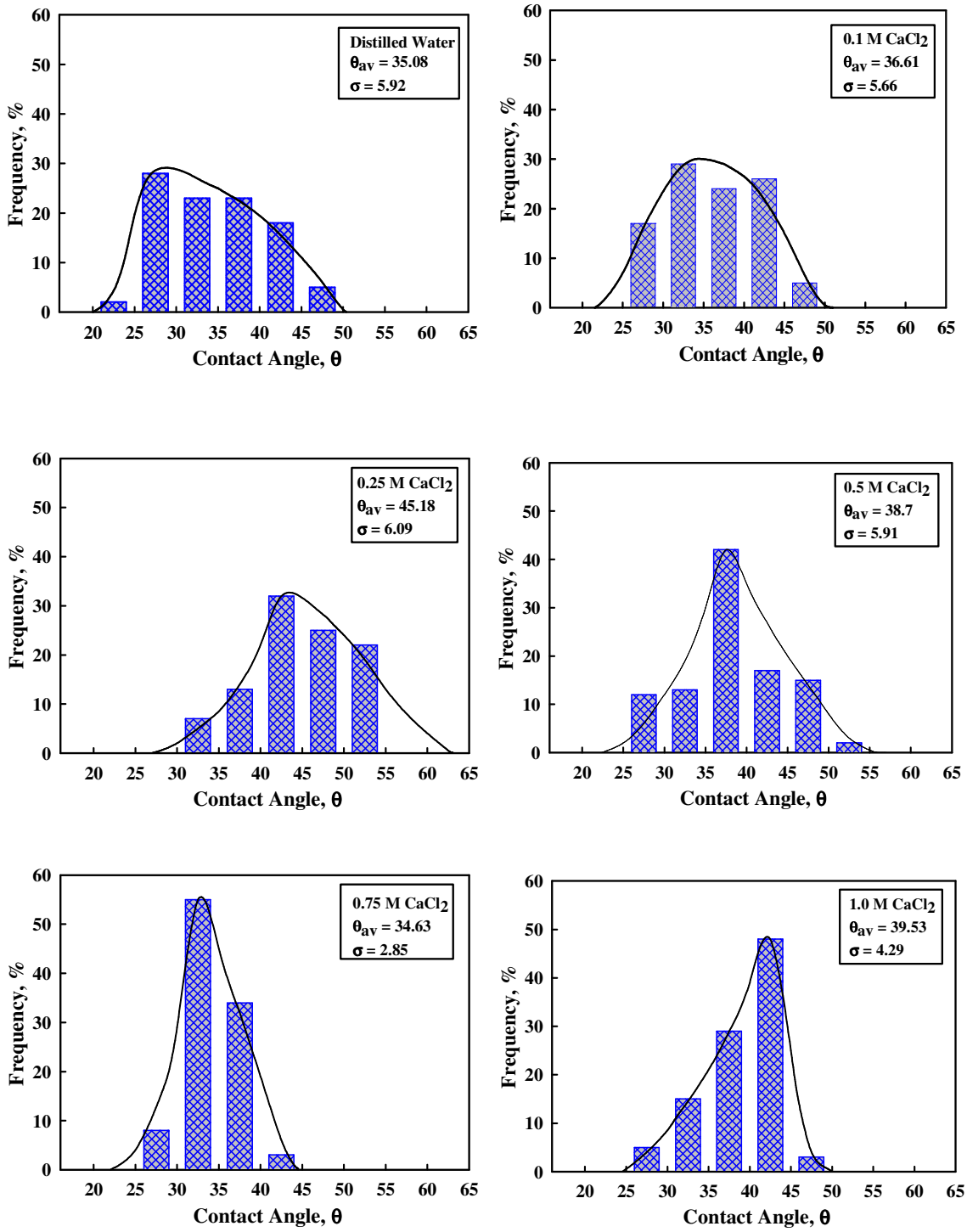

Figure 4.66. Contact Angle graphs for samples prepared with $CaCl_2$

4.5. Rheology Measurements

Rheology is important in ceramic processing. To understand the particle interactions the rheology experiments were conducted using both distilled water and solutions of NaCl and $CaCl_2$ at different concentrations. The solution pH used was natural (~ pH 10) since it is far away from the PZC value. Additions of ions, however, changed the pH of solutions from 8 to 10. The solid/liquid ratio used in this study was 60% by (w/v). In real sistems this ratio is much higher and varies between 2.56 – 3.35 (Zhang et al. 2004). For a fine slip high solid percentages are preferred to retard segregation, to increase the casting rate, to produce a more uniform cast, and to possibly obtain a higher green density.

Figures from 4.67 to 4.77 show the rheological behaviour of IPS Empress 2 veneer powder as a function of shear rate versus shear stress and viscosity versus shear rate curves. As it is seen from the figures that suspensions prepared using distilled water showed Newtonian behavior. The change of shear stress as a function of shear rate was linear and the change of viscosity as a function of shear rate was constant as in the case of newtonian systems. This shows that there is no flocculation of particles in the absence of any ions in the system. Addition of NaCl brings the system slightly shear thickening behavior at the lowest concentration. The slight increase of viscosity as a function of shear rate is the indication of this. However increasing concentration changed the behavior from shear thickening to shear thinning behavior (pseudoplastic) that is flocculation in the system. The decrease observed with shear rate is the indication of this behavior. This decrease increased with an increase in concentration. In the case of $CaCl_2$, there is no shear thickening behavior at the lowest concentration studied. The behavior was always shear thinning for all the concentrations studied. It is also known that most ceramic suspensions show shear thinning behaviour (King 2002). That is where flocculation occurs between the particles in the system.

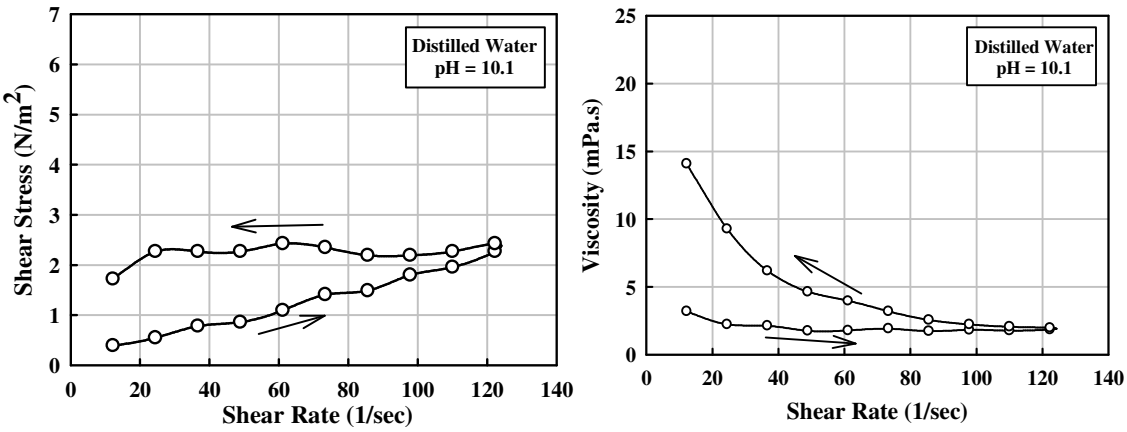

Figure 4.67. Rheological behaviour of IPS Empress 2 veneer powder in distilled water

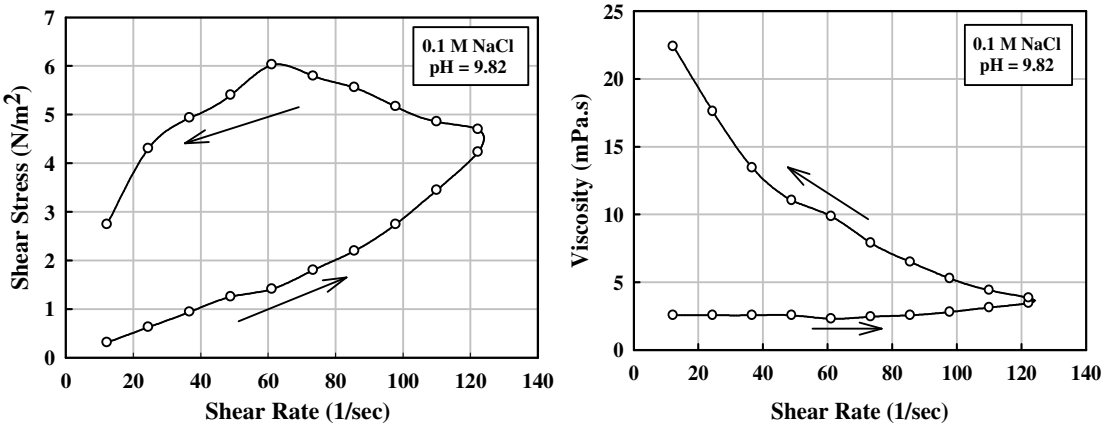

Figure 4.68. Rheological behaviour of IPS Empress 2 veneer powder in 0.1 M NaCl

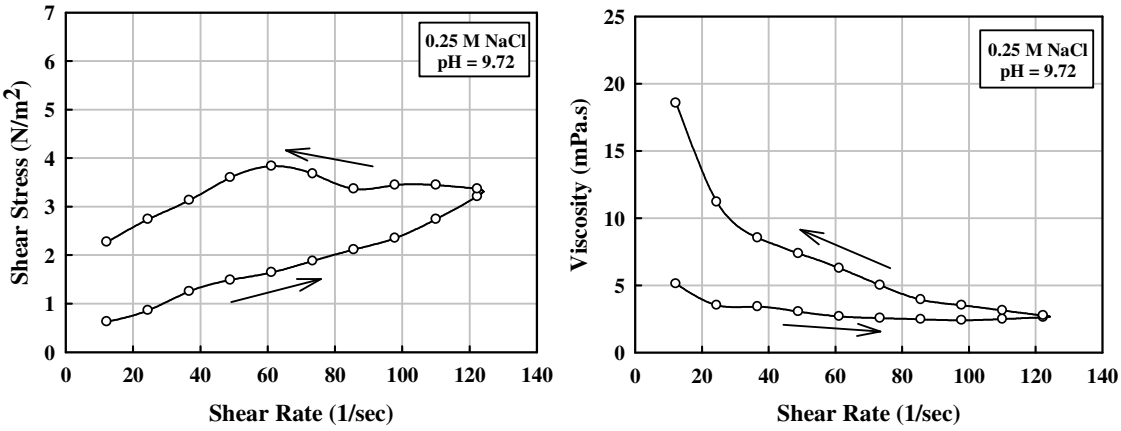

Figure 4.69. Rheological behaviour of IPS Empress 2 veneer in 0.25 M NaCl

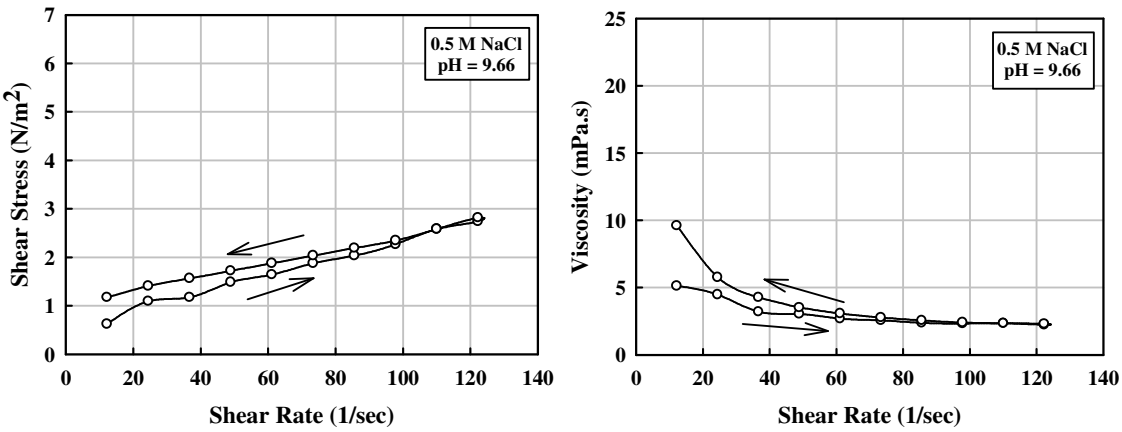

Figure 4.70. Rheological behaviour of IPS Empress 2 veneer in 0.5 M NaCl

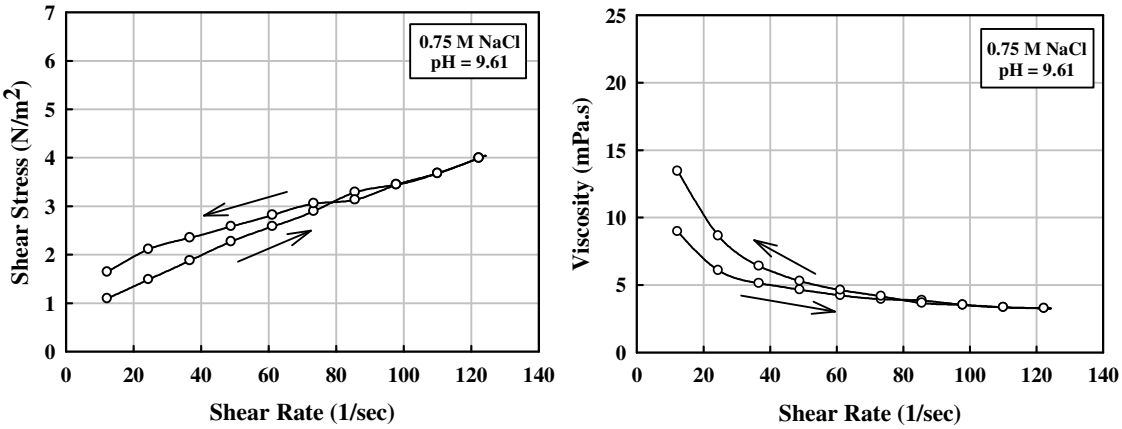

Figure 4.71. Rheological behaviour of IPS Empress 2 veneer in 0.75 M NaCl

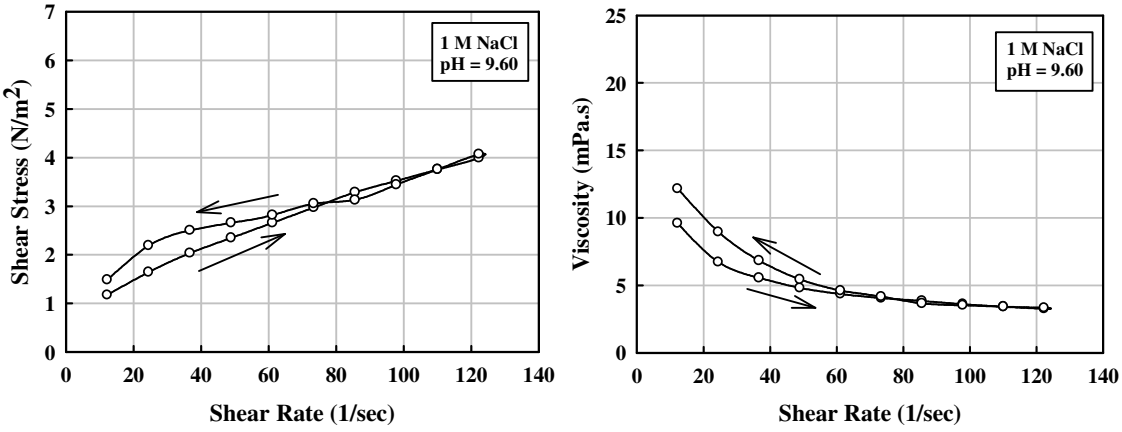

Figure 4.72. Rheological behaviour of IPS Empress 2 veneer in 1M NaCl

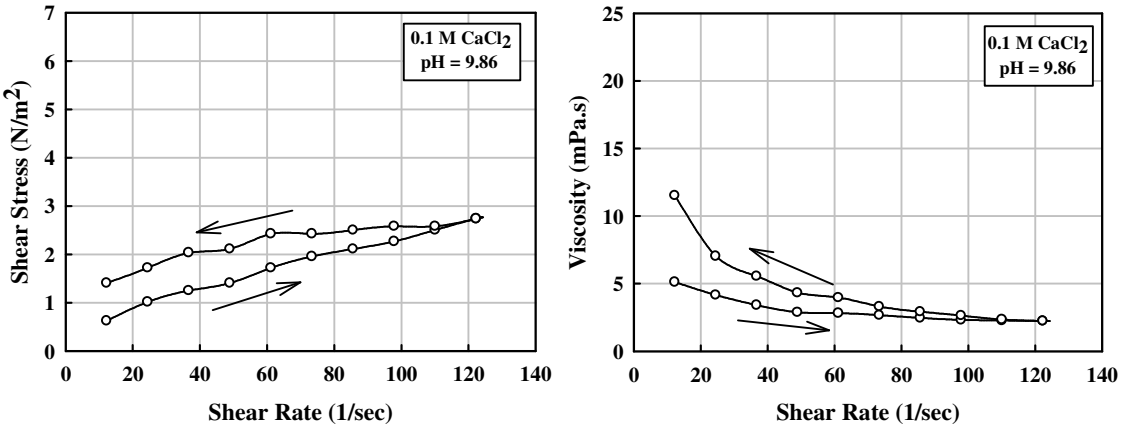

Figure 4.73. Rheological behaviour of IPS Empress 2 veneer in 0.1 M $CaCl_2$

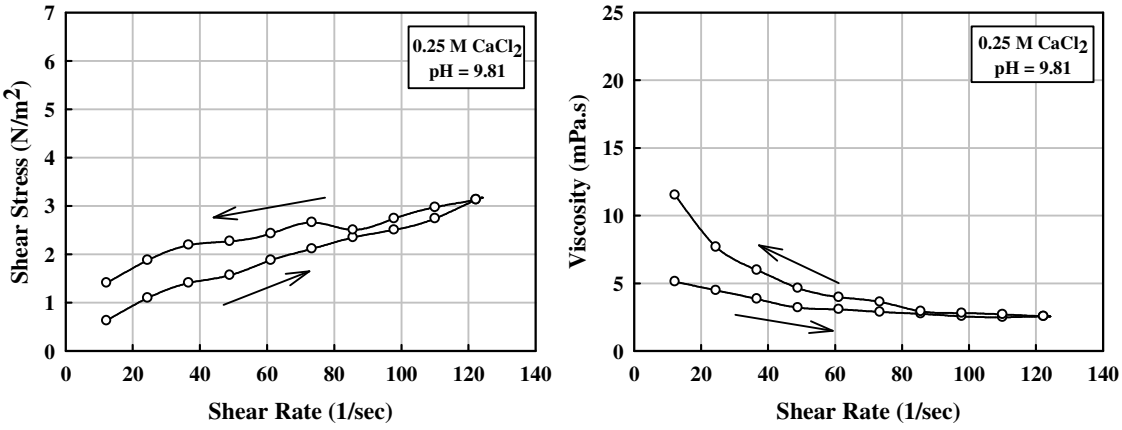

Figure 4.74. Rheological behaviour of IPS Empress 2 veneer in 0.25 M $CaCl_2$

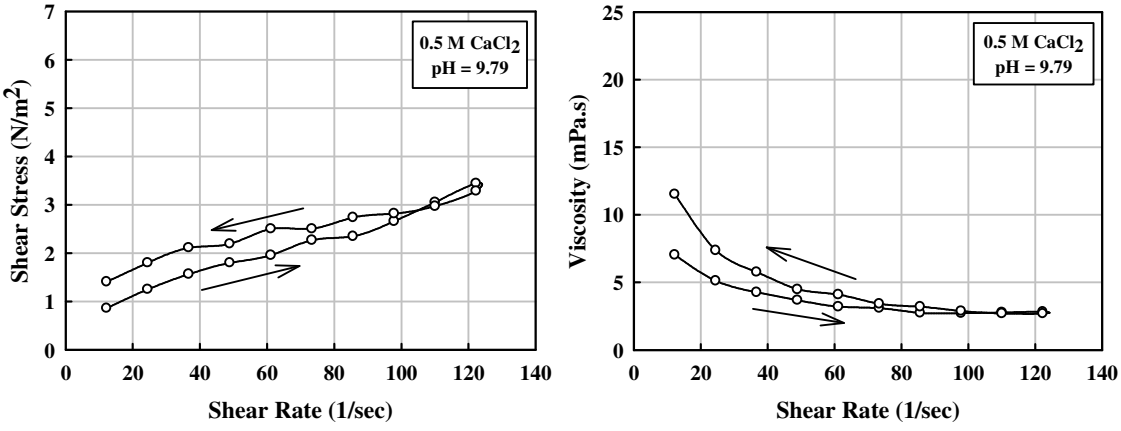

Figure 4.75. Rheological behaviour of IPS Empress 2 in 0.5 M $CaCl_2$

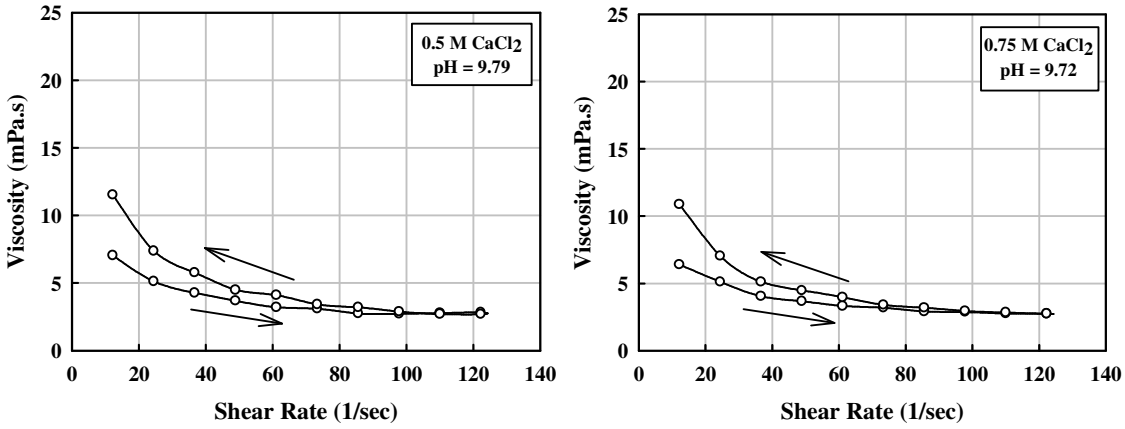

Figure 4.76. Rheological behaviour of IPS Empress 2 veneer in 0.75 M $CaCl_2$

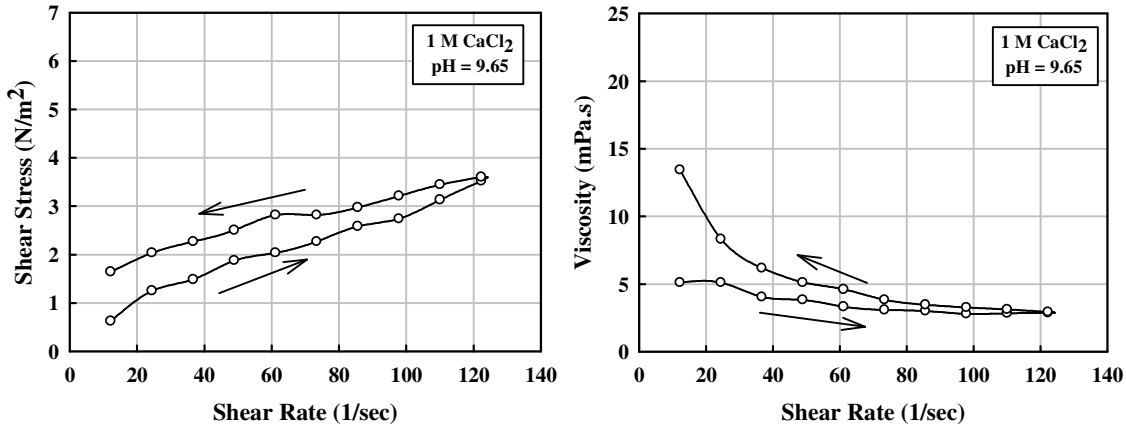

Figure 4.77. Rheological behaviour of IPS Empress 2 veneer in 1 M $CaCl_2$

As seen in Figure 4.78 electrolytes affect the viscosity of the system. $CaCl_2$ increases viscosity first and than decreases whereas NaCl increases with an increase in concentration.

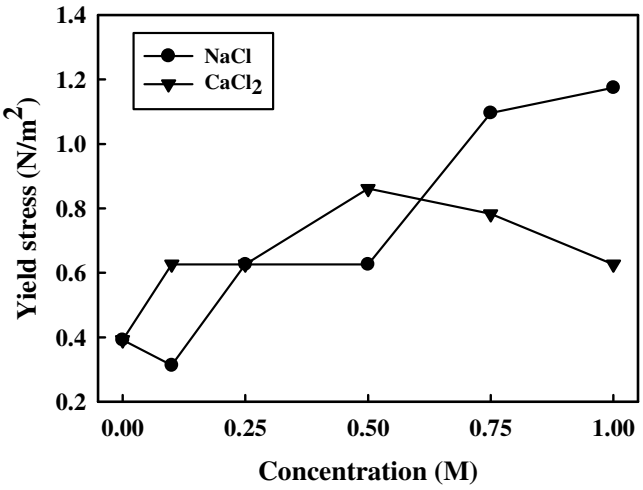

Figure 4.78. Yield Stress versus Concentration Graph for Electrolytes at Different Concentrations

The gelation process is known to be reponsible for producing the shear-thinning behaviour. When gelation exist, particles are constantly subjected to forces which pull them in and cause them to join the forming gel structures. When gel structures are sheared, the greater the imposed shear rate, the more gel structure is broken, and generally, the lower will be the suspension's measured viscosities. The limiting (minimum) viscosity in shear-thinning fluids occur when gel structures have been totally disrupted and all particles travel as individuals. When shear stresses are reduced, gel structures will reform and suspension viscosity will increase. When shear stresses are removed, shear flow will stop and gelation will cause the complete structure reform.

As a result increasing electrolyte concentration in the system starts gelation and bring particles together. This is another mechanism besides interparticle realations (agglomeration) that has to be considered in the system. In previous sections, interactions between particles were discussed using DLVO theory and surface roughness was related to particle-particle interactions. Even in the presence of low concentrations of electrolytes (0.1 M), there is a considerable decrease in the energy barier obtained from DLVO theory for particles to agglomerate. This agglomeration makes system unstable and causes an increase in surface roughness. However, after this concentration surface roughness starts decreasing again due to the gelation process as discussed in above paragraphs. Ceramic suspensions that have gel like form give smooth surfaces.

CHAPTER 5

CONCLUSION

In this study, determination of the particle interactions-rheology-surface rouphness relationship for dental ceramics was studied. Various electrolyte ($CaCl_2$, NaCl) concentrations were tested to determine whether they give smooth surfaces.

The size and charge of powder used was measured prior to experiments. Particle size of the powder was found to change between 500 nm and 2600 nm depending on pH of the suspension and it was 1602 nm in case of natural pH (6.86) where the experiments of this study were conducted. Zeta potential measurements were also conducted to determine the electrostatic charge of the powder surface. These studies were done as a function of pH and PZC (point of zero charge) of the suspension was determined which was found to be around pH 3. Surface charge was negative in case of natural pH and affected by addition of electrolytes. NaCl changed only the magnitute of the charge while $CaCl_2$ changed both the magnitute and the sign of surface charge. This is most probably due to the adsorption of $CaCl_2$ on surface. DLVO theory was used to investigate the effect of electrolytes on the stability of the powder/water system and the potential energy curves were obtained. As expected the stability of the system decreases with increasing electrolyte concentration and valency. Electrical double layer thickness was calculated to be 3032 A^o in case of distilled water. It decreased down to 9.6, 6.06, 4.3, 3.5 and 3.03 A^o in case of NaCl (0.1, 0.25, 0.5, 0.75, 1.0 M) and 4.8, 3.03, 2.14, 1.75 and 1.52 A^o in case of $CaCl_2$ (0.1, 0.25, 0.5, 0.75, 1.0 M) recpectively. The energy barier height decreased from 650 Joules down to 350, 250, 150, -100 and –70 Joules in case of NaCl and 200, 100, 0, -40 and –60 Joules $CaCl_2$ respectively.

Rheological studies were also conducted to investigate the particle interactions through flow behaviour of suspensions. It is found that the ceramic powder suspensions (60 wt %) showed Newtonian behaviour (no flocculation) in absence of electrolytes and non-Newtonian behaviour (shear-thinning) in the presence of electrolytes due to gelation in the system.

Surface roughness of ceramic surfaces were investigated using both AFM and profilometer. However, profilometer was found to be more suitable technique rather than AFM to investigate the surface roughness of dental ceramics. Because AFM has a

low vertical range therefore cannot scan the whole surface. If AFM is used, large numbers of measurements should be done to get a meaningful idea about surface roughness which is time consuming. Therefore, in this study the results of profilometer was used to relate with particle interactions. It was found that there was a direct relation with the surface roughness and the contact angle results which were also conducted to investigate surface roughness. Increasing surface roughness increased the contact angle values obtained. The mean contact angle values obtained were so similar to the surface roughness values obtained with profilometer as a function of electrolyte concentration. However, the relation between the surface roughness and the electrolyte concentration was found to be complex. While surface roughness increased at low electrolyte concentrations, it decreased at higher electrolyte concentrations. This behaviour explained with agglomeration of particles at low concentrations and the gelation in the system at high concentrations.

REFERENCES

ADA Council on Scientific Affairs, 2003. "Direct and Indirect Restorative Materials", *The Journal of the American Dental Association*. Vol.134, No.4, pp. 463 – 472.

Adamson, A.W., 1967. *Pysical Chemistry of Surfaces*. Second Edition. (Wiley, USA), pp. 358 – 359.

Aksoy, G., Polat, H., Polat, M. and Coskun, G., 2006. "Effect of Various Treatment and Glazing (Coating) Techniques on the Roughness and Wettability of Ceramic Dental Restorative Surfaces", *Colloid and Surfaces B: Biointerfaces.* Vol. 53, Issue 2, pp. 254-259.

Anusavice, K.J., 1992. "Degradability of Dental Ceramics", *Advances in Dental Research*. Vol.6, No.1, pp. 82 – 89.

Barnes, H.A., Hutton, J.F., and Walters, K., 1989. *An Introduction to Rheology.* (Elsevier, Amsterdam), pp. 1 – 4.

Bergstörm, L., 1997. "Hamaker constants of Inorganic Materials", *Advances in Colloid and Interface Science*, Vol.70, pp. 125 – 169.

Bai, C., 2000. *Scanning Tunneling Microscopy and Its Applications*. (Springer, Shangai), pp. 105 – 106.

Bargeman, D. and Vader, F.V.V., 1972. "Van der Wals Forces Between Immersed Particles", *Journal of Electroanalytical Chemistry and Interfacial Electrochemistry.* Vol. 37, pp. 45 – 52.

Bhat, S.V., 2002. *Biomaterials*. (Kluwer Academic Publishers, Dordrecht), p.39.

Bico, J., Tordeux, C. and Quèrè, D., 2001. "Rough Wetting", *Europhysics Letters.* Vol.55, No.2, pp. 214–220

Binnig, G., Quate, C.F., and Gerber, C., 1986. "Atomic Force Microscope", *Physical Review Letters.* Vol.56, No.9, pp. 930 – 933.

Brookfield Engineering, 2005. *More Solutions To Sticky Problems.* (Boston), pp. 14 – 17.

Butt, H.J., Cappella, B., Kappl, M., 2005. "Force Measurements with the Atomic Force Microscope: Technique, Interpretation and Applications", *Surface Science Reports*. Vol.59, pp. 1 – 152.

Büttner, H. and Gerlach, E., 1970. "Van der Waals-Interaction of Ionic and Covalent Crystals", *Chemical Physics Letters.* Vol.5, Issue.2, pp. 91 – 92.

Callister Jr., W. D., 2001. *Fundamentals of Materials Science and Engineering*. Fifth Edition (Wiley, New York). p. 485.

Chauvy, P.F; Madore, C.; Landolt, D, 1998. "Variable Length Scale Analysis of Surface Topography: Characterisation of Titanium Surfaces for Biomedical Applications", *Surface and Coatings Technology*. Vol.110, No.1, pp. 48 – 56.

Cho, Y.J, Koo, Y.P, Jeon, J.H, 2002. "Surface Profile Estimation by Digital Filtering for Wear Volume Calculation", *Wear*. Vol.252, No.3, pp. 173–178.

Combe, E. C., 1986. *Notes on Dental Materials*. Fifth Edition (Churchill Livingstone, Edinburgh). pp. 96 – 99.

Crispin, B.J., 1994. *Contemporary Esthetic Dentistry: Practice Fundamentals*. (Quintessence, Tokyo), p.156.

Davis, E.J. and Stout, K.J., 1982. "Stylus Measurement Techniques: A Contribution to the Problem of Parameter Variation", *Wear*. Vol.83, No.1, pp. 49 – 60.

Dinger, D. R., 2005. *Characterization Techniques for Ceramists*. (Morris Publishing, Kearney) pp. 33 – 145

Feng, A., McCoy, C., Munir, Z.A., and Cagliostro, D., 1998. "Wettability of Transition Metal Oxide Surfaces", *Materials Science and Engineering A*. Vol.242, Issues 1 – 2, pp. 50 – 56.

Fowkes, F.M., 1967. "Intermolecular and Interatomic Forces at Interfaces", in *Surfaces and Interfaces I: Chemical and Physical Characteristics,* edited by J.J. Burke, N.L. Reed and V. Weiss (Syracuse University Pres, New York), Vol.1, p. 199.

Franks, G.F., 2002. "Zeta Potentials and Yield Stresses of Silica Suspensions in Concentrated Monovalent Electrolytes: Isoelectric Point Shift and Additional Attraction", *Journal of Colloid and Interface Science.* Vol.249, Issue.1, pp. 44 – 51.

Funk, J.E. and Dinger, D.R., 1994. *Predictive Process Control of Crowded Particulate Suspensions: Applied to Ceramic Manufacturing*. (Kluwer Academic Publishers, Dordrecht), pp. 254 – 328.

Girifalco, L.A. and Good, R.J., 1957. "A Theory for the Estimation of Surface and Interfacial Energies. I. Derivation and Application to Interfacial Tension", *The Journal of Physical Chemistry.* Vol.61, No.7, pp. 904 – 909.

Graves, G.A. Jr., Hentrich, R.L. Jr., Stein, H.G.; and Bajpai, P.K., 1972. "Resorbable Ceramic Implants in Bioceramics", in *Engineering and Medicine, Part I*, edited by C.W. Hall, S.F. Hullbert, S.N. Levine, and F.A. Young (Wiley, New York), pp. 91 – 115.

Guenther, K.H., Wierer, P.G., and Bennett, J.M., 1984. "Surface Roughness Measurements of Low-Scatter Mirrors and Roughness Standards," *Applied Optics*, Vol.23, No.21, p. 3820.

Hamaker, H.C., 1937. "The London – Van der Waals Attraction Between Spherical Particles", *Physica*, Vol.4, Issue.10, pp. 1058 – 1072.

Heintze, S.D., 1998. "Bridges Made of All-Ceramic Materials (IPS Empress 2) Indications, Clinical Aspects, Prognosis", in *Ivoclar-Vivadent Report* (Lichtenstein). No.12, pp. 11 – 12.

Hench, L.L., 1980. "Biomaterials", *Science.* Vol.208, No.4446, pp. 826 – 831.

Hench, L.L., 1991. "Bioceramics: From Concept to Clinic". *Journal of the American Ceramic Society*, Vol.74, No.7, pp. 1487 – 1510.

Hench, L.L., 1993. "Bioceramics: From Concept to Clinic". *American Ceramic Society Bulletin*, Vol.74, No.272, pp. 93 – 98.

Hentrich, R.L. Jr., Graves, G.A. Jr., Stein, H.G., and Bajpai, P.K., 1971. "An Evaluation of Inert and Resorbable Ceramics for Future Clinical Applications". *Journal of Biomedical Materials Research*. Vol.5, Issue.1 pp. 25 – 51.

Herczynska, E. and Proszynska, K., 1962. "Adsorption of H^+ and OH^- Ions on Various Metallic and Oxide Surfaces. Part I. The Isoelectrical Points. Part II. The Adsorption Isotherms", *Polish Academy of Sciences. Institute of Nuclear Research*, Warsaw, Report No: 372/V

Hiemenz, P.C. and Rajagopalan, R., 1997. *Principles of Colloid and Surface Chemistry*. (Marcel Dekker, New York), p.252, 464.

Hogg, R, Healy, T.W. and Fuerstenau, D.W., 1966. "Mutual Coagulation of Colloidal Dispersions", *Transaction of the Faraday Society.* Vol.62, pp. 1638 – 1651.

Höland, W. And Frank, M., 1994. "Material Science of Empress Glass-Ceramics" in *Ivoclar-Vivadent Report* (Lichtenstein). No.10, p.3.

IPS Empress 2 2004. *Instructions for Use Catalogue*. (Lichtenstein), p.29.

Johansen, P.G. and Buchanan, A. S., 1957. "An Application of the Microelectrophoresis Mmethod to the Study of the Surface Properties of Insoluble Oxides" *Australian Journal of Chemistry.* Vol.10,No. 4, pp. 398 – 403.

Johnson, M.L., 2000. "*Characterization of Geotechnical Surfaces via Stylus Profilometer" MSc. Thesis*, Georgia Tech, Atlanta.

Johnson, R.E. and Dettre, R.H.,1964. "Contact Angle, Wettability and Adhesion", Advances in Chemistry Series Vol. 43, *American Chemical Society,* pp. 112 – 135.

Johnson S. B., Scales P.J. and Healy T.W., 1999. "The Binding of Monovalent Electrolyte Ions on α-alumina. I. Electroacoustic Studies at High Electrolyte Concentrations", *Langmuir*. Vol.15, No.8, pp. 2836 – 2843.

Kingery, W.D., Bowen, H.K. and Uhlmann, D.R., 1976. *Introduction to Ceramics*. Second Edition (Wiley, New York), p.368.

Krupp, H., Schnabel, W. and Walter, G., 1972. "The Lifshitz-Van der Waals Constant: Computation of the Lifshitz-Van der Waals Constant on the Basis of Optical Data", *Journal of Colloid and Interface Science.* Vol.39, Issue.2, pp. 421 – 423.

Liang, Y., Hilal, N., Langston, L. and Starov, V. 2007. "Interaction Forces Between Colloidal Particles in Liquid: Theory and Experiment", *Advances in Colloid and Interface Science.* Article in Press.

Loehman, R.E., 1993. *Characterization of Ceramics*. (Butterworth-Heinemann, Boston), pp. 272 – 286.

Machesky M., Wesolowski D.J., Palmer D.A. and Ichiro-Hayashi K., 1998. "Potentiometric Titrations of Rutile Suspensions to 250°C", *Journal of Colloid Interface Science*. Vol.200, No.2, pp. 298 – 309.

McCabe, J.F., 1990. *Anderson's Applied Dental Materials*, Seventh Edition. (Blackwell Scientific, Oxford), p.73.

McKay, G., 1996. *Use of Adsorbents for the Removal of Polluntants from Wastewaters*. (CRC Press, USA), pp. 40 – 41.

McLean, J W., 1979. *The Science and Art of Dental Ceramics: Volume I: The Nature of Dental Ceramics and Their Clinical Use*. (Quintessence Publishing, Illionis), pp.34 – 49.

McMillan, P.W., 1979. *Glass-Ceramics*, Second Edition. (Academic Press Inc., London), p.12.

Meyer, E. and Bennewitz, R., 2004. *Scanning Probe Microscopy: The Lab on a Tip*. (Springer, Heidelberg), p. 45.

Miller, J.D., Veeramasuneni, S., Drelich, J.,Yalamanchili, M.R. and Yamauchi, G., 1996. "Effect of Roughness as Determined by Atomic Force Microscopy on the Wetting Properties of PTFE Thin Films" *Polymer Engineering and Science*. Vol.36, No. 14, pp. 1849 – 1855.

Morris, V.J., Kirby, A.R. and Gunning, A.P., 1999. *Atomic Force Microscopy for Biologists*. (Imperial College Press, London), p.1, 44.

Netz, R. R. and Andelman, D., 1997. "Roughness-Induced Wetting", *Physical Review E.* Vol.55, No.1, pp. 687 – 700.

Park, J.B. and Bronzino, J.D., 2003. *Biomaterials: Principles and Applications*. (CRC Press, Florida), p.21.

Park, J.B. and Lakes, R.S., 1992. *Biomaterials: An Introduction*. (Springer-Plenum Press, New York), p.3, p.29.

Parks, G.A., 1965. **"**The Isoelectric Points of Solid Oxides, Solid Hydroxides, and Aqueous Hydroxo Complex Systems", *Chemical Reviews*. Vol.65, No.2, pp. 177 – 198.

Parsegian, V.A., 2006. *Van der Waals Forces: A Handbook for Biologists, Chemists, Engineers, and Physicists.* (Cambridge University Press, USA), pp. 5 – 8.

Podczek, F., 1998. "Measurement of Surface Roughness of Tablets Made From Polyethylene Glycol Powders of Various Molecular Weight", *Pharmacy and Pharmacology Commununications*. Vol.4, pp. 179 – 182.

Polat, H. and Chander, S. 1999. "Adsorption of PEO/PPO Triblock Co-Polymers and Wetting of Coal", *Colloid and Surfaces. A: Physicochemical and Engineering Aspects*. Vol.146, Issues. 1 – 3, p. 199 – 212.

Polat, M. 1999. "A Review of the Theory of Interactions Between Particles Dispersed in Aqueous Media, I. The Electrical Double Layer", *The Journal of Ore Dressing*. Vol.1, Issue.2, pp. 7 – 35.

Polat, M. and Polat, H., 2000. "A Review of the Theory of Interactions Between Particles Dispersed in Aqueous Media, II. Van der Waals Interactions", *The Journal of Ore Dressing.* Vol.2, Issue.3, pp. 21 – 48.

Polat, M. and Polat, H., 2000. "A Review of the Theory of Interactions Between Particles Dispersed in Aqueous Media, III. Electrostatic and Structural Interactions and the DLVO Theory", *The Journal of Ore Dressing.* Vol.2, Issue.4, pp. 1 – 16.

Ponsonnet, L., Reybeier, K., Jaffrezic, N., Comte, V., Lagneau, C., Lissac, M. and Martelet, C., 2003. "Relationship Between Surface Properties (Roughness, Wettability) of Titanium and Titanium Alloys and Cell Behaviour", *Materials Science and Engineering C*. Vol.23, Issue.4, pp. 551 – 560.

Ricci, D. and Braga, P.C., 2004. "How the Atomic Force Microscope Works", in *Atomic Force Microscopy: Biomedical Methods and Applications,* edited by P.C. Braga and D.Ricci (Humana Press, New Jersey), pp. 3 – 11.

Ricci, D. and Braga, P.C., 2004. "Imaging Methods in Atomic Force Microscopy", in *Atomic Force Microscopy: Biomedical Methods and Applications,* edited by P.C. Braga and D. Ricci (Humana Press, New Jersey), pp. 13 – 17.

Riippi, M., Antikainen, O., Niskanen, T. and Yliruusi, J., 1998. "The Effect of Compression Force on Surface Structure, Crushing Strength, Friability, and Disintegration Time of Eythromycin Acistrate Tablets", *European Journal of Pharmaceutics and Biopharmaceutics*. Vol.46, Issue.3, pp. 339 – 345.

Robinson, M., Pask, J.A., and Fuerstenau, D. W., 1964. "Surface Charge of Alumina and Magnesia in Aqueous Media", *Journal of the American Ceramic Society*. Vol.47, No. 10, pp. 516 – 520.

Rosenblum, M.A. and Schulman, A., 1997. "A Review of All-Ceramic Restorations", *The Journal of the American Dental Association.* Vol.128, No.3, pp. 297 – 307.

Ruotsalainen, M., Heinämäki, J., Antikainen, O. and Yliruusi, J., 2002. "Time-Dependent Dimensional Changes and Film Adhesion of Coated Tablets", *S.T.P. Pharma Sciences*. Vol.12, No.6, pp. 385–389.

Salako, M., Podczeck, F. and Newton, M., 1998. "Investigations into the Deformability and Tensile Strength of Pellets", *International Journal of Pharmaceutics*. Vol.168, No.1, pp. 49 – 57.

Seitavuopio, P., Rantanen, J. and Yliruusi, J., 2003. "Tablet Surface Characterisation by Various Imaging Techniques", *International Journal of Pharmaceutics*. Vol.254, No.2, pp. 281–286.

Seitavuopio, P., Rantanen, J. and Yliruusi, J., 2005. "Use of Roughness Maps in Visualisation of Surfaces", *European Journal of Pharmaceutics and Biopharmaceutics*. Vol.59, No.2, pp. 351 – 358.

Settle, F., 1997. *Handbook of Instrumental Techniques for Analytical Chemistry*. (Prentice-Hall, New Jersey), pp. 341 – 342.

Shaw, D.J., 1992. *Introduction to Colloid and Surface Chemistry.* (Butterworth-Heinemann, Massachusetts), pp. 244 – 251.

Sinzinger, S.F. and Jahns, J., 2003. *Microoptics*. (Wiley, Weinheim), p.79 – 80.

Sonnefeld, J., Löbbus M., and Vogelsberger W., 2001. "Determination of Electric Double Layer Parameters for Spherical Silica Particles Under Application of the Triple-Layer Model Using Surface Charge Density Data and Results of Electrokinetic Sonic Amplitude Measurements", *Colloids and Surfaces A: Physicochemical and Engineering Aspects*. Vol.195, No.1, pp. 215 – 225.

Stookey, S.D., 1956. *Verfahren zur Herstellung Kristalliner Oder Glaskristalliner Gegenstände*. Dtsch Patent No. 1045056.

Sverjensky, D.A., 2005. "Prediction of Surface Charge on Oxides in Salt Solutions: Revisions for 1:1 (M^+L^-) Electrolytes", *Geochimica et Cosmochimica Acta.* Vol.69, No:2, pp. 225 – 257.

Tamai, Y. And Aratani, K., 1972. "Experimental Study of the Relation between Contact Angle and Surface Roughness" *The Journal of Physical Chemistry*. Vol.76, No.22, pp. 3267 – 3271.

Van der Wal, Bouwe Pieter, 2006. "*Static and Dynamic Wetting of Porous Teflon® Surfaces", Ph.D. Thesis*, (The Netherlands), pp. 11 – 13.

Van Noort, R., 2002. *An Introduction to Dental Materials*. (Mosby, UK), pp.231 – 242.

Van Oss, C.J., 1994. *Interfacial Forces in Aquoeus Media.* (Marcel Dekker, New York), pp. 1 – 2.

Wagberg, P. and Johansson, P.-A, 1993. "Surface Profilometry—A Comparison Between Optical and Mechanical Sensing on Printing Papers", *Tappi Journal*, Vol.76, No.12, pp. 115–121.

WEB_1, 2006. Ceramic Oxide: Ag2O Silver Oxide, 18/08/2006. http://ceramic-materials.com/cermat/oxide

WEB_2, 2007. Feature Article: Get the Roll Surface Right, 07/02./2007 http://www.ptonline.com/articles/200403fa3.html

WEB_3, 2007. Figure – Nature Methods, 07/02/2007. http://www.nature.com/nmeth/journal/v3/n12/fig_tab/nmeth1206-973_F1.html

WEB_4, 2007. Nanotechnology/STM, 07/02/2007. http://en.wikibooks.org/wiki/Nanotechnology/STM

WEB_5, 2006. Atomic Force Microscopy: Theory, Practice,Applications, 26/09/2006. http://www.afmuniversity.org/chapter7.html

WEB_6, 2007. EDX Analysis and WDX Analysis, 07/02/2007. http://www.siliconfareast.com/edxwdx.htm

Wenzel, R.N., 1936. "Resistance of Solid Surfaces to Wetting by Water", *Industrial and Engineering Chemistry*, Vol. 28, No. 8, pp. 988 -994

Wenzel, R.N., 1949**.** "Surface Roughness and Contact Angle", *Journal of Physical Chemitry*, Vol.53, No.9, pp. 1466 – 1467.

Wiesendanger, R., 1994. *Scanning Probe Microscopy and Spectroscopy: Methods and Applications*. (Cambridge University Press, Cambridge). p.213.

Williamson, J.B.P., 1967 "The Microtopography of Surfaces" *Proceedings of the Institution of Mechanical Engineers*. Vol.182, pp. 21 – 30.

Wolansky,G. and Marmur, A., 1998. "The Actual Contact Angle on a Heterogeneous Rough Surface in Three Dimensions", *Langmuir*. Vol.14, No.18, pp. 5292 - 5297.

Wolansky, G. and Marmur, A., 1999. "Apparent Contact Angles on Rough Surfaces: the Wenzel Equation Revisited" *Colloids and Surfaces A: Physicochemical and Engineering Aspects.* Vol.156, No.1, pp. 381–388

Zeta-Meter Inc. "*Zeta Potential: A Complete Course in 5 Minutes"*. (Staunton, USA), pp. 2 – 4.

Zetasizer Nano Series User Manual, 2004. Malvern Instruments Ltd. (Worcestershire UK). Issue 1.1, pp. 15.1 – 15.3.

Zhang, Y., Griggs, J.A. and Benham, A.W., 2004. "Influence of Powder/Liquid Mixing Ratio on Porosity and Translucency of Dental Porcelains" *Journal of Prosthetic Dentistry*. Vol.91:128 – 135.